Continuous Carbonyl Sulfide Fluxes in a Tallgrass Prairie

Using the Flux-Gradient Method

BY

Benjamin M. Alsip
B.A., Knox College, 2000

THESIS

Submitted as partial fulfillment of the requirements
for the degree of Master of Science in Earth and Environmental Sciences
in the Graduate College of the
University of Illinois at Chicago, 2017

Chicago, Illinois

Defense Committee:

Max Berkelhammer, Chair and Advisor, Earth and Environmental Sciences
Kathryn Nagy, Earth and Environmental Sciences
D'Arcy Meyer-Dombard, Earth and Environmental Sciences

Dedicated to those who never stop learning.

ACKNOWLEDGMENTS

I owe a debt of gratitude to the department—professors and graduate students alike. Without their advice, guidance, and inspiration—before, during, and potentially after graduation—it's likely that this process would have changed my career, but it certainly wouldn't have changed my life. At the top of this list could only be my advisor, Max Berkelhammer, who has a razor-sharp mind and the patience of a saint. My committee provided direction and molding early on in the process that made the experience go smoothly. Much is owed to all of them for their unique input, which extends to before my time in graduate school began.

Roser Matamala and David Cook (both at Argonne National Laboratory) have been exceptionally helpful in letting us run the sampling experiment at Fermilab—now in its second year—as well as with access to the eddy covariance data. Chris Whelan (University of Illinois at Chicago, Biological Sciences) braved the tick horde on multiple occasions to provide much-needed assistance in identifying prairie plant species.

Lastly, a number of very important people in my life had to put up with me being absent through large chunks of time during the entire career-change process. They knew that I had to do this to find my peace.

BMA

TABLE OF CONTENTS

1 INTRODUCTION 1
1.1 Ecosystem Research at Fermi 1
1.2 Drivers of Ecosystem Change 4
1.3 Literature Review 9
1.3.1 OCS Introduction 9
1.3.2 Stomatal Conductance 11
1.3.3 Conditions for a Carbonyl Sulfide Gross Primary Productivity Proxy 13
1.3.4 Laser Absorption Spectrometry Advancements 14
1.4 Purpose 15
1.5 Hypotheses 16

2 METHODS 17
2.1 Field Sites 17
2.2 Experimental Setup 20
2.3 Site Visit Standard Operating Procedures 21
2.4 Calibration 22
2.5 Data Procedure 23
2.5.1 During Campaign 24
2.5.2 After Campaign 25

3 RESULTS 29
3.1 Concentrations 29
3.2 Carbonyl Sulfide Concentration Diel Cycle 36
3.3 Carbonyl Sulfide Minima and Carbon Dioxide Maxima 39
3.4 Carbonyl Sulfide Gradients 40
3.5 Daytime Carbonyl Sulfide Flux and Gross Primary Productivity 42
3.6 Carbonyl Sulfide Flux Diel Cycle 48
3.7 Nighttime Carbonyl Sulfide Flux and Transpiration 50
3.8 Statistical Analysis of Nighttime Carbonyl Sulfide Flux 55
3.8.1 Linear Regressions 55
3.8.2 High-Flux vs. Low-Flux Percentiles 58
3.8.3 Nighttime Carbonyl Sulfide Flux Compared to the Previous Day 62

4 DISCUSSION 65
4.1 Carbonyl Sulfide Flux in a Tallgrass Prairie 65
4.2 Carbonyl Sulfide Flux and Gross Primary Productivity 67
4.3 Comparison of Gross Primary Productivity Estimates 70
4.4 Nighttime Stomatal Conductance and Transpiration 72
4.5 Humidity and Water Stress 75
4.6 Inferring Ecosystem Responses to Climate Change 76

5 CONCLUSIONS 79
5.1 Overview 79
5.2 Further Study 80

TABLE OF CONTENTS, *continued*

6 BIBLIOGRAPHY 81

7 APPENDIX.....89

8 VITA 97

LIST OF TABLES

Table 1. Mean daytime OCS fluxes from tallgrass prairie (Fermi), peak-season corn (BND), and senescent corn (EF). 45

Table 2. Mean nighttime OCS fluxes from tallgrass prairie (Fermi), peak-season corn (BND), and senescent corn (EF). 51

Table 3. Mean nighttime transpiration from the tallgrass prairie (Fermi), peak-season corn (BND), and senescent corn (EF). 55

Table 4. F_{leaf} night:day ratios (%) at the tallgrass prairie (Fermi), peak-season corn (BND), and senescent corn (EF). 64

Table 5. Whole-night (n) linear regressions, F_{leaf} vs. eight ecosystem variables, sorted by R^2 92

Table 6. First half-night (n_1) linear regressions, F_{leaf} vs. eight ecosystem variables, sorted by R^2. 92

Table 7. Second half-night (n_2) linear regressions, F_{leaf} vs. eight ecosystem variables, sorted by R^2. 93

Table 8. Whole-night (n) linear regressions, F_{eco} vs. eight ecosystem variables, sorted by R^2 93

Table 9. First half-night (n_1) linear regressions, F_{eco} vs. eight ecosystem variables, sorted by R^2. 94

Table 10. Second half-night (n_2) linear regressions, F_{eco} vs. eight ecosystem variables, sorted by R^2. 94

LIST OF FIGURES

Figure 1. Temperature anomaly for Illinois by 2100 with respect to 1900. 6
Figure 2. Leaf-level day and night fluxes of OCS, CO_2, and H_2O. 10
Figure 3. Comparison of OCS flux and CO_2 flux vs. transpiration of different plant species. 12
Figure 4. OCS sampling sites referenced. 18
Figure 5. Historic mean temperature and precipitation at the Fermi tallgrass prairie. 19
Figure 6. Most predominant plant species on site through the campaign. 19
Figure 7. Sampling inlets at the Fermi tallgrass prairie. 21
Figure 8. Calibrations against secondary standard in the field. 23
Figure 9. Nighttime F_{leaf} vs. u* at all sites. 27
Figure 10. OCS measurements made at Fermi and WLEF. 30
Figure 11. Concentrations of OCS, CO_2, CO, and H_2O at 0.32 m throughout the campaign. 32
Figure 12. Fermi midday mean above-canopy OCS and CO_2 concentrations. 33
Figure 13. Fermi in-canopy OCS and CO_2 concentrations. 34
Figure 14. In-canopy OCS concentrations at BND and EF. 35
Figure 15. Mean in-canopy OCS vs. CO_2 concentrations at BND and EF. 36
Figure 16. Mean Fermi OCS diel cycle at all four inlets. 37
Figure 17. Select 20-day Fermi OCS concentration diel cycles. 38
Figure 18. BND and EF OCS diel cycles. 39
Figure 19. In-canopy OCS minimum and CO_2 maximum. 40
Figure 20. Select 20-day Fermi OCS gradient diel cycles. 41
Figure 21. Fermi mean daytime (10:00–15:00) OCS fluxes. 42
Figure 22. Fermi daily F_{leaf} and FPAR throughout the campaign. 43
Figure 23. Fermi FPAR vs. F_{leaf} throughout the campaign. 44
Figure 24. Fermi daily F_{leaf} vs. GPP_{Re}. 46
Figure 25. GPP_{OCS} vs. GPP_{Re}. 47
Figure 26. Fermi mean OCS flux diel cycle. 48
Figure 27. Select 20-day Fermi OCS flux diel cycles. 49
Figure 28. Fermi mean nighttime (22:00–04:00) OCS fluxes. 50

LIST OF FIGURES, *continued*

Figure 29. Fermi nighttime transpiration (mean = 0.0364). 53
Figure 30. Fermi nighttime E_n vs. F_{leaf} (A) and E_n vs. VPD (B). 54
Figure 31. Fermi F_{eco} and F_{leaf} vs. WS. 57
Figure 32. High (blue) and low (red) nighttime OCS fluxes vs. WS. 59
Figure 33. High (blue) and low (red) nighttime OCS fluxes vs. VPD. 60
Figure 34. High (blue) and low (red) nighttime OCS fluxes vs. OCS. 61
Figure 35. High (blue) and low (red) nighttime OCS fluxes vs. CO_2. 62
Figure 36. F_{leaf} night:day ratios at Fermi. 63
Figure 37. F_{leaf} and GPP_{Re} at Fermi. 68
Figure 38. Air temperature and SWC at Fermi, DOY 250–275. 69
Figure 39. GPP_{OCS} and variable LRU through the period of observation. 72
Figure 40. Fermi nighttime transpiration (E_n) vs. CO_2 concentration. 74
Figure 41. Fermi nighttime transpiration (E_n) vs. relative humidity (R_h) and soil water content (SWC). 76
Figure 42. BND soil map (https://websoilsurvey.nrcs.usda.gov). 89
Figure 43. EF soil map (https://websoilsurvey.nrcs.usda.gov). 90
Figure 44. Fermi soil map (https://websoilsurvey.nrcs.usda.gov). 91
Figure 45. High (blue) and low (red) nighttime OCS fluxes vs. R_n. 95
Figure 46. High (blue) and low (red) nighttime OCS fluxes vs. SWC. 95
Figure 47. High (blue) and low (red) nighttime OCS fluxes vs. T_a. 96
Figure 48. High (blue) and low (red) nighttime OCS fluxes vs. T_s. 96

LIST OF ABBREVIATIONS

ABA	Abscisic acid
BND	Bondville, IL; peak-season corn site
CO	Carbon monoxide (ppb)
CO_2	Carbon dioxide (ppm)
DOY	Day of year
EF	Energy Farm, Urbana, IL; senescent corn site
E_n	Nighttime transpiration (proxy in units of pmol hPa m^{-2} s^{-1})
F_{eco}	Ecosystem OCS flux (pmol m^{-2} s^{-1})
F_{leaf}	Vegetation OCS flux (pmol m^{-2} s^{-1})
F_{OCS}	OCS flux (pmol m^{-2} s^{-1})
Fermi	Fermilab, Batavia, IL; tallgrass prairie
FPAR	Absorbed PAR fraction (%)
F_{soil}	Soil OCS flux (pmol m^{-2} s^{-1})
GPP	Gross primary productivity (µmol m^{-2} s^{-1})
GPP_{OCS}	Gross primary productivity (µmol m^{-2} s^{-1}), from OCS flux
GPP_{Re}	Gross primary productivity (µmol m^{-2} s^{-1}), from nighttime respiration
g_s	Stomatal conductance
H_2O	Water
H_2S	Hydrogen sulfide
LGR	Los Gatos Research laser absorption spectrometer
LRU	Leaf relative uptake ratio of OCS:CO_2
MIU	Multiport inlet unit
NEE	Net ecosystem exchange, or CO_2 flux (µmol m^{-2} s^{-1})
NOAA	National Oceanic and Atmospheric Administration
OCS or COS	Carbonyl sulfide (ppt)
PAR	Photosynthetically active radiation (µmol m^{-2} s^{-1})
R_{eco}	Ecosystem respiration
$R_{e,day}$	Daytime respiration
$R_{e,night}$	Nighttime respiration
R_n	Net radiation (W m^{-2})
SOC	Soil organic carbon
SWC	Soil water content (%)
T_a	Air temperature (°C)
T_s	Soil temperature (°C)
u*	Wind friction velocity (m s^{-1})
UIC	University of Illinois at Chicago
VPD	Vapor pressure deficit (hPa)
WS	Wind speed (m s^{-1})
WUE	Water use efficiency, biomass gained per water transpired

SUMMARY

An ecosystem's carbonyl sulfide (OCS or COS) flux is a powerful proxy for plant-controlled carbon and water exchange. This study is the first to apply the OCS flux-gradient method to constrain gross primary productivity (GPP) and nighttime transpiration. It is also one of only a few OCS studies in grassland ecosystems, which are characterized by complex species distributions that vary temporally. A laser absorption spectrometer measured OCS fluxes during the growing season at the Fermi tallgrass prairie eddy covariance site in Batavia, Illinois, USA. Ambient atmospheric concentrations of OCS, carbon monoxide (CO), carbon dioxide (CO_2), and water vapor (H_2O) were sampled at 1 Hz frequency at four different heights within and above the vegetation canopy from May to October, 2016. We observed a well-defined seasonal cycle of OCS concentrations that tracked the Northern Hemisphere growing season. The data also show a strong diel cycle in concentrations, above-canopy gradients, and OCS fluxes associated with changes in radiation and atmospheric stability. Nighttime OCS in the canopy dropped to a minimum of 17.6 ± 9.5 ppt, which, to our knowledge, is the lowest tropospheric OCS concentration ever observed in the free atmosphere. Close coupling of OCS and CO_2 concentrations was demonstrated (R^2 = 0.654, p < 0.001) even as the season and species makeup evolved. We converted OCS concentration gradients to ecosystem OCS fluxes using the net ecosystem exchange of carbon dioxide from existing eddy covariance data on site. OCS fluxes reached a maximum uptake of -102 ± 9.5 pmol m^{-2} s^{-1} on June 18. After correcting for soil OCS fluxes using a published empirical model, we compared GPP derived from OCS flux-gradients (mean = -23.3 µmol m^{-2} s^{-1}) against GPP derived from ecosystem respiration (mean = -19.2 µmol m^{-2} s^{-1}), and the two methods were well-correlated (R^2 = 0.566, p < 0.001, RMSE =

8.81, n = 150). Ratios of OCS flux night:day indicate nighttime canopy conductance was ~8% of daytime conductance. In this first field study of its kind, we demonstrated that the OCS flux-gradient method to constrain GPP has great potential to improve ecosystem carbon budget closure.

1 INTRODUCTION

1.1 Ecosystem Research at Fermi

Ecosystem research in the tallgrass prairie at the Fermi National Accelerator Laboratory (Fermilab) in Batavia, Illinois, dates back to 1975 when a series of prairie restorations were undertaken on land that had been cultivated for at least a century (*Jastrow*, 1987; *Cook et al.*, 1988; *Allison et al.*, 2005; *Matamala et al.*, 2008). By 2002, a total of 452 ha on the grounds of Fermilab had been converted from tilled agricultural land to restored tallgrass prairie (*Matamala et al.*, 2008). This conversion substantially increased the landscape's carbon sink, returning carbon to the soil that conventional tilled agriculture liberated to the atmosphere. For example, microbial biomass carbon was over two times greater in a 25-year-old prairie restoration (1230 μg g^{-1}) than in a corn or soy agriculture plot (both, 478 μg g^{-1}; *Allison et al.*, 2005). After 100 years following restoration, these soils will likely have recovered 3.5 kg C m^{-2}, or half of their initial soil organic carbon (SOC) stocks (*Matamala et al.*, 2008).

The resulting soil chronosequence of restored prairie has provided many opportunities to investigate various carbon cycle dynamics pertaining especially to land use change and soil sequestration of carbon. Tallgrass prairie soils are among the most productive soils in the world (*Jastrow*, 1987; *Cook et al.*, 1988), and the chronosequence offered an opportunity to understand the specific properties of soil prairies that lead to such high levels of productivity. Common agricultural practices (e.g., tilling) disrupt soil structure, reducing soil macroaggregates, which leads to increased erosion, decreased porosity, and other conditions that inhibit air, water, and nutrient cycling within soils (*Tisdall and Oades*, 1982; *Jastrow*, 1987). An early sampling campaign of the chronosequence produced a model suggesting that within

5–10 years following cultivation, a restored prairie would recover a macroaggregate fraction (85-90%) close to that of prairie remnant (~95%), but it would take 56 seasons to reach 99% of an undisturbed (i.e., remnant) prairie (*Jastrow*, 1987, 1996). The rate of recovery to pre-disturbance conditions is driven by recolonization of root and mycorrhizal hyphae (*Cook et al.*, 1988). By the eighth growing season following restoration, predominant prairie grass species contributed to a root mass and fine root fiber structure (*Cook et al.*, 1988) conducive to soil aggregate stability (*Tisdall and Oades*, 1982; *Oades*, 1984; *Jastrow*, 1987, 1996; *Cook et al.*, 1988; *Miller and Jastrow*, 1990; *Jastrow et al.*, 1998).

Research at the Fermi prairie soil chronosequence also helped characterize the role of macroaggregates, roots, and mycorrhizal hyphae in increasing soil carbon stores (*Elliott*, 1986; *Jastrow*, 1996). *Andropogon gerardii* colonized with mycorrhizal fungi demonstrated higher rates of photosynthesis than non-colonized specimens, indicating the possibility of an increased carbon sink (*Miller et al.*, 2002). This enhanced carbon sink potential, however, was due less to the abundance of fungi following cultivation, but rather their impact on soil structure (*Allison et al.*, 2005). The timescales over which prairie restorations see carbon stores return to pre-cultivation levels vary. Aboveground biomass rapidly returns to the carbon storage levels of remnant prairie in 13 years, and belowground plant carbon stores return on a decadal scale, it takes microbial biomass and soil organic carbon (SOC) hundreds of years to return to remnant prairie levels (*Matamala et al.*, 2008).

In order for soils to sequester carbon belowground, plants aboveground need to draw down carbon dioxide (CO_2) from the atmosphere and convert the CO_2 to biomass. To understand the controls on aboveground carbon fixation, fluxes of carbon into and out of an

ecosystem can be measured. The AmeriFlux Network (http://ameriflux.lbl.gov) was designed to aggregate information on the carbon, water, and energy exchange at the land-air interface from many sites in order to generate fundamental information on the processes that mediate the terrestrial drawdown and exchange of carbon. The tallgrass prairie at Fermilab, which is part of the AmeriFlux network, is one of only a few sites dedicated to restored grasslands. Recently, AmeriFlux data from the Fermi tallgrass prairie site was used to characterize how carbon exchange in eight grasslands responds to annual variations in precipitation from 1980 to 2012 (*Petrie et al.*, 2016). Three eastern and three western Great Plains grassland sites were studied, as well as two sites located outside of the Great Plains: one in the southwest, and the Fermi site in the northeast. Relative to the three eastern grasslands, net plant carbon drawdown (i.e., the difference between ecosystem respiration and GPP) at Fermi was 1347% greater (*Petrie et al.*, 2016). The increased carbon sink is commonly observed in eastern grasslands, which receive more precipitation than western grasslands (*Derner et al.*, 2006; *Zhang et al.*, 2011; *Petrie et al.*, 2016). The climatic and ecosystem conditions at Fermi allowed for maximized carbon uptake: Fermi was wetter than most sites, cooler than the eastern grasslands, and had the lowest vapor pressure deficit (VPD), which is inversely related to relative humidity, of all sites (*Petrie et al.*, 2016). Whereas the conditions observed made Fermi exceptionally productive, environmental conditions and management practices can drastically change the carbon budget of prairies. Grasslands can switch from net carbon sinks to sources with less precipitation than average years (*Flanagan et al.*, 2002; *Zhang et al.*, 2010b, 2011; *Petrie et al.*, 2016) or controlled burning (*Zhang et al.*, 2011; *Vargas et al.*, 2012; *Logan and Brunsell*, 2015; *Petrie et al.*, 2016). These carbon exchange responses will be more predictable

for eastern grasslands than western grasslands under climate change (*Petrie et al.*, 2016). However, analyses using eddy covariance data to estimate plant uptake of CO_2 are uncertain (*Reichstein et al.*, 2005; *Commane et al.*, 2015), which will be detailed in the next section.

The Fermi tallgrass prairie provides an ideal location to study the processes limiting above and belowground productivity because it is comprised of some of the most productive soils in the world (*Jastrow*, 1987; *Cook et al.*, 1988), and situated in the region of highest gross primary productivity in North America (*Hilton et al.*, 2017). Further, as land use decisions such as biofuel production, prairie restoration, and food production become increasingly complex in a changing climate, quantifying the impact of these decisions on regional and global carbon cycles is critical. It is precisely the question of how carbon exchange and land use change intersect that inspired the research presented here.

1.2 Drivers of Ecosystem Change

Illinois ecosystems are undergoing rapid change. Factors driving these changes include, but are not limited to, land use change and a warming climate. Frequently, land use change in Illinois represents a conversion from heterogeneous native prairie ecosystems into homogeneous agricultural plots, representing a loss of SOC. The reverse is also true in areas undergoing prairie restoration initiatives, where stocks of SOC can be replenished (*Allison et al.*, 2005; *Matamala et al.*, 2008).

Ecosystem responses to land use change and climate change will include shifts in carbon and water budgets. Converting ecosystems to agriculture may temporarily increase aboveground carbon storage with an overall increase in plant biomass, but this is somewhat offset by decreases in SOC (*Beniston et al.*, 2014; *Lawler et al.*, 2014). Hydrologically, converting

land to agriculture has been associated with a decrease in soil water retention, increasing runoff (*Wright and Wimberly*, 2013). The combination of higher atmospheric CO_2 and increased heat and water stress predicted for Illinois (*Hayhoe et al.*, 2010) can generate multiple ecosystem responses. Increased photosynthetic production has been observed as a resulted of higher atmospheric CO_2 (*Keenan et al.*, 2013, 2014), but reduced photosynthesis also has been observed (*Piao et al.*, 2008; *Barichivich et al.*, 2013). Prolonged heat and water stress results in drought and can bring about a reduction of photosynthetic production (*Ciais et al.*, 2005; *Zhang et al.*, 2016), and early senescence (*Zhang et al.*, 2016). It is ultimately difficult to predict whether changing climate and atmosphere CO_2 will increase or decrease the strength of the carbon sink and how much this trajectory will vary between ecosystems.

One way to assess changing water and carbon budgets is through the concept of water-use efficiency (WUE), which is the ratio of biomass gained from the assimilation of atmospheric CO_2 (gross primary productivity, GPP) to the water transpired (E). For WUE to be useful in assessing the impacts of land use change, GPP and E both need to be constrained and the ratio of these two quantities represents WUE (i.e., GPP/E). Previous work on this topic has been limited because GPP cannot be directly measured and, whereas transpiration can be estimated during the day, it cannot be measured effectively during the night (E_n). Historically, indirect estimates of GPP have been used to close the carbon budget along with an assumption that E_n is close to zero. This assumption has been challenged recently, with research demonstrating substantial nighttime transpiration (*Rawson and Clarke*, 1988; *Green et al.*, 1989; *Matyssek et al.*, 1995; *Donovan et al.*, 1999; *Snyder et al.*, 2003; *Caird et al.*, 2007; *Fisher et al.*, 2007; *Coupel-Ledru et al.*, 2016). In terms of WUE, water transpired at night is “wasted” because it

occurs in the absence of photosynthesis. The increasing temperatures expected with climate change could reduce WUE due to higher evaporative demand. Models indicate nighttime temperatures in Illinois will warm faster by 2100 than daytime temperatures (Figure 1; +6.7°C and +5.3°C, respectively, with respect to 1900; average of all models for Illinois, CMIP5 ensemble, business-as-usual emissions scenario; *Taylor et al.*, 2012) driving conditions that would force greater nighttime transpiration.

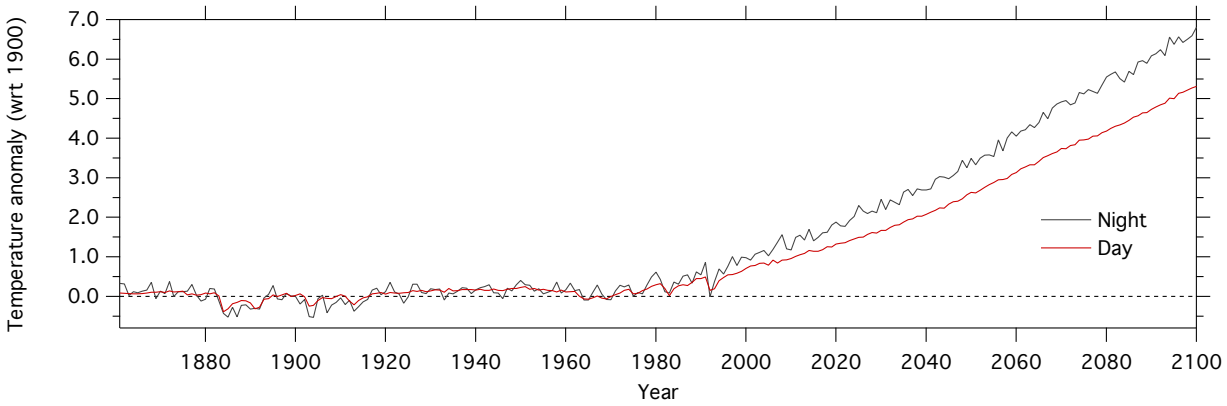

Figure 1. Temperature anomaly for Illinois by 2100 with respect to 1900. Illinois daytime temperatures are expected to rise by ~5.3°C, and nighttime temperatures by ~6.7°C. Average of all models for Illinois, CMIP5 ensemble, business-as-usual emissions scenario (Taylor et al., 2012).

Constraining the terms driving WUE is exceptionally important in the Midwest, which has the highest GPP of any region in North America (*Hilton et al.*, 2017). Therefore, WUE should be considered in any land-use decision that seeks to balance food, energy, water, and ecosystem services concerns. However, existing methods of estimating GPP and E_n are limited.

The widely-used eddy covariance method of estimating GPP requires turbulent conditions in the boundary layer, the lowest portion of the troposphere under the influence of

Earth's surface (*Stull*, 2012). Frequently at night, the boundary layer is sufficiently stable that not only turbulence but also diffusion influences the exchange of gas between the surface and atmosphere. This results in large gaps in the data that must be interpolated by a process known as, "gap-filling." This technique assumes stability between meteorological conditions and carbon, water, and energy fluxes on a seasonal scale that does not reflect shorter-term variability (*Reichstein et al.*, 2005). Total daytime carbon fluxes are the sum of photosynthesis (GPP) and the simultaneous respiration of CO_2 from plants and the soil. The partitioning of eddy covariance data into its constituent flux components (i.e., flux-partitioning) to estimate GPP, relies on extrapolating the CO_2 flux at night when GPP is 0 ($R_{e,night}$) to obtain an indirect estimate of daytime respiration ($R_{e,day}$). This estimate of $R_{e,day}$ allows for an estimate of respiration-based gross primary productivity (GPP_{Re}; *Reichstein et al.*, 2005; *Commane et al.*, 2015). In productive ecosystems such as Fermi, ecosystem respiration is systematically overestimated by temperature-dependent night-to-day extrapolations of respiration (*Reichstein et al.*, 2005). Recent work has demonstrated that this overestimation is largely due to the inhibition of daytime respiration because respiration is inhibited by light (*Kok*, 1949; *Heskel et al.*, 2013; *Sun et al.*, 2014; *Wehr et al.*, 2016).

Water fluxes are similarly confounded. For example, when partitioning ecosystem latent heat flux, distinguishing between evaporation and transpiration presents methodological challenges (*Yakir and Wang*, 1996; *Jasechko et al.*, 2013; *Berkelhammer et al.*, 2016a). Similarly, constraining E_n has not been considered necessary, because it was assumed that transpiration was negligible at night when photosynthesis ceases. The need to constrain nighttime water loss became evident when it was demonstrated that E_n can reach up to 30% of daytime water loss

(*Rawson and Clarke*, 1988; *Green et al.*, 1989; *Matyssek et al.*, 1995; *Donovan et al.*, 1999; *Snyder et al.*, 2003; *Caird et al.*, 2007; *Fisher et al.*, 2007; *Coupel-Ledru et al.*, 2016). Furthermore, nighttime temperatures are expected to increase faster than the daytime, forcing nighttime VPD to rise faster than daytime VPD (*Taylor et al.*, 2012; *Coupel-Ledru et al.*, 2016), leading to an increase in the rate at which plants lose water at night (*Herzog et al.*, 1998; *Benyon*, 1999; *Oren et al.*, 2001; *Daley and Phillips*, 2006; *Caird et al.*, 2007; *Fisher et al.*, 2007; *Kavanagh et al.*, 2007; *Coupel-Ledru et al.*, 2016). In this context, understanding the forcings of E_n among different plant species becomes increasingly important and should be included in land use decisions. One common method of E_n estimation uses sap flow, where the velocity of a heat pulse introduced in the xylem stream is converted to sap flow rate, and converted again to transpiration (*Fisher et al.*, 2007). This approach is typically only done on woody plants, and it is not robust enough to use sap flow from a few individual grass species to represent the entire ecosystem.

New ecosystem-scale methods of constraining GPP and E_n (i.e., when GPP = 0) are needed to provide quantitative estimates of WUE, which in turn can be used to assess the carbon and water cycle impacts of land use change. Once validated, such methods will reduce the variability among regional GPP estimation methods that, at present, differ widely in their estimation of GPP in North America (*Huntzinger et al.*, 2012; *Schaefer et al.*, 2012; *Guanter et al.*, 2014; *Hilton et al.*, 2017).

1.3 Literature Review

1.3.1 OCS Introduction

The application of carbonyl sulfide (OCS or COS) to constrain GPP (*Blonquist et al.*, 2011; *Asaf et al.*, 2013) and E_n (*Seibt et al.*, 2010) is a novel method to close ecosystem carbon and water budgets. OCS is a trace atmospheric gas with concentrations ~500 ppt (*Montzka et al.*, 2007). OCS is produced by direct emission from the oceans, oxidation of marine carbon disulfide (CS_2) and dimethyl sulfide (C_2H_6S), as well as generated from anthropogenic sources (*Montzka et al.*, 2007). OCS sinks are dominated by vegetative uptake, which suggests its usefulness as a tracer for GPP during the day (*Campbell et al.*, 2008) and stomatal conductance at night (*Seibt et al.*, 2010). Known and unknown atmospheric leaf-level fluxes of carbon, water, and OCS are detailed below (Figure 2).

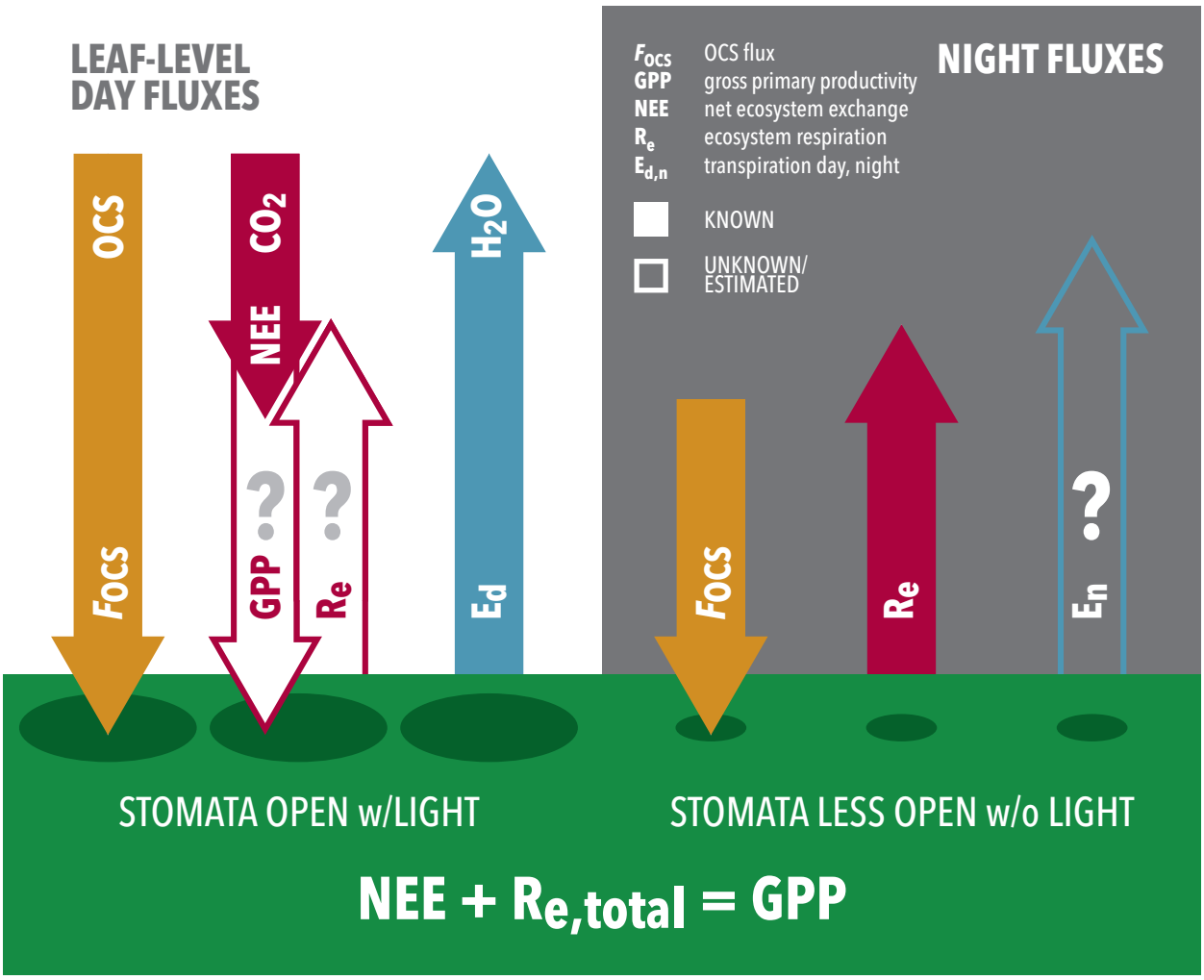

Figure 2. Leaf-level day and night fluxes of OCS, CO_2, and H_2O. Measured nighttime CO_2 respiration is extrapolated to daytime respiration, which is systematically overestimated using the eddy covariance method of flux partitioning and contingent upon turbulent conditions (Reichstein et al., 2005). The total CO_2 flux of the system (NEE) is measured. Methods of measuring E_n (e.g., sap flow) are logistically infeasible in grassland ecosystems. OCS provides a solution to constrain both GPP and E_n based on its one-way diffusion into plants controlled by stomatal conductance (g_s; Seibt et al., 2010; Blonquist et al., 2011; Asaf et al., 2013; Berkelhammer et al., 2013).

OCS and CO_2 follow the same diffusion pathway across the stomata and into the mesophyll, where the hydrolysis reaction (Equation 1), catalyzed by carbonic anhydrase, completely consumes OCS rapidly (*Asaf et al.*, 2013).

$$OCS + H_2O \text{ —> } H_2S + CO_2 \qquad (1)$$

The resulting hydrogen sulfide (H_2S) may perform a number of plant biology functions, including providing an alternate form of sulfur for protein synthesis (*Lamers et al.*, 2013; *Calderwood and Kopriva*, 2014), increasing resistance to pathogens (*Rausch and Wachter*, 2005; *Bloem et al.*, 2007; *Papenbrock et al.*, 2007; *Calderwood and Kopriva*, 2014), as well as signaling responses to drought, hypoxia, and toxicity stresses (*Wang et al.*, 2010; *Zhang et al.*, 2010a; *Jin et al.*, 2011; *Cheng et al.*, 2013; *Sun et al.*, 2013; *Calderwood and Kopriva*, 2014). This one-way hydrolysis reaction distinguishes OCS from CO_2, with the latter being partially respired by plants as well as soil microorganisms (*Asaf et al.*, 2013).

1.3.2 Stomatal Conductance

Stomata are small openings on plant leaves and stems that mediate gas exchange between plant leaves and the atmosphere through increased or decreased stomatal aperture (*Hetherington and Woodward*, 2003). The rate at which a given gas can transfer through these openings is quantified using stomatal conductance (g_s). Enhanced levels of CO_2 decrease g_s (*Kimball and Idso*, 1983; *Morison and Gifford*, 1983; *Wand et al.*, 1999; *Flexas and Medrano*, 2002; *Reichstein et al.*, 2002; *Hetherington and Woodward*, 2003; *Morgan et al.*, 2004, 2011; *Caird et al.*, 2007; *Zhang et al.*, 2016), which decreases canopy transpiration and increases soil water content (SWC; *Field et al.*, 1995; *Morgan et al.*, 2004, 2011).

A key difference between CO_2 and OCS fluxes at the ecosystem-level is that their uptake is driven by different mechanisms. Photosynthesis drives CO_2 flux, which means that the CO_2 flux into an ecosystem drops to zero when there is no sunlight. On the other hand, OCS flux (F_{OCS}) is driven by g_s and does not require light for the hydrolysis reaction to occur (*Seibt et al.*,

2010; *Berkelhammer et al.*, 2014). This difference is indicated in Figure 3 below where OCS tracks transpiration even in the absence of light due to incomplete stomatal closure.

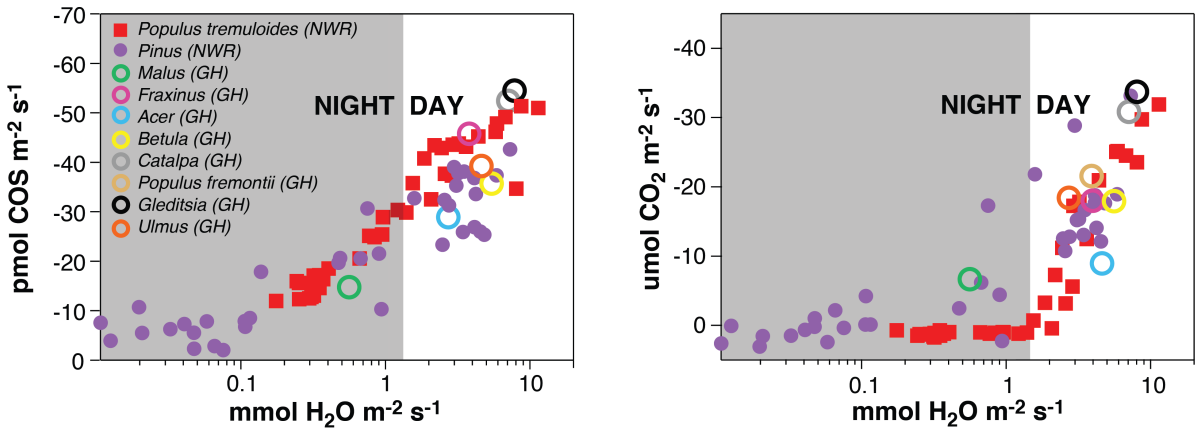

Figure 3. Comparison of OCS flux and CO_2 flux vs. transpiration of different plant species. In the left panel, plants consume OCS and lose water (transpiration) at rates along a linear slope that crosses from day into night, indicating that plant stomata are only partially closed. The slope between transpiration and OCS flux remains stable for these 10 plant species. In the right panel, CO_2 flux becomes a source to the atmosphere (respiration) in the absence of sunlight, but transpiration continues. Thus, OCS flux is controlled by stomatal conductance rather than photosynthesis. Adapted from Berkelhammer et al. (2014).

Therefore, the effects of increased CO_2 projected under climate change may increase WUE as plants increase the amount of biomass assimilated through photosynthesis at a smaller water cost. The stomatal response to rising CO_2 is referred to as the "fertilization effect" and it has been observed over the last few decades (*Keenan et al.*, 2013, 2014). Whereas these effects will make plants more efficient and drought-resistant, plants will not be immune to the effects of extreme and prolonged droughts, when even increased SWC stores are depleted (*Morgan et al.*, 2011). Questions remain, however, as to how ecosystem respiration (R_{eco}) is responding to decreased g_s. Studies demonstrate changes in both directions: net increases in carbon storage

(*Keenan et al.*, 2014) and increases of R_{eco} to the atmosphere (*Piao et al.*, 2008; *Barichivich et al.*, 2013). Disparities in the literature such as these highlight the need for better constraints on GPP and plant water use.

1.3.3 Conditions for a Carbonyl Sulfide Gross Primary Productivity Proxy

The utility of OCS as a tracer for GPP depends on three conditions at the ecosystem-scale: (1), that OCS diffuses with CO_2 along the same pathway (*Stimler et al.*, 2010); (2), that there is no corresponding respiration-like mechanism of OCS as there is with CO_2 (*Stimler et al.*, 2010); and (3), that OCS does not interact with CO_2 during diffusion (*Stimler et al.*, 2010). These conditions need to be adjusted to include a fourth condition when applied at the ecosystem-scale. Because F_{OCS} also includes flux from non-vegetative sources, such as soils and senescent vegetation (*Kesselmeier et al.*, 1999; *Kuhn*, 1999; *Simmons et al.*, 1999; *Van Diest and Kesselmeier*, 2008; *Liu et al.*, 2010; *Maseyk et al.*, 2012; *Berkelhammer et al.*, 2014; *Whelan et al.*, 2016), the final condition thus states that (4) non-plant OCS fluxes must be negligible relative to plant fluxes (*Montzka et al.*, 2007; *Campbell et al.*, 2008; *Blonquist et al.*, 2011).

The first three conditions have been rigorously tested and met in the leaf-level studies of Stimler et al. (2010), but results from recent field studies have generated debate regarding the fourth condition of non-plant OCS fluxes (*Maseyk et al.*, 2012, 2014, *Whelan et al.*, 2013, 2016; *Berkelhammer et al.*, 2014; *Billesbach et al.*, 2014). Soil microbial communities also produce carbonic anhydrase such that soil waters are capable of consuming OCS via hydrolysis (*Seibt et al.*, 2006; *Wingate et al.*, 2008; *Berry et al.*, 2013). The resulting soil flux (F_{soil}) is dominated by soil biological and physical properties. Soil flux is controlled by the deposition velocity of OCS through water-filled pore spaces, which is in turn a function of bulk density (*Van*

Diest and Kesselmeier, 2008; *Berry et al.*, 2013). Research has characterized F_{soil} as a negligible sink relative to leaf OCS flux (F_{leaf}; *Van Diest and Kesselmeier*, 2008; *Liu et al.*, 2010; *Berkelhammer et al.*, 2014; *Billesbach et al.*, 2014; *Whelan et al.*, 2016), thus minimally altering contributions to overall ecosystem OCS flux (F_{eco}). However, positive soil fluxes were also observed, typically under drier and hotter conditions (*Berkelhammer et al.*, 2014; *Billesbach et al.*, 2014; *Whelan et al.*, 2016). The results of the soil incubation studies of Whelan et al. (2016) suggest that these OCS soil sources are unique to agricultural ecosystems, but not all incubated agricultural soils demonstrate an OCS source. In short, any study seeking to apply F_{OCS} as a proxy for GPP should include an estimate of the soil contribution to total ecosystem OCS flux.

1.3.4 Laser Absorption Spectrometry Advancements

Advancements in laser spectrometry have been integral to the application of F_{OCS} as a GPP proxy. Early field observations of ambient atmospheric OCS mixing ratios were sampled in flasks and transported to the lab for analysis by gas chromatography-mass spectrometry (*Montzka et al.*, 2007; *Campbell et al.*, 2008; *Blonquist et al.*, 2011). This discrete measurement approach lacked the frequency to reveal the controls on F_{OCS} at different timescales (*Commane et al.*, 2015). High-frequency OCS measurements are now possible with mid-infrared dual quantum cascade laser spectrometer used by Stimler et al. (2009) to sample leaf-scale OCS, CO_2, and H_2O dynamics at 1 Hz; results were consistent with flask-sampled gas chromatography-mass spectrometry methods. The first *in situ* ecosystem-scale field measurements were made by Asaf et al. (2013) using the QCL spectrometer. The novel F_{OCS} measurements resulted in a direct measurement of GPP (denoted as GPP_{OCS}) that agreed with the traditional respiration-based method of estimating GPP (GPP_{Re}) within ±15% (*Asaf et al.*,

2013). Whereas Asaf et al. (2013) drew from the well-established eddy covariance method to measure F_{OCS}, Meredith et al. (2014) showed how vertical concentration gradients could be used to determine the flux using the trace gas similarity theory and the flux-gradient method.

With the high-frequency laser spectrometer field measurement campaign of Asaf et al. (2013) and the theoretical possibility of applying the flux-gradient method developed in Meredith et al. (2014), the groundwork was established for future studies to evaluate OCS flux across different ecosystems.

1.4 Purpose

This study is the first season-long continuous application of the OCS flux-gradient method. High-frequency *in situ* OCS measurements were used to determine continuous OCS fluxes and then to constrain gross primary production and nighttime transpiration in a tallgrass prairie ecosystem in Illinois. To our knowledge, there have been no OCS flux-gradient studies conducted in a tallgrass prairie, where multiple species coexist and the plant distribution changes between years and through the growing season. Upon validation of the applicability of the OCS flux-gradient method in a tallgrass prairie, ecosystem responses to projected climate scenarios are inferred. More broadly, this project aims to contribute to the growing body of scientific literature establishing OCS as a tracer for GPP, so that carbon budget estimates at the ecosystem, regional, and global level may be assessed and improved.

1.5 Hypotheses

1. Continuous measurements of OCS gradients can be used to derive the OCS flux in a tallgrass prairie ecosystem.
2. OCS fluxes follow a seasonal cycle associated with changes in local gross primary productivity.
3. Gross primary productivity derived from OCS flux (GPP_{OCS}) is comparable to GPP derived from respiration (GPP_{Re}).
4. OCS flux can be used as a proxy for nighttime stomatal conductance and transpiration.
5. Nighttime stomatal conductance and transpiration vary with changes in atmospheric humidity and water stress.

2 METHODS

2.1 Field Sites

Two proof-of-concept laser spectroscopy campaigns were conducted in the summer and early fall of 2015. The first was conducted from July 20–27, 2015 at the Bondville Fluxnet eddy covariance site (40.006225°, -88.290400°) in Bondville, Illinois, USA (Figure 4; site map with all locations referenced shown) where an agricultural corn ecosystem at growing season peak was sampled. The soil at the Bondville site is primarily silty clay loam and silt loam (https://websoilsurvey.nrcs.usda.gov). The second campaign was conducted from September 9–25, 2015 at the Energy Farm AmeriFlux eddy covariance site (40.062789°, -88.196157°) in Urbana, Illinois, USA where a senescent agricultural corn ecosystem was sampled. The soil at Energy Farm is primarily silt loam (https://websoilsurvey.nrcs.usda.gov).

From May 17–October 23, 2016 (n days = 159), a laser spectroscopy campaign was conducted at the Fermi tallgrass prairie AmeriFlux eddy covariance site (41.840617°, -88.240920°) in Batavia, Illinois, USA. Sampling spanned the majority of the 2016 growing season, from initial late-spring GPP increase until productivity ceased and vegetation senesced in September–October. Prior to being restored to a tallgrass prairie in 1989, the silt loam soil (https://websoilsurvey.nrcs.usda.gov) had been farmed for over 100 years. The site was chosen for a number of scientific and logistical reasons. The site had an existing eddy covariance tower established in 2004, as well as hardwired electrical supply that would minimize data loss due to power shortages and enabled temperature control of the instrument enclosure. The proximity of the site to the PIs also factored into its selection.

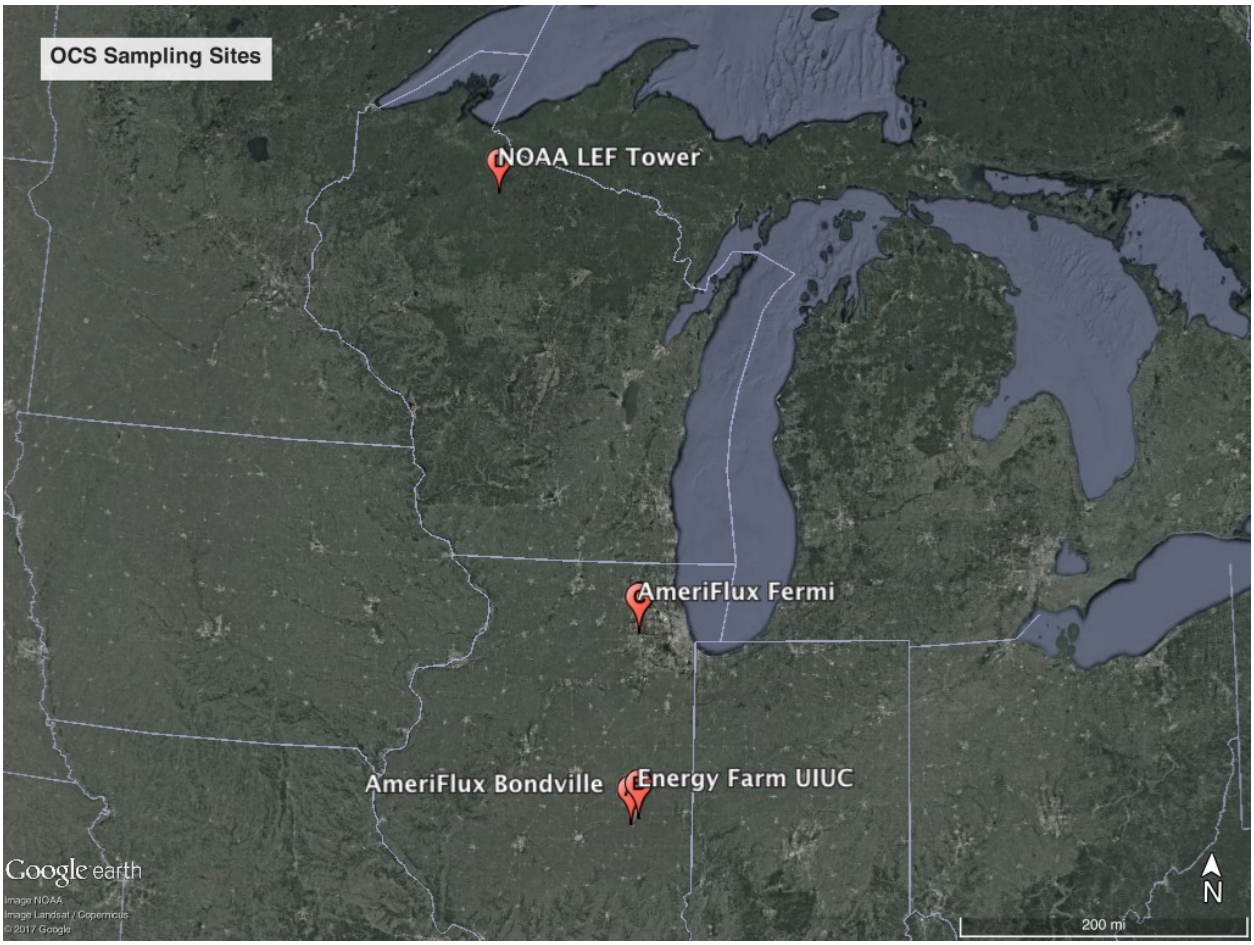

Figure 4. OCS sampling sites referenced. AmeriFlux Bondville, IL, sampled July 20–27, 2015. Energy Farm at UIUC, Urbana, IL, sampled September 9–25, 2015. Fermi AmeriFlux tallgrass prairie AmeriFlux site, Batavia, IL, sampled May 17–October 23, 2016. The NOAA Earth System Laboratory, Global Monitoring Division has measured OCS at WLEF tower in Park Fals, WI since October 7, 2006 (https://www.esrl.noaa.gov/gmd/dv/site/LEF.html).

The Fermi tallgrass prairie receives an annual average of 975 mm of precipitation and an additional 808 mm of snow per year. The annual average high temperature is 14.9°C, with an average low of 2.64°C. The historic average temperatures for the time of year of the campaign (May–October) are 24.5°C high, 10.7°C low, with 590 mm of precipitation, and 5 mm of snow (Figure 5; historic averages for Aurora, IL; intellicast.com).

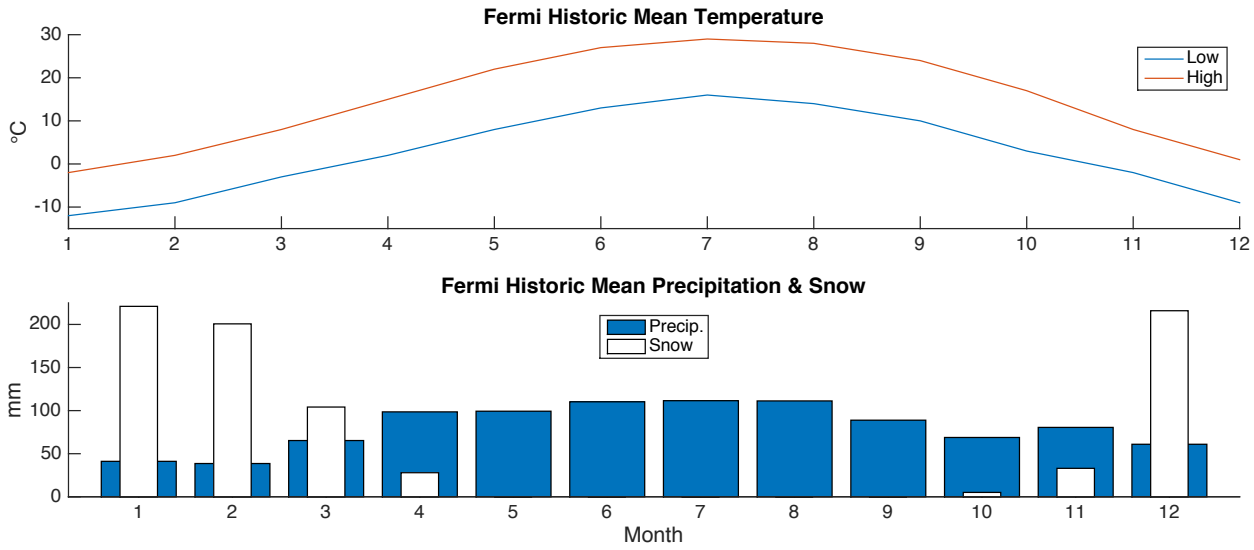

Figure 5. Historic mean temperature and precipitation at the Fermi tallgrass prairie. Data for nearby Aurora, IL. (http://www.intellicast.com/Local/History.aspx?unit=C&location=USIL0062)

Plant species identification was conducted with the aid of field biologist, Christopher Whelan (Department of Biological Sciences, UIC). A photo log cataloging identified species was maintained to track species shifts, and the four most populous species are pictured below (Figure 6). The most predominant species throughout the season was Goldenrod (*Solidago*). Milkweed (*Asclepias syriaca*), Reed Canary Grass (*Phalaris arundinacea*), and Rosinweed (*Silphium integrifolium*) were also prominent at different times.

Figure 6. Most predominant plant species on site through the campaign. From left to right, Goldenrod (Solidago), Reed Canary Grass (Phalaris arundinacea), Milkweed (Asclepias syriaca), Rosinweed (Silphium integrifolium).

2.2 Experimental Setup

The Los Gatos Research laser absorption spectrometer (hereafter denoted as the LGR) that measures OCS, CO_2, CO, and H_2O was installed within an existing enclosure that protected it from inclement weather. An air conditioner was installed outside of the enclosure to maintain stable laser temperatures (mean = 41.9°C; σ^2 = 0.0170°C), minimizing instrument drift (See section 2.4). Operational pressure of the LGR was ~59.0 Torr, with a cavity flow-through rate of 0.7 L min^{-1}.

To measure the gradients of the different gas species, four filtered inlets (1-2 µm filters, Savillex Corporation, polytetrafluoroethylene, chemically and biologically inert) were installed on the eddy covariance tower (Figure 7). From top to bottom, the inlets and their respective heights were

1. Top of tower: 4.4 m
2. Middle high: 2.2 m
3. Middle low: 1.2 m
4. Soil: 0.32 m

Figure 7. Sampling inlets at the Fermi tallgrass prairie. Eddy covariance tower (left) with four filtered inlets (three pictured, the fourth is obscured by the grasses) photographed on June 19, 2016. Detail of a hanging inlet (right).

Teflon tubing was run from the inlets down the tower and horizontally to the enclosure. The 8.7 m distance from the bottom of the tower to the enclosure was spanned by a PVC pipe that protected the Teflon tubing from degradation by exposure to inclement weather and damage during site visits. Each of the four Teflon lines was connected to a port on the back of the multiport inlet unit, which switched the port being sampled by the LGR in a programmed sequence. The non-sequential port-switching order and duration was programmed in software onboard the LGR. Ports were sampled for seven minutes (420 one-second measurements) at a time, resulting in a complete vertical gradient approximately every 30 minutes.

2.3 Site Visit Standard Operating Procedures

Site visits were conducted weekly. On every visit, data were retrieved and canopy height was measured using the same goldenrod plant as a representative of the majority of the canopy. Photos were taken for the species photo log to track species and phenology shifts.

Filters on the inlets were replaced on two- to three-week intervals to minimize airborne particulate matter from entering the LGR or restricting air flow through the Teflon lines. Soil samples from the top 10–15 cm were taken on the same two- to three-week interval, and were frozen in the lab at ~-10°C.

2.4 Calibration

Before deployment, the LGR was calibrated to a National Oceanic & Atmospheric Administration – Global Monitoring Division (NOAA GMD) reference gas standard (OCS = 314.1 ppt). Per the procedure noted in Berkelhammer et al. (2016b), secondary atmospheric standards stored in 3785 cm^3 stainless steel tanks lined with SilcoNert (*Whelan et al.*, 2013) were filled to 1800 psi at a local SCUBA shop. These tanks were sampled in the field approximately every ten days to calculate instrument drift. Upon conclusion of the campaign, instrumental drift was calculated by sampling the NOAA GMD standard once more, and fitting a robust linear regression (slope = -0.188) through all OCS calibration values (Figure 8). This slope was used to correct raw observations of OCS concentration over the time series. Analytical error was calculated as the standard deviation of the difference of consecutive midday OCS measurements made above the canopy, and found to be ± 9.5 ppt.

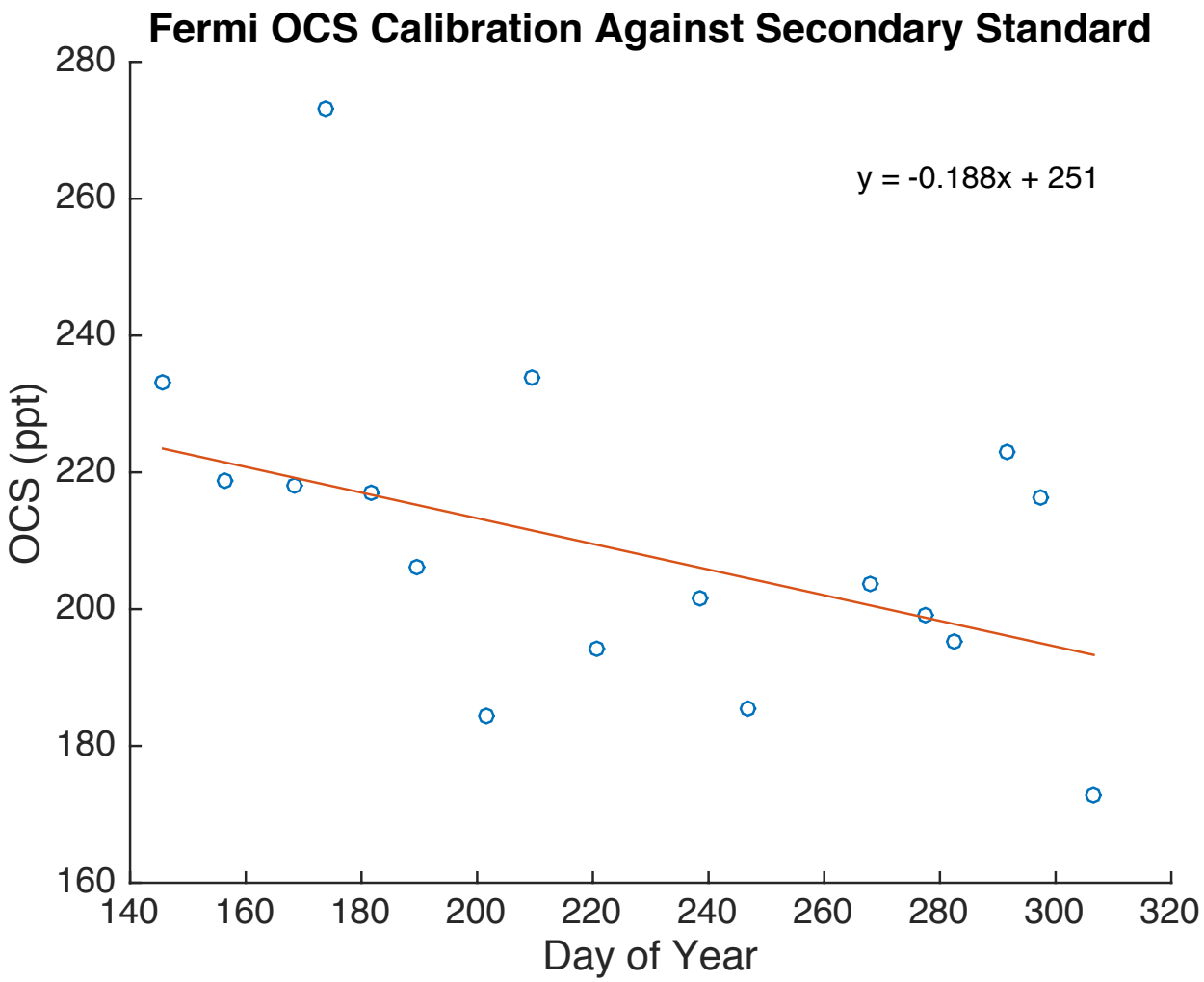

Figure 8. Calibrations against secondary standard in the field. Secondary standard was sampled against the primary NOAA GMD standard upon the completion of the campaign. The resulting slope (-0.188) fit through these points was used to correct for the long term drift of the LGR.

2.5 Data Procedure

Data processing was done in two stages: during-campaign and after-campaign. To calculate F_{OCS}, net ecosystem exchange (NEE, or CO_2 flux) from the eddy covariance data is required at a minimum. Other variables from the eddy covariance data were used to characterize energy exchange and meteorological conditions at the site: wind friction velocity (u*), fraction of absorbed photosynthetically active radiation (FPAR), net radiation (R_n), wind

speed (WS), air temperature (T_a), soil temperature (T_s), and soil water content (SWC). Data processing proceeded in this order:

Concentration measurement —> gradient calculation—>
quantitative flux —> estimate GPP_{OCS} from flux (2)

Concentrations and gradients were processed and calculated during the campaign; fluxes and GPP were calculated after sampling concluded.

Gradients and fluxes are reported throughout this manuscript with negative values representing sinks and positive values representing sources to the atmosphere.

2.5.1 During Campaign

After each site visit, data were imported and processed in Mathworks Matlab software (R2015a release). Processing began by removing data during periods when conditions would invalidate results. Such conditions included prolonged site visits, and periods when the LGR was not at optimal temperature (i.e., < 40°C). Gas concentration measurements (e.g., CO, OCS, H_2O and CO_2) were separated by height. Data per species and per port were then averaged over five minutes (300 counts) after excluding the first two minutes of measurements at each height. Vertical gradients between different inlets (i.e., $\Delta OCS / \Delta Z$) were then calculated and analyzed throughout the campaign. The gradient is related to the flux, but the flux cannot be quantitatively inferred from the gradient without knowledge of the eddy diffusivity. Performing this processing throughout the campaign not only allowed us to monitor ecosystem response to shifting phenology, it also ensured that the LGR was operating under safe conditions that would yield reliable data.

2.5.2 After Campaign

Eddy covariance and meteorological data, with periods gap-filled when boundary layer conditions lacked the turbulence required for measurement, were synchronized with the high-frequency laser data. The NEE from the eddy covariance system and CO_2 gradients from the LGR were used to calculate the ecosystem OCS flux (F_{eco}) according to Equation 3 (*Meredith et al.*, 2014):

$$F_{eco} = NEE * \Delta OCS/\Delta CO_2 \quad (3)$$

To account for soil contribution to F_{eco}, F_{soil} was estimated (Equations 4–10) using the method detailed in Whelan et al. (2016):

$$F_{soil,abiotic} = \exp^{\alpha} * \exp^{\beta Ts} \quad (4)$$

$$F_{opt} = -0.00986T_s^2 + 0.197T_s + -9.32 \quad (5)$$

$$\theta_{opt} = 0.287T_s + 14.5 \quad (6)$$

$$F_{\theta g} = (-0.0119T_s^2) + 0.110T_s + -1.18 \quad (7)$$

$$a = \ln(F_{opt} / F_{\theta g}) (\ln(\theta_{opt} / \theta_g) + (\theta_g/\theta_{opt}) - 1)^{-1} \quad (8)$$

$$F_{soil,biotic} = F_{opt} (\theta_i/\theta_{opt})^a \exp(-a((\theta_i/\theta_{opt})-1)) \quad (9)$$

$$F_{soil} = F_{soil,biotic} + F_{soil,abiotic} \quad (10)$$

where $F_{soil,biotic}$ and $F_{soil,abiotic}$ are the portion of biotic and abiotic processes contributing to soil OCS flux, respectively, α and β are fitting parameters (-6.12, and 0.096, respectively), T_s is observed soil temperature (°C), F_{opt} is the maximum biotic uptake, θ_{opt} is optimum SWC, $F_{\theta g}$ is the flux at constant SWC, a is the curve shape constant, θ_g (0.35) was held constant to generalize for all temperature and moisture combinations, and θ_i is observed SWC. Abiotic and biotic soil flux components were estimated with calculations 4–9, and summed to F_{soil} (Equation

10). It should be noted that observations of SWC were not available for the Bondville and Energy Farm campaigns. To estimate SWC observations at these sites, data was used from the Cosmic-ray Soil Moisture Observing System (COSMOS) project (http://cosmos.hwr.arizona.edu), which has probes in place at the Bondville AmeriFlux site. Finally, F_{leaf} (Equation 11) is the difference of ecosystem and soil OCS fluxes:

$$F_{leaf} = F_{eco} - F_{soil} \quad (11)$$

A final set of filters were applied to the data to nullify erroneous scenarios when positive fluxes resulted from negative gradients, or vice versa. To reduce the effect of outlying fluxes, all data were removed outside of the 2nd and 98th percentile. As previously noted, eddy covariance requires turbulence in the boundary layer. Data from the Fermi tallgrass prairie was only used when the friction velocity (u*) exceeded a threshold of 0.29 m s^{-1}, which was determined following Papale et al. (2006) and Reichstein et al. (2005). A weaker threshold was used for the Bondville and EF sites, because such a rigorous threshold forced all the data to be rejected. For these sites, a u* threshold was chosen by plotting nighttime OCS fluxes against u*, and visually determining that the fluxes did not become unstable at low u* (Figure 9). Accordingly, a u* threshold of 0.15 m s^{-1} was chosen to filter as few nighttime values as possible, whereas still being within an acceptable u* threshold range of 0.15–0.25 m s^{-1} (*Papale et al.*, 2006).

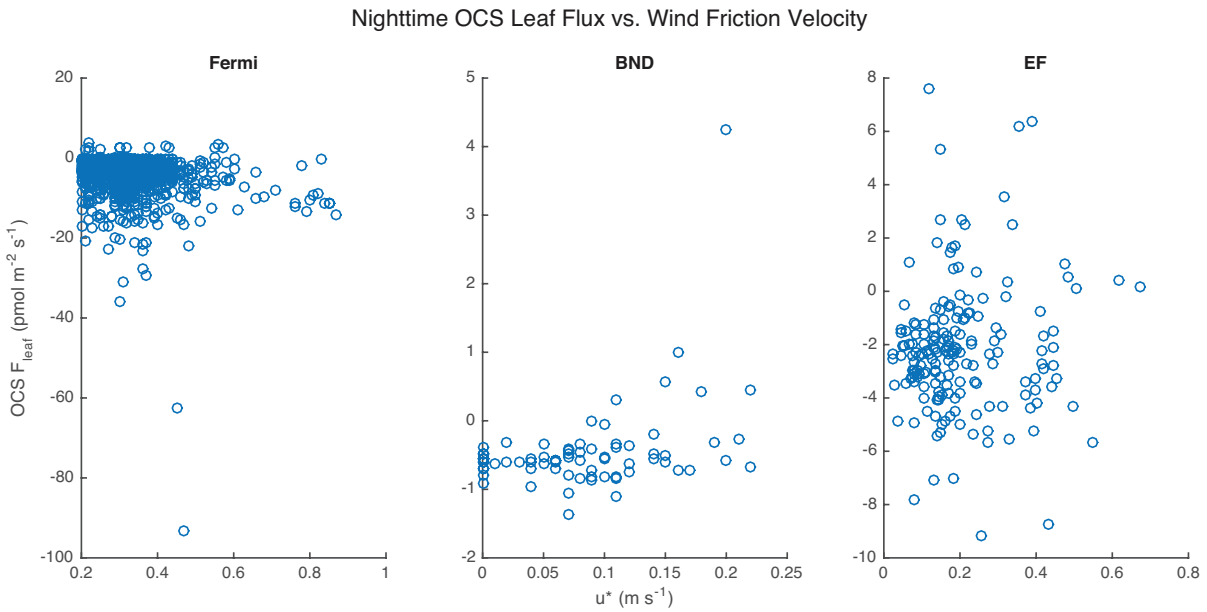

Figure 9. Nighttime F_{leaf} vs. u at all sites. The Fermi u* threshold of 0.29 m s^{-1} was an output of the Reichstein method. Bondville (BND) and Energy Farm (EF) u* thresholds were selected visually as 0.15 m s^{-1} due to stable F_{leaf} across u* values.*

Lastly, GPP_{OCS} was calculated using the relationship (Equation 5) from Asaf et al. (2013):

$$GPP_{OCS} = (F_{leaf} / LRU) * ([CO_2]/[OCS]) \quad (12)$$

Leaf relative uptake (LRU) is the normalized unitless ratio of OCS and CO_2 assimilation rates (i.e., OCS ppt / CO_2 ppm, with units removed), here estimated at 1.6. It must be acknowledged that whereas LRU is variable, separate investigations have justified the use of a constant LRU of 1.6 under conditions when sufficient sunlight is present (*Stimler et al.*, 2010, 2012; *Asaf et al.*, 2013; *Berkelhammer et al.*, 2014; *Billesbach et al.*, 2014; *Hilton et al.*, 2017). The resulting direct GPP_{OCS} will be compared to the estimated GPP_{Re}, which relies on temperature-based extrapolations to estimate daytime respiration as detailed in Reichstein et al. (2005) and Commane et al. (2015).

Applying principles of Fick's Law allows for the calculation of an E_n proxy. The H_2O gradient between the saturated leaf stomata and the atmosphere is represented by VPD and F_{leaf} functions as g_s, which can be thought of as a specialized diffusion coefficient. Multiplying the two terms results in units of pmol hPa m^{-2} s^{-1} (Equation 13), which have been normalized using the lowest and highest values across observations at the three sites (Equation 14). The resulting values are on a unitless index (0–1) representing water lost by plants in the absence of photosynthesis. Note that when relative humidity is 100% (i.e., VPD = 0), E_n is 0.

$$E_{n,i} = -(F_{leaf} * VPD) \quad (13)$$

$$E_n = (E_{n,i} - E_{n,min}) / (E_{n,max} - E_{n,min}) \quad (14)$$

3 RESULTS

The 2016 campaign at the Fermi tallgrass prairie spanned 159 days, from day of year (DOY) 138–297 (May 17–October 23). During this time, only two minor interruptions of the power supply to the LGR—each less than an hour—impeded sampling. Observations in time made by the laser spectrometer totaled 14,527,069. At each of those observations, 36 parameters were recorded, for a grand total of 522,974,484 individual data points. Nearly 60 million of these points were concentrations of the H_2O, CO, CO_2, and OCS.

The experimental setup was reinstalled in the early spring of 2017, and a new campaign began on DOY 99 (April 9) and is expected to run until mid-October of this year. This data will not be presented in the thesis because the experiment is ongoing.

3.1 Concentrations

To validate data quality, which is necessary for testing any of the hypotheses (e.g., *continuous measurements of OCS gradients will be used to derive OCS flux in a tallgrass prairie ecosystem*), atmospheric mixing ratios of OCS at the Fermi tallgrass prairie were compared against the nearest NOAA Global Monitoring Division site making weekly OCS measurements during this same time period (Figure 10). The WLEF tower (447 m, sampling above the boundary layer at 396 m) in Park Falls, Wisconsin (~500 km to the north of the Fermi site), is located in a northern hardwood and aspen forest. The Fermi data and WLEF data showed great parity, even to the point where a mid-season pause (DOY ≈ 200–235, mid-July–mid-August) in the Northern Hemisphere drawdown of OCS was shown in both data sets. This alignment, not only of concentrations, but of sensitivity to seasonal OCS dynamics as well, suggests the

accuracy of the Fermi tallgrass prairie measurements, surprising regional homogeneity, and the possibility of OCS in constraining regional-scale carbon budget processes.

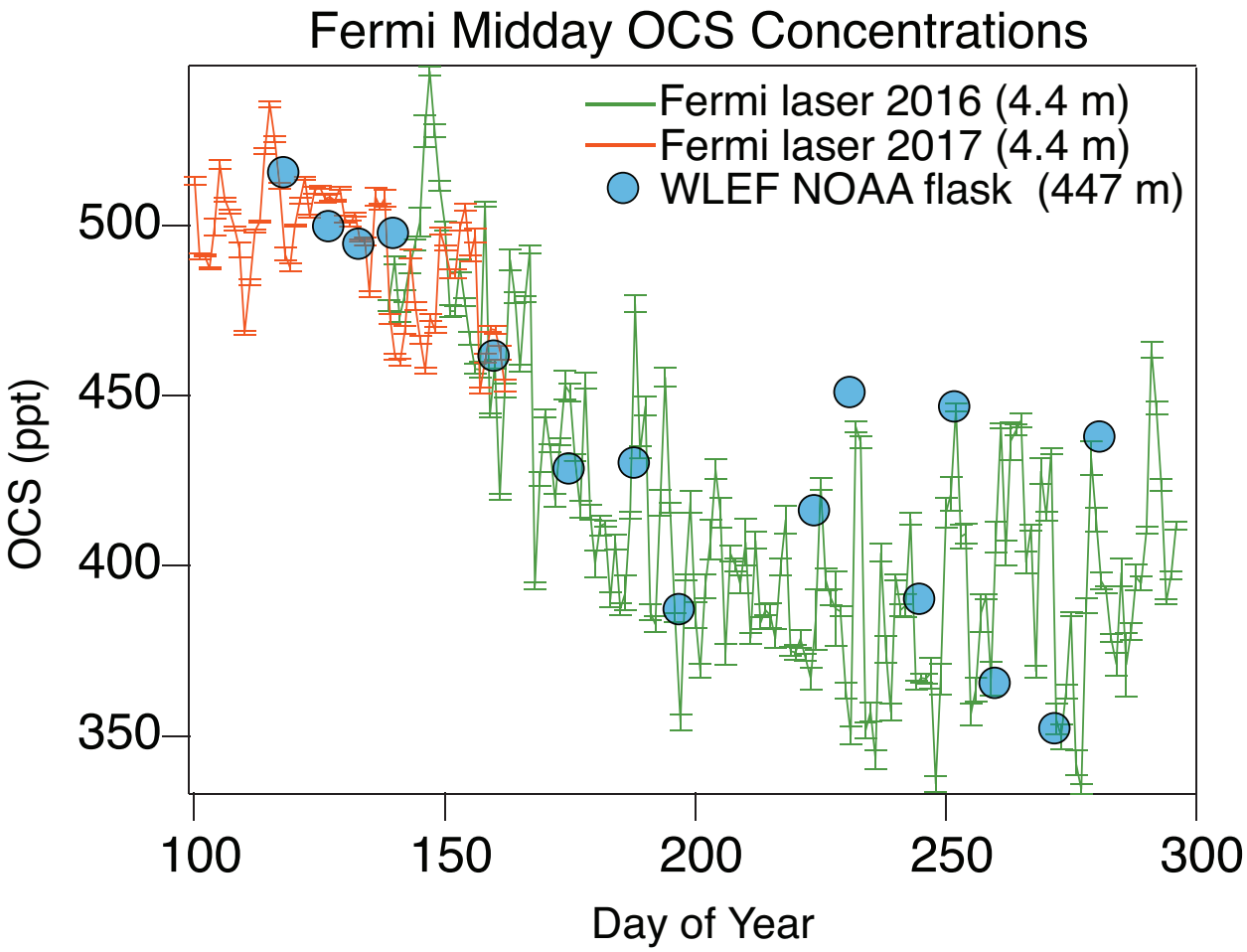

Figure 10. OCS measurements made at Fermi and WLEF. Comparison of midday averaged 4.4 m OCS concentrations alongside the tall-tower (447 m, sampling at 396 m) NOAA flask data from the Park Falls, Wisconsin WLEF site (~500 km north of Fermi). Both data sets show parity in the seasonal cycle of OCS, including a mid-summer pause (DOY ≈ 200–235 ≈ mid-July–mid-August) in the northern hemisphere drawdown of OCS. The data also show higher frequency variability associated with diurnal processes.

Our data comparison with the WLEF site shows the accuracy of these long-term measurements on a seasonal scale. Higher frequency variation occurs as well, with OCS, CO_2,

CO, and H_20 following distinct diel cycles. In the absence of photosynthesis, plants and soils continue to consume OCS and vegetation becomes a CO_2 source as respiration dominates. This cycle results in simultaneous OCS minima and CO_2 maxima at night (Figure 11A and 11B). Concentrations of CO spike usually in sync with localized effects of morning commutes (i.e., 7–10am) before soil drawdown reduces CO (Figure 11C). The lack of OCS and CO_2 during the morning when CO spikes, shows that the former two gases are only minimally affected by local pollution. Midday CO spikes are likely caused by the operation of agricultural or landscaping activity nearby on Fermilab grounds. Concentrations of H_2O shift with the summer air temperature, increasing as warmer air holds more water until mid-summer, and decreasing in the second half of the season (Figure 11D).

The Northern Hemisphere OCS cycle follows the annual cycle of plant productivity, which leads to decreasing concentration until DOY ≈ 265–275 (Figure 12A; mid- to late-September) when senescence diminishes productivity, and atmospheric OCS concentrations increase again. The seasonal CO_2 cycle reaches its minimum earlier on DOY (201) at 390 ppm (Figure 12B). Close negative coupling of OCS and CO_2 concentrations at the prairie site were observed (Figure 13; $R^2 = 0.654$, $p < 0.001$).

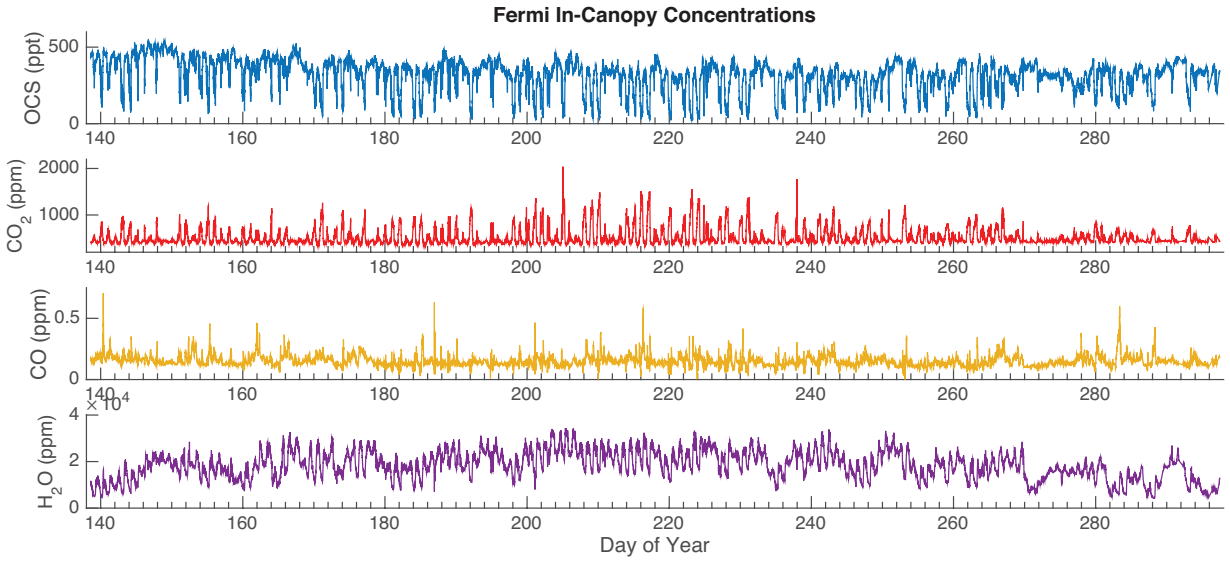

Figure 11. Concentrations of OCS, CO_2, CO, and H_2O at 0.32 m throughout the campaign. Nighttime valleys (OCS) and peaks (CO_2) frequently coincide. The seasonal decrease of OCS in the northern hemisphere is also shown from May until mid- to late-September when it will continue to increase until the following spring. CO spikes are typically the localized effects of morning commute emissions, with other midday spikes resulting from agricultural or landscaping machinery. Concentrations of H_2O increase with air temperature as the warmer air holds more moisture until midsummer when air temperatures decrease and the trend reverses.

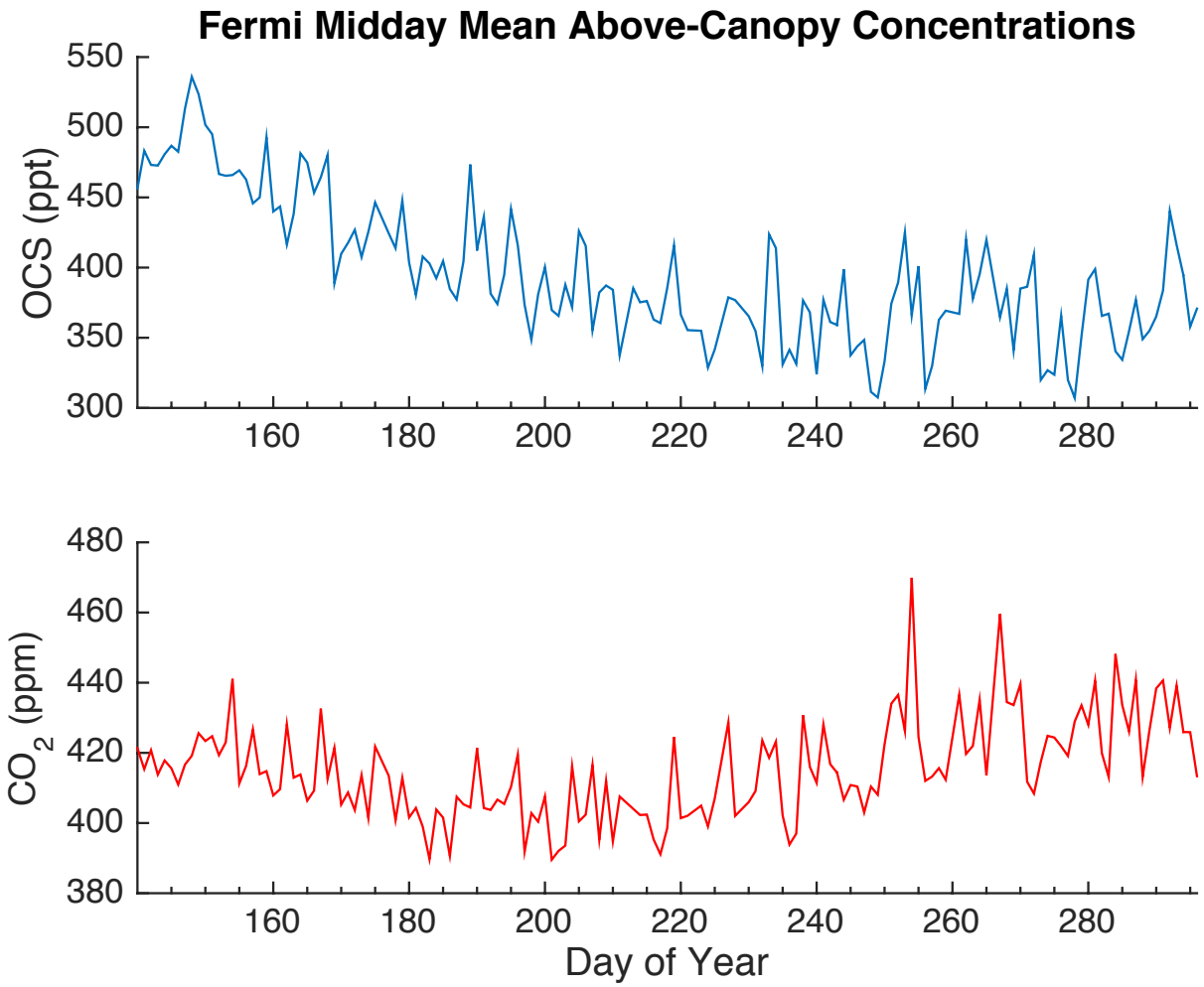

Figure 12. Fermi midday mean above-canopy OCS and CO_2 concentrations. The Northern hemisphere seasonal cycles of OCS and CO_2 are both dominated by plant uptake, with the observed CO_2 minimum of 390 ppm occurring on DOY 201 (July 19). The OCS minimum is reached later in the season (307.4 ppt; DOY 249 = September 5), with concentrations that increase until the following spring.

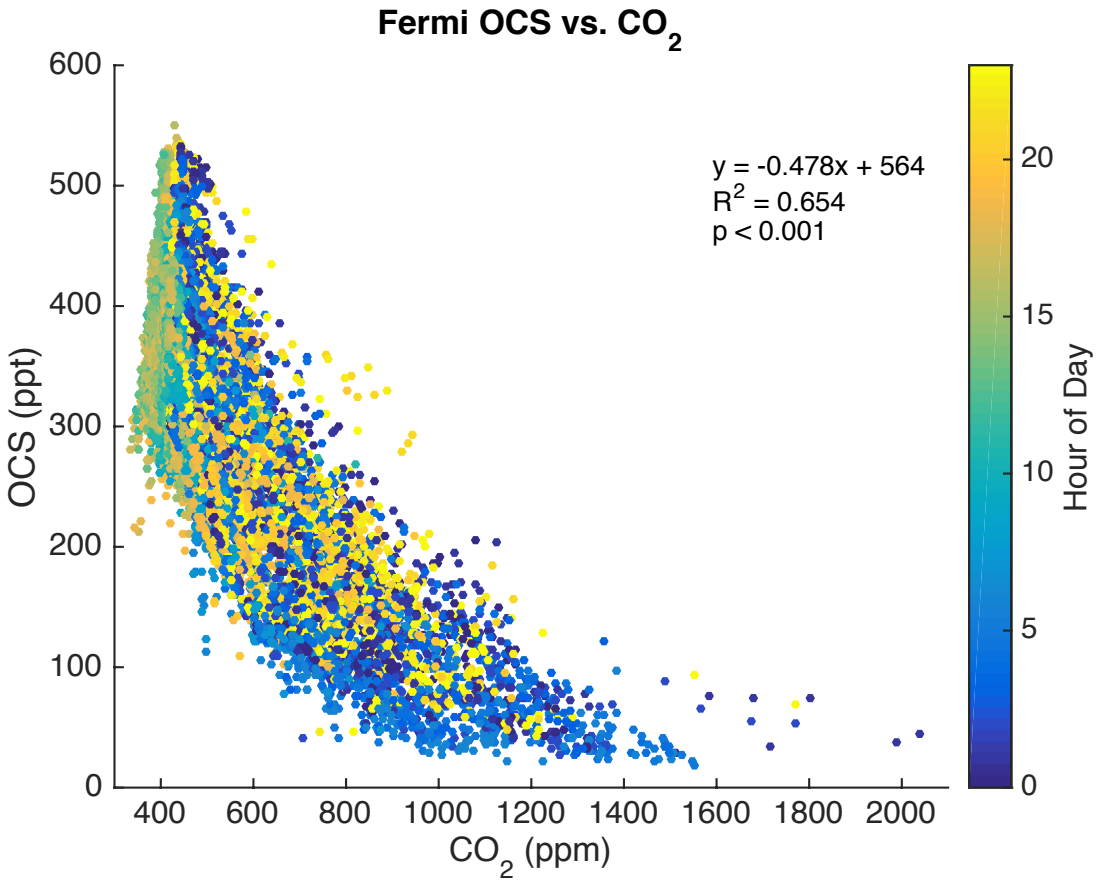

Figure 13. Fermi in-canopy OCS and CO_2 concentrations. Robust linear regression demonstrates significant correlation between OCS and CO_2 (R^2 = 0.654, $p < 0.001$). The sharp delineation primarily comprised of midday (10:00–15:00) points from upper-left to mid-left demonstrates the seasonal drawdown of both OCS and CO_2.

Measurements from the productive agricultural corn site (Bondville, hereafter denoted as BND) and the senescent agricultural corn site (Energy Farm, hereafter denoted as EF) show similar diel cycle concentration patterns to Fermi over their short-term sampling campaigns (Figure 14; 7 and 16 days, respectively). Spikes of OCS concentration well above atmospheric mixing ratios were observed in the in-canopy EF data, where late-day OCS increased to a maximum 780 ± 15 ppt. Levels of daytime OCS above the canopy during the peak growing season at BND (mean = 392 ± 13 ppt) and later in the season when corn was in senescence at EF (mean = 420 ± 15 ppt) were in keeping with the Northern Hemisphere OCS cycle. Above-canopy

OCS concentrations at Fermi during the same times as BND and EF were 386 and 378 ± 9.5 ppt respectively.

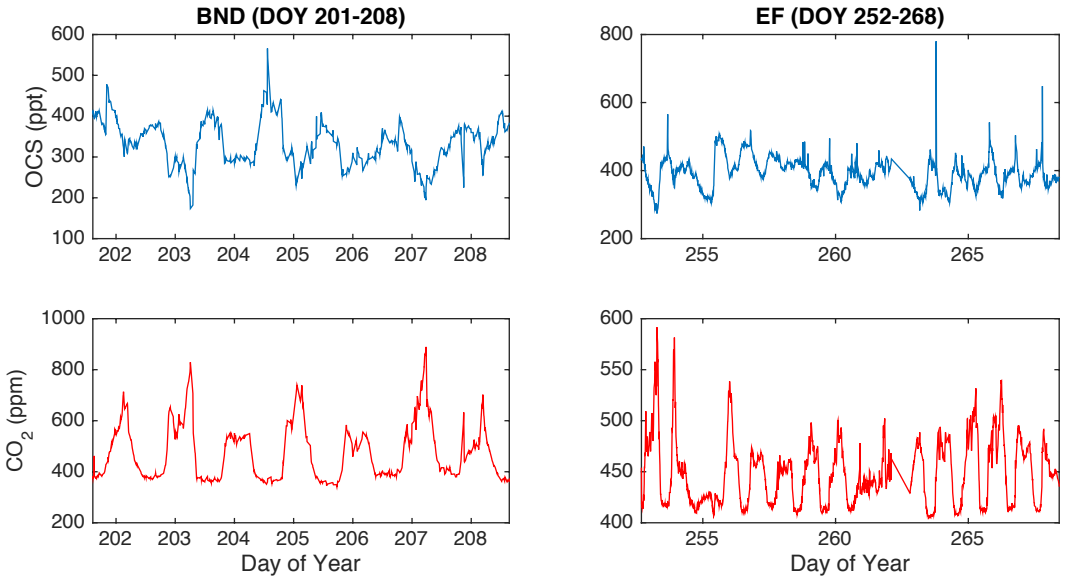

Figure 14. In-canopy OCS concentrations at BND and EF. Late-day spikes are seen in the senescent crops at EF, possibly indicating an OCS source.

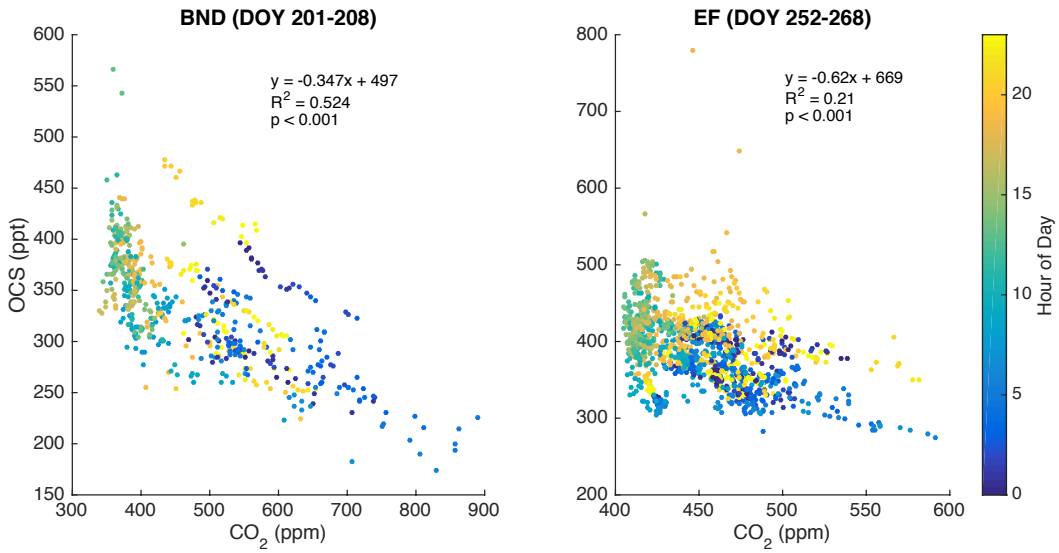

Figure 15. Mean in-canopy OCS vs. CO_2 concentrations at BND and EF. Robust linear regression shows higher correlation between the two gases in peak-season (BND: $R^2 = 0.524$, $p < 0.001$) as opposed to senescent corn (EF: $R^2 = 0.210$, $p < 0.001$).

Concentrations of OCS and CO_2 at the two agricultural sites were less correlated than at Fermi. The peak season corn demonstrated higher correlation between OCS and CO_2 than the senescent corn (Figure 15A, BND: $R^2 = 0.524$, $p < 0.001$; Figure 15B, EF: $R^2 = 0.210$, $p < 0.001$).

3.2 Carbonyl Sulfide Concentration Diel Cycle

OCS diel cycle concentrations over a 24-hour period during the campaign (Figure 16) were in line with expectations. Lowered nighttime concentrations resulted from ecosystems uptake of OCS within a stable boundary layer. The canopy progressively depleted OCS until thermal convection and turbulence resumed at dawn, and OCS was mixed to the surface from the free troposphere. After dawn, OCS concentrations increased until sunlight waned in the late-afternoon. The same process affected the CO_2 diel cycle, but in reverse. At night, the

canopy respired CO_2 into a stable boundary layer, where concentrations rose until turbulent mixing resumed at dawn.

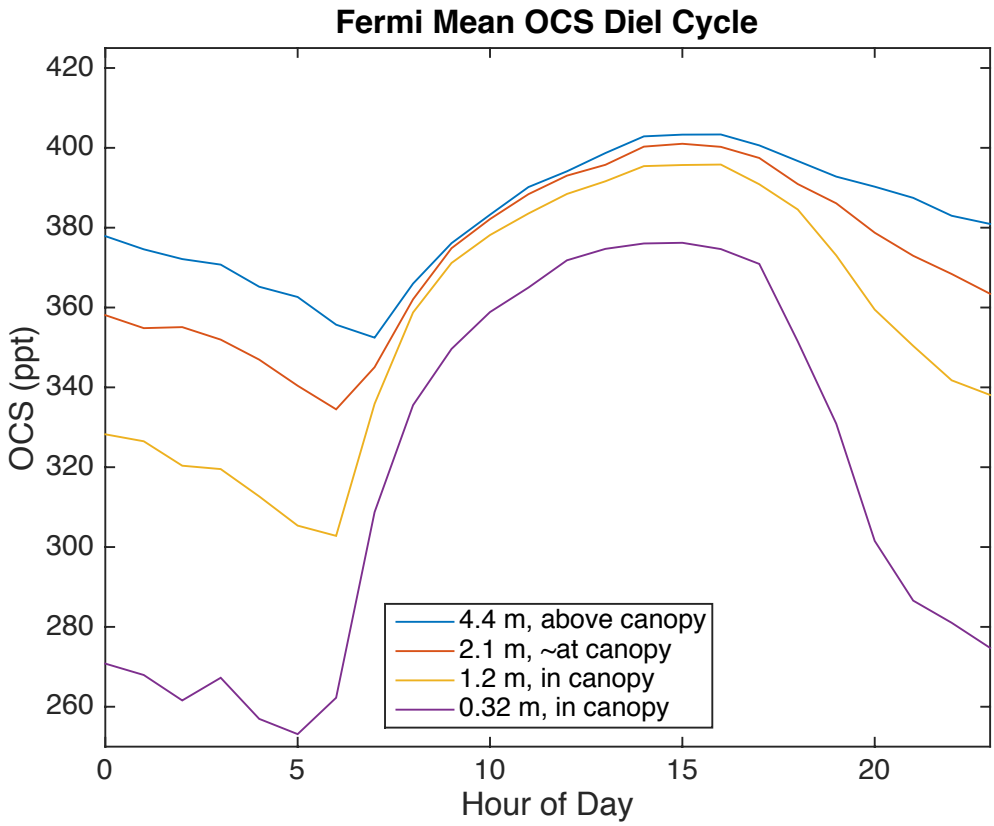

Figure 16. Mean Fermi OCS diel cycle at all four inlets. OCS is demonstrated mixing in from the upper-atmosphere during the day, and then the canopy depletes those OCS concentrations at night.

A distinct feature of the OCS diel cycle is the sharp dip in OCS concentrations in the third inlet (1.2 m) at or around dawn. This dip was present in the other inlets as well, only less pronounced. This diel pattern likely indicates that there was progressive uptake of OCS during the night resulting in canopy air with very low concentrations. These OCS-depleted pockets of

air near the soil may have been mobilized and registered successively upward through each inlet above as these pockets of air were mixed upwards.

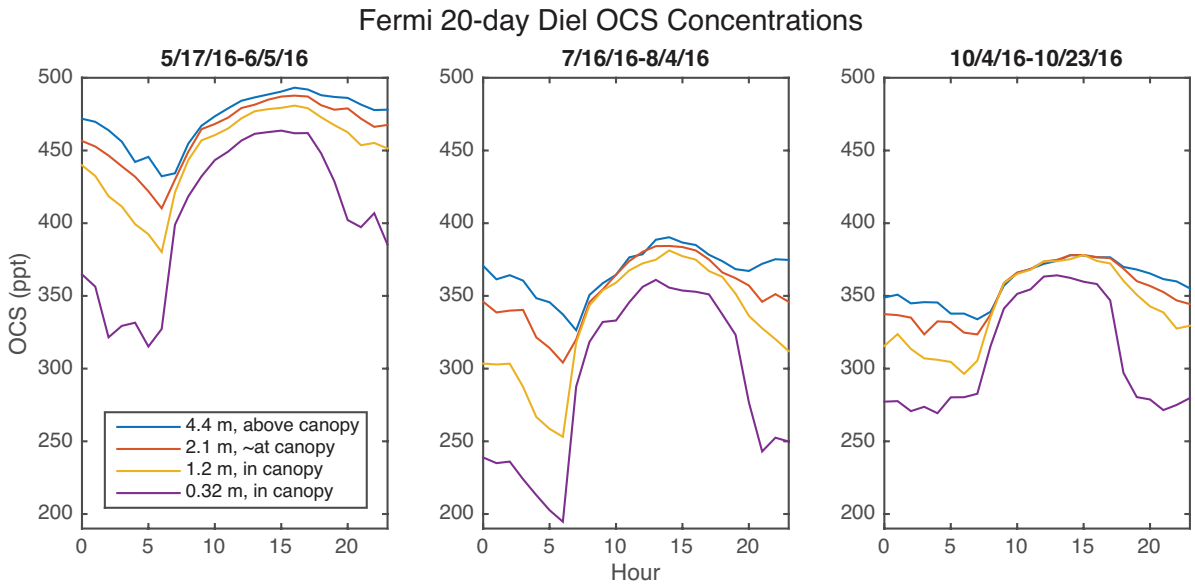

Figure 17. Select 20-day Fermi OCS concentration diel cycles. The (A) beginning, (B) middle, and (C) end of growing season are shown, with progressively less difference in amplitude between the day and night demonstrated.

The sharp, pre-dawn dip in OCS concentrations was also present in 20-day means of OCS diel cycles (Figure 17A and 17B), when OCS dropped to nearly steady concentrations through the night at each inlet until daytime turbulence resumed. Variation from daytime to nighttime OCS concentrations varied the least at the end of the growing season when plant uptake had largely ceased (Figure 17C).

At the two corn sites, diel cycles reflected the seasonal productivity of the crop. Peak season corn registered strong midday vertical gradients even with turbulent replenishment of

OCS (Figure 18A). Senescent corn did not reproduce these gradients, and concentrations at all heights tracked one another throughout the 24-hour period (Figure 18B).

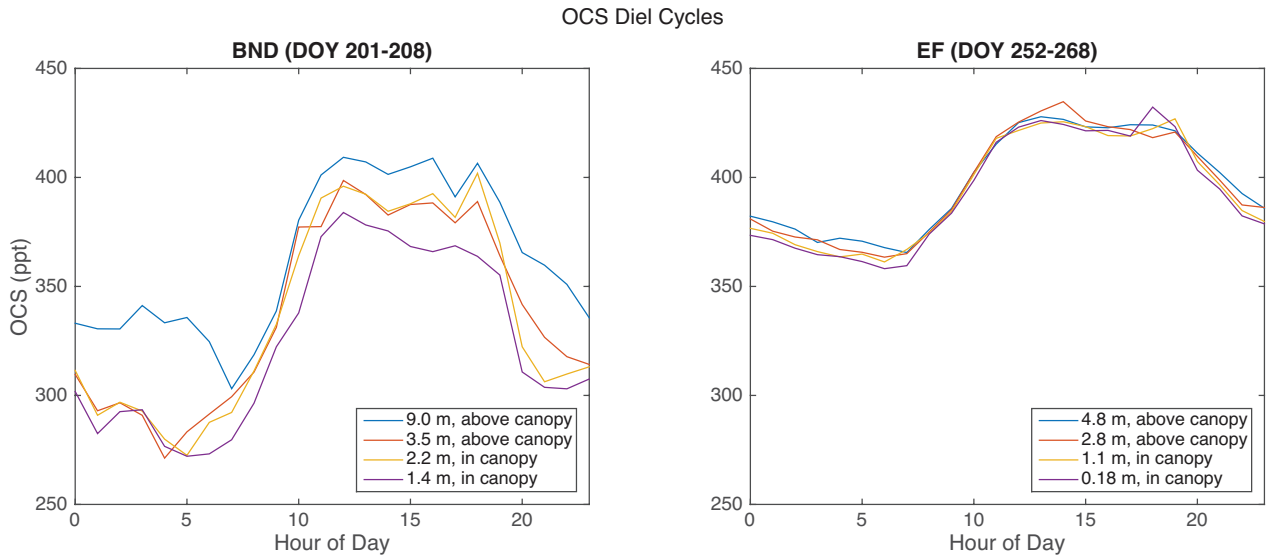

Figure 18. BND and EF OCS diel cycles. Strong midday vertical OCS gradients in the presence of turbulent mixing were observed in peak corn (BND) when concentrations at the highest inlet were ~30 ppt higher than those sampled near the ground. Vertical gradients were largely absent in senescent corn, where OCS concentrations at all heights tracked one another.

3.3 Carbonyl Sulfide Minima and Carbon Dioxide Maxima

Also of note are the minimum OCS and maximum CO_2 in-canopy concentrations (Figure 19), which both occurred at night in the absence of turbulent mixing. The lowest OCS measured was 17.6 ± 9.5 ppt on DOY 223 (August 10), which, to our knowledge, is the lowest OCS measurement made in the free atmosphere. The maximum CO_2 was 2040 ppm on DOY 205 (July 23), which is five times larger than average concentrations in the atmosphere. Examples of very high CO_2 and low OCS periods are illustrated in Figure 19. These observations are likely a demonstration of boundary layer stability combined with the dense, irregular canopy of a

tallgrass prairie, in which exceptionally windless nights allowed for pockets of stable air to become OCS-depleted and CO_2-enriched without turbulent mixing from the boundary layer to replenish OCS concentrations or disperse respired CO_2.

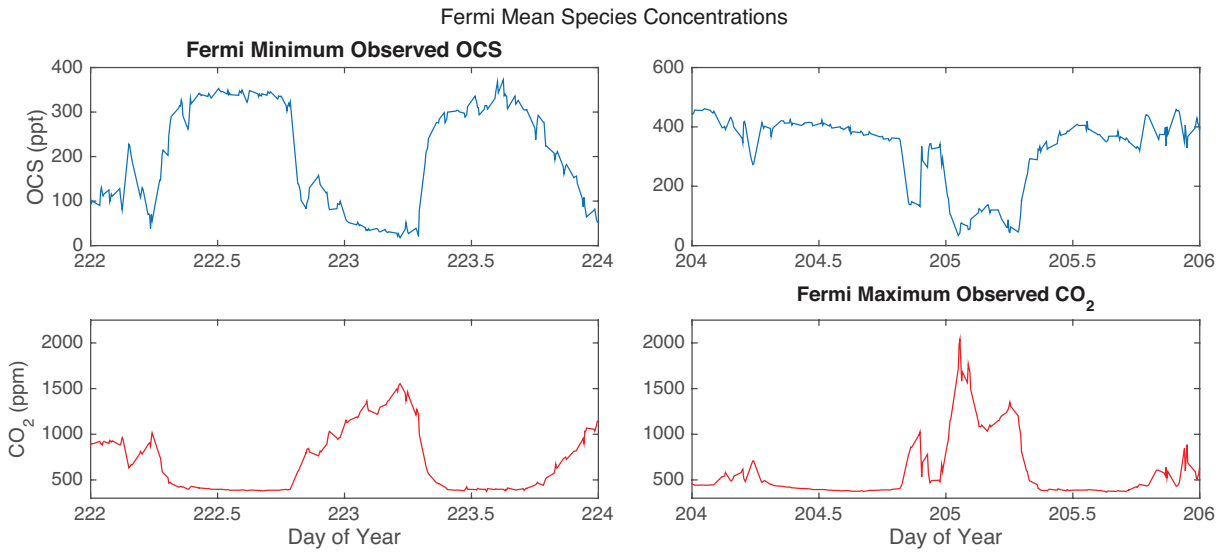

Figure 19. In-canopy OCS minimum and CO_2 maximum. OCS and CO_2 concentrations on the days of year when an OCS minimum concentration of 17.6 ± 9.5 ppt (upper left, DOY 223 = August 10, 2016) and a CO_2 maximum concentration of 2040 ppm (lower right, DOY 205 = July 23, 2016) were observed. The corresponding CO_2 (lower-left) and OCS (upper-right) concentrations are included to demonstrate the high correlation between the two gases.

3.4 Carbonyl Sulfide Gradients

Vertical gradients of OCS were our real-time proxy for assessing flux throughout the Fermi field campaign before the data allowing flux calculations were available. The strongest daytime OCS gradients (-11.8 ± 9.5 pmol mol $^{-1}$ m^{-1}) were observed early in the growing season in June as the prairie built the majority of its mass above ground and root density increased below ground (Figure 20A). OCS gradients were much more prominent at night when boundary

layer turbulence was minimal. Nighttime gradients reached a minimum of -35.6 ± 9.5 pmol m^{-1} in late July (Figure 20B). Daytime and nighttime gradients increase thereafter, with daytime gradients of > -5 ± 9.5 pmol m^{-1} in October (Figure 20C).

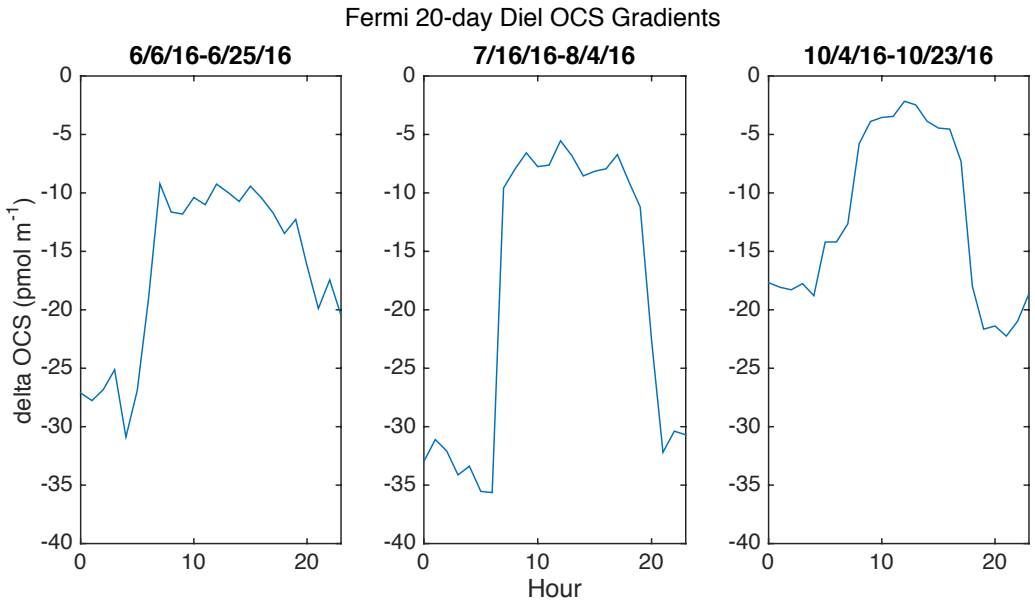

Figure 20. Select 20-day Fermi OCS gradient diel cycles. The (A) beginning, (B) middle, and (C) end of growing season are shown. The largest daytime gradient is at beginning of season (-11.8 ± 9.5 pmol m^{-1}); largest nighttime gradient in middle of season (-35.6 ± 9.5 pmol m^{-1}). Daytime gradient approaches zero near end of season.

3.5 Daytime Carbonyl Sulfide Flux and Gross Primary Productivity

In the presence of a turbulent boundary layer, observations of mean daytime (10:00–15:00) F_{eco} at the Fermi tallgrass prairie were -39.1 ± 9.5 pmol m^{-2} s^{-1} (Figure 21). Mean daytime F_{leaf} was -36.3 ± 9.5 pmol m^{-2} s^{-1}. According to the model of Whelan et al. (2016) F_{soil} (mean = -2.78 ± 9.5 pmol m^{-2} s^{-1}) was never an OCS source, with maximum F_{soil} at -0.171 ± 9.5 pmol m^{-2} s^{-1}, validating assertions that F_{soil} has a negligible effect on the total ecosystem flux from this site. Leaf OCS flux was typically an order of magnitude larger than F_{soil}, which clearly demonstrated that fluxes were dominated by plant uptake in agreement with previous investigations that directly measured F_{soil} (*Berkelhammer et al.*, 2014; *Maseyk et al.*, 2014; *Whelan et al.*, 2016)

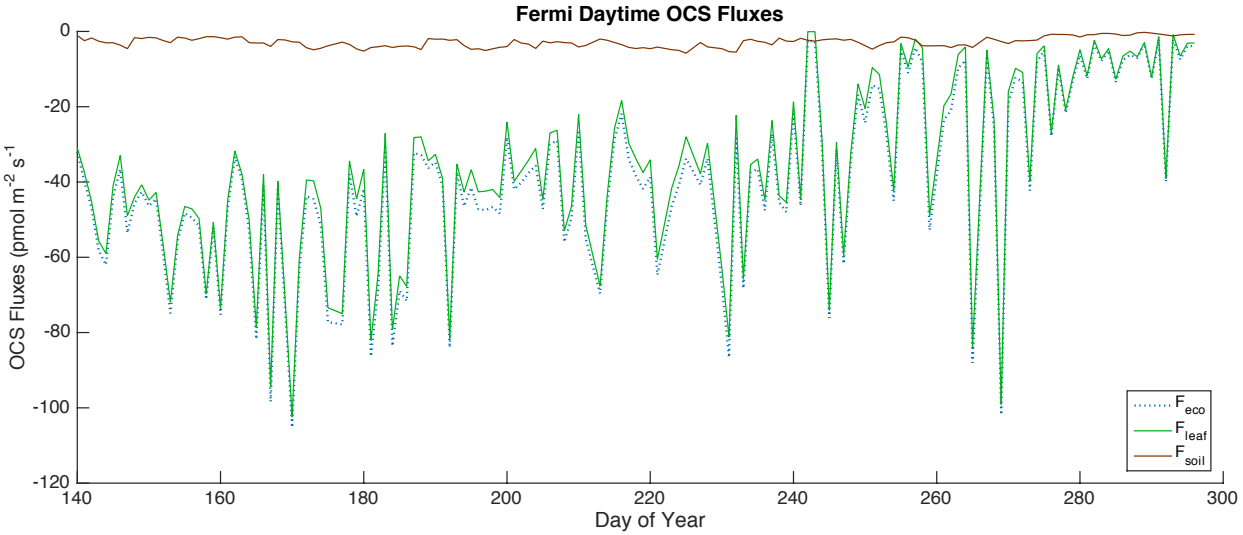

Figure 21. Fermi mean daytime (10:00–15:00) OCS fluxes. Strength of OCS sink declines through the year. F_{soil} remains negative, adding to F_{leaf} (mean = -36.3 ± 9.5 pmol m^{-2} s^{-1}), which is the larger OCS sink by an order of magnitude.

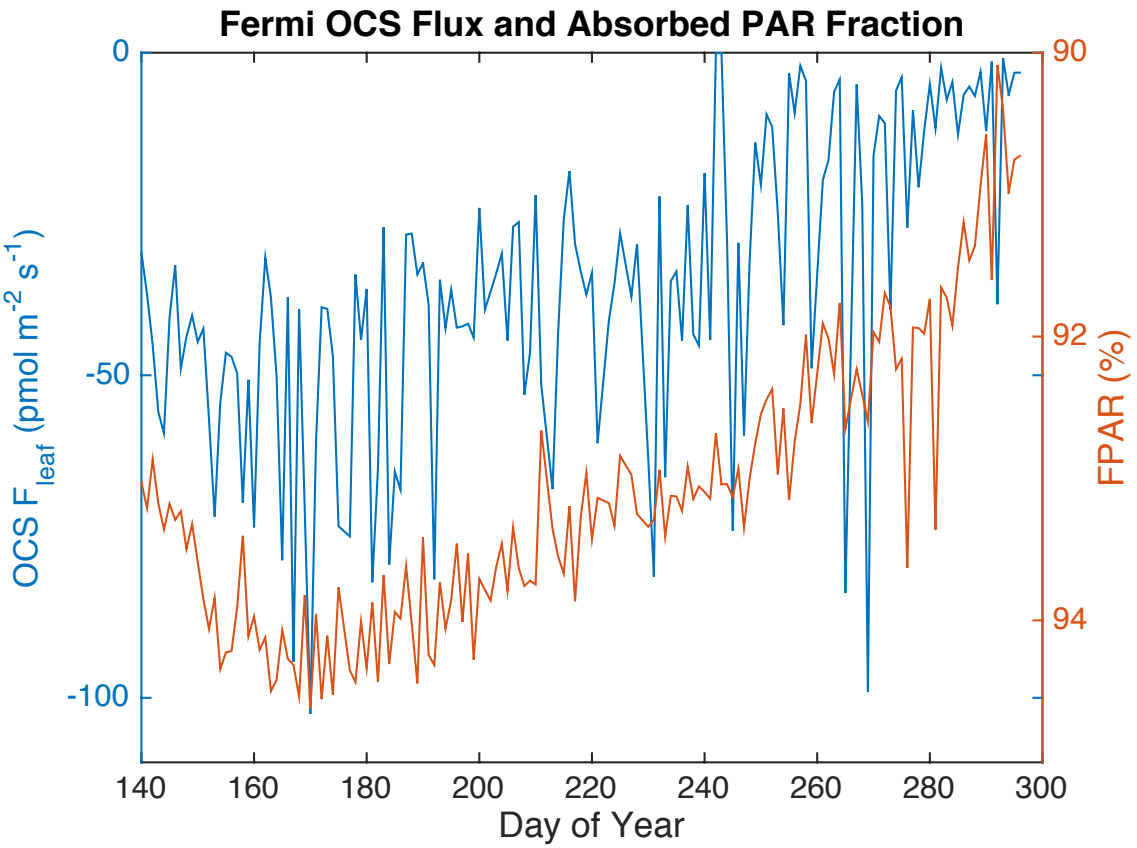

Figure 22. Fermi daily F_{leaf} and FPAR throughout the campaign. Strongest signals of each coincide on DOY 170 (June 18).

Daytime leaf OCS flux tracked canopy absorption of photosynthetically active radiation (PAR) throughout the season, represented here as FPAR (Figure 22), where the strongest OCS flux (-102 ± 9.5 pmol m^{-2} s^{-1}) coincides with the largest absorption of PAR (94.6%) early in the growing season (DOY 170 = June 18). There was significant correlation (R^2 = 0.437, $p < 0.001$) between F_{leaf} and FPAR, with higher FPAR resulting in stronger F_{leaf} (Figure 23).

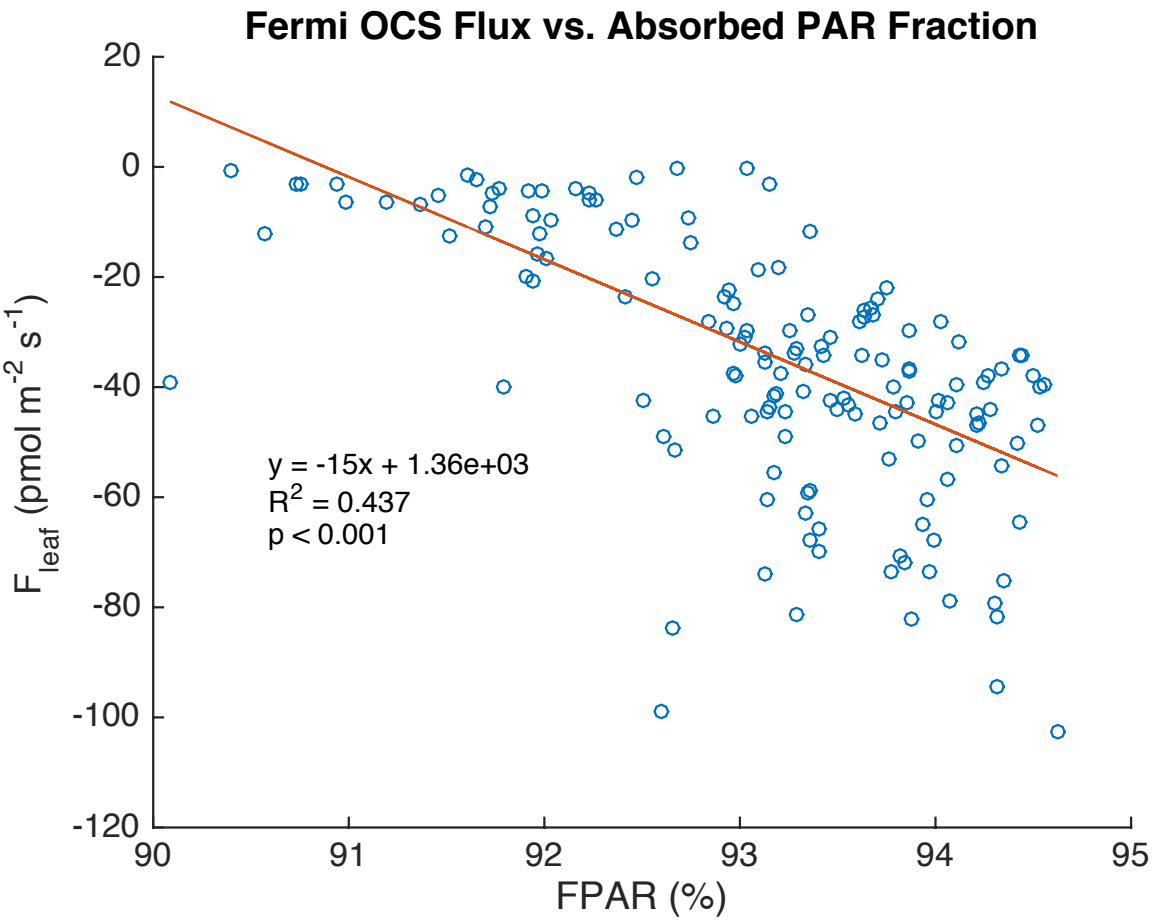

Figure 23. Fermi FPAR vs. F_{leaf} throughout the campaign. Stronger OCS fluxes correspond to higher fractions of absorbed PAR indicating a significant correlation between photosynthesis and OCS flux regulated by stomatal conductance.

With vegetation dominating OCS uptake, daytime fluxes observed in the agricultural corn fields during the middle of the season (BND) and after the onset of senescence (EF) reflect these middle and end points of the annual cycle. Daytime mean leaf fluxes for the mid-season corn at BND were strongly and consistently negative, with a mean F_{leaf} of -79.3 ± 13 pmol m^{-2} s^{-1}. Senescent corn F_{leaf} was far weaker (mean = -0.437 ± 15 pmol m^{-2} s^{-1}), and indicated three days when F_{leaf} was positive, but only one of those days resulted in an OCS emission once F_{soil} sinks were incorporated.

These same mid-season and senescent periods at the prairie site demonstrated a markedly different OCS flux pattern. The uptake of OCS at Fermi during the same time as BND was less than half as strong, with a mean F_{leaf} of -36.6 ± 9.5 pmol m^{-2} s^{-1}. The prairie site, however, demonstrated a stronger OCS sink later into the transition from summer to fall and remained negative, with a mean daily F_{leaf} two orders of magnitude larger than the EF corn, at -20.3 ± 9.5 pmol m^{-2} s^{-1} (Table 1). Whereas peak corn OCS uptake is more than twice as strong as the prairie during the same DOYs, more GPP is retained on average over the course of the longer growing season.

Table 1. Mean daytime OCS fluxes from tallgrass prairie (Fermi), peak-season corn (BND), and senescent corn (EF).

Site	*Vegetation*	*DOYs*	F_{leaf} *(pmol* m^{-2} s^{-1}*)*	F_{soil} *(pmol* m^{-2} s^{-1}*)*
Fermi	Tallgrass Prairie	138-297	-36.3 ± 9.5	-2.78 ± 9.5
BND	Corn	201-208	-79.3 ± 13	-0.327 ± 13
Fermi	Tallgrass Prairie	201-208	-36.6 ± 9.5	-3.05 ± 9.5
EF	Corn	252-268	-0.437 ± 15	-0.291 ± 15
Fermi	Tallgrass Prairie	252-268	-20.3 ± 9.5	-3.05 ± 9.5

Linear regressions of OCS leaf fluxes and GPP_{Re} were made to test the second hypothesis (*OCS fluxes will follow a seasonal cycle associated with changes in local gross primary productivity*). As was expected with daytime correlations of F_{leaf} and GPP, the relationships between plant uptake of OCS and CO_2 were significant. The widely-used flux partitioning

method of Reichstein (2005) yielded a GPP_{Re} that was well-correlated (R^2 = 0.652, $p < 0.001$) with daytime F_{leaf} (Figure 24).

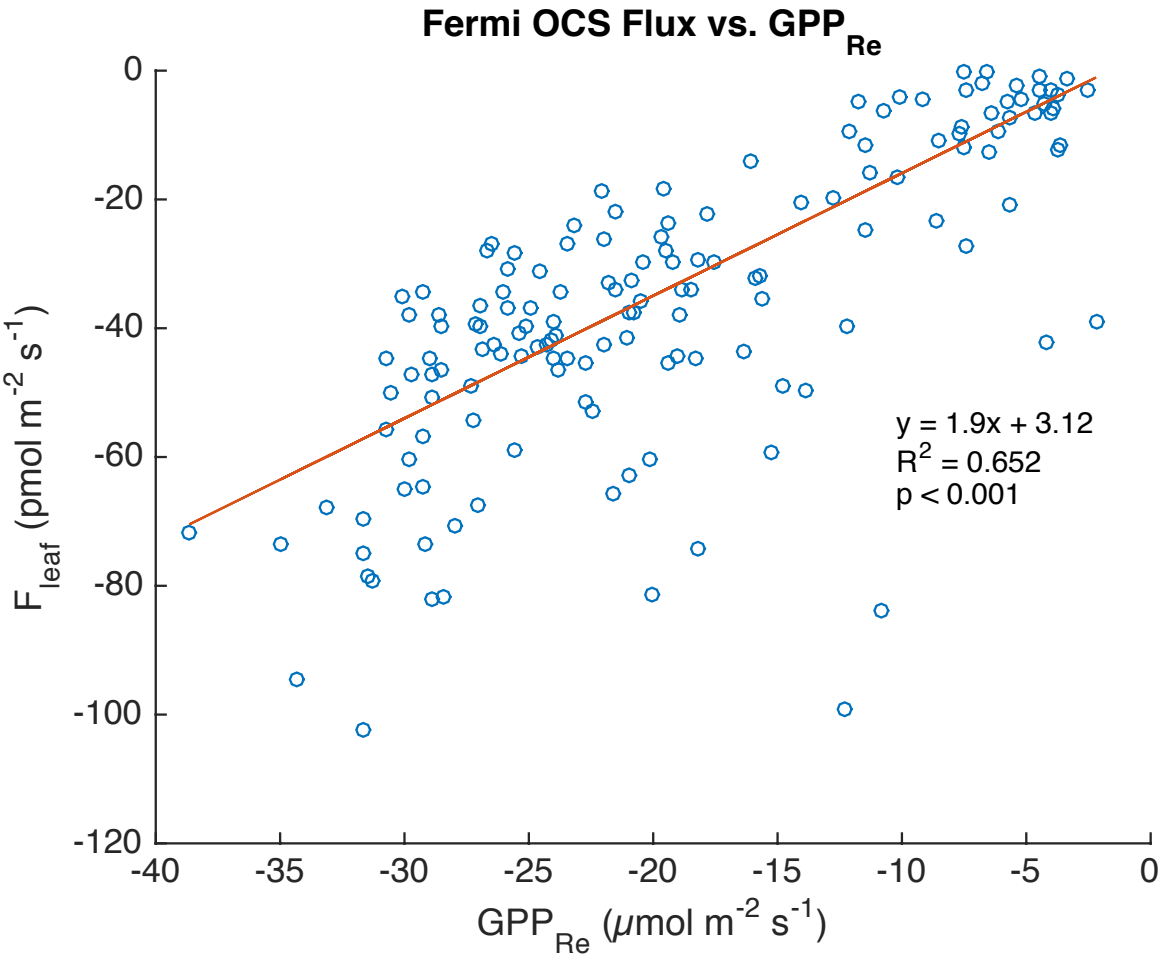

Figure 24. Fermi daily F_{leaf} vs. GPP_{Re}. Observed leaf OCS flux is well-correlated with respiration-derived GPP (R^2 = 0.652, $p < 0.001$).

To assess the validity of using a constant leaf uptake ratio (LRU = OCS:CO_2 = 1.6) in calculating GPP_{OCS} (*Stimler et al.*, 2010, 2012; *Asaf et al.*, 2013; *Berkelhammer et al.*, 2014; *Billesbach et al.*, 2014; *Hilton et al.*, 2017), equation 12 was rearranged to solve for the site-

specific LRU using observed OCS and CO_2 concentrations, F_{leaf}, and the GPP_{Re} estimate. This yielded a median LRU of 1.67.

Comparing the two methods of obtaining gross primary productivity validated the third hypothesis (GPP_{OCS} will be comparable to GPP_{Re}). GPP_{OCS} and GPP_{Re} (mean = -23.3 and -19.2 µmol m^{-2} s^{-1} respectively) were significantly correlated (Figure 25; R^2 = 0.566, p < 0.001, RMSE = 8.81, n = 150). This estimate of GPP, based on observed OCS flux-gradients, constrains the unknown GPP term of the carbon budget above (Figure 2), leaving only one unknown that can now be solved for: daytime ecosystem respiration.

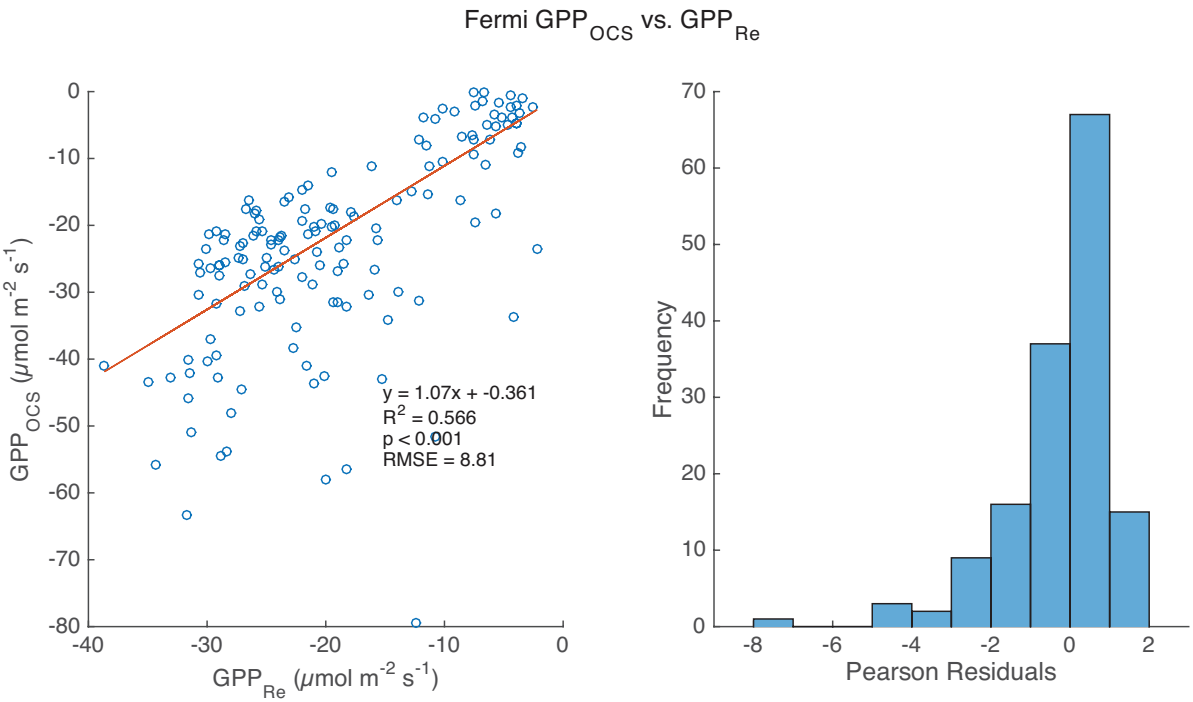

Figure 25. GPP_{OCS} vs. GPP_{Re}. GPP_{OCS} correlated well with the widely-used GPP_{Re} extrapolated from nighttime respiration values (R^2 = 0.566, p < 0.001, RMSE = 8.81, n = 150).

3.6 Carbonyl Sulfide Flux Diel Cycle

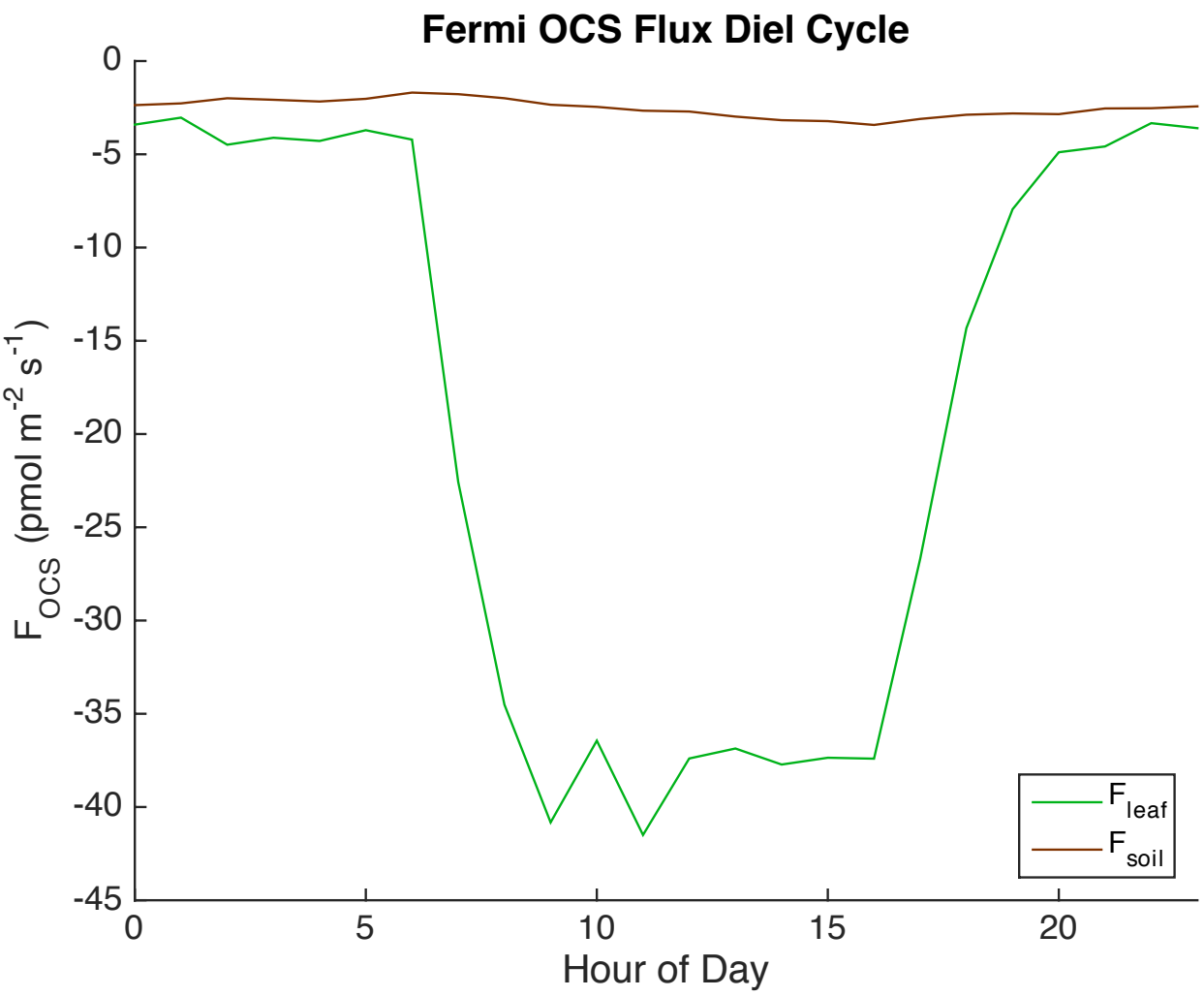

Figure 26. Fermi mean OCS flux diel cycle. Daytime F_{leaf} dominated the cycle from 06:00–22:00, with nighttime F_{leaf} values of ~3 pmol m^{-2} s^{-1} only slightly stronger than F_{soil}.

The mean diel cycle of OCS fluxes in the prairie was dominated by daytime leaf OCS uptake from 06:00–20:00 when mean F_{leaf} remained relatively stable (Figure 26; mean = -36.3 ± 9.5 pmol m^{-2} s^{-1}). Nighttime F_{leaf} was generally constant at ~-3 pmol m^{-2} s^{-1}. The F_{soil} diel cycle had a much smaller amplitude than the F_{leaf}. Around dawn, F_{soil} began to increase from a minimum of -1.69 ± 9.5 pmol m^{-2} s^{-1} to a maximum flux of -3.43 ± 9.5 pmol m^{-2} s^{-1} at 16:00.

The magnitude of the F_{leaf} diel cycle decreased through the season (Figure 27). The strongest daytime F_{leaf} coincided with the maximum GPP values in the middle of June (~-60 ± 9.5 pmol m^{-2} s^{-1}). From the mid-June maximum until the end of observation, the amplitude of the F_{leaf} diel cycle diminished. During October, mean daytime F_{leaf} was limited to -16.1 ± 9.5 pmol m^{-2} s^{-1}, and the mean difference between day and night was less than 10 ± 9.5 pmol m^{-2} s^{-1}. Across the growing season, F_{soil} strength at night increased from ~-3 pmol m^{-2} s^{-1} to values between ~-1 and 0 pmol m^{-2} s^{-1}.

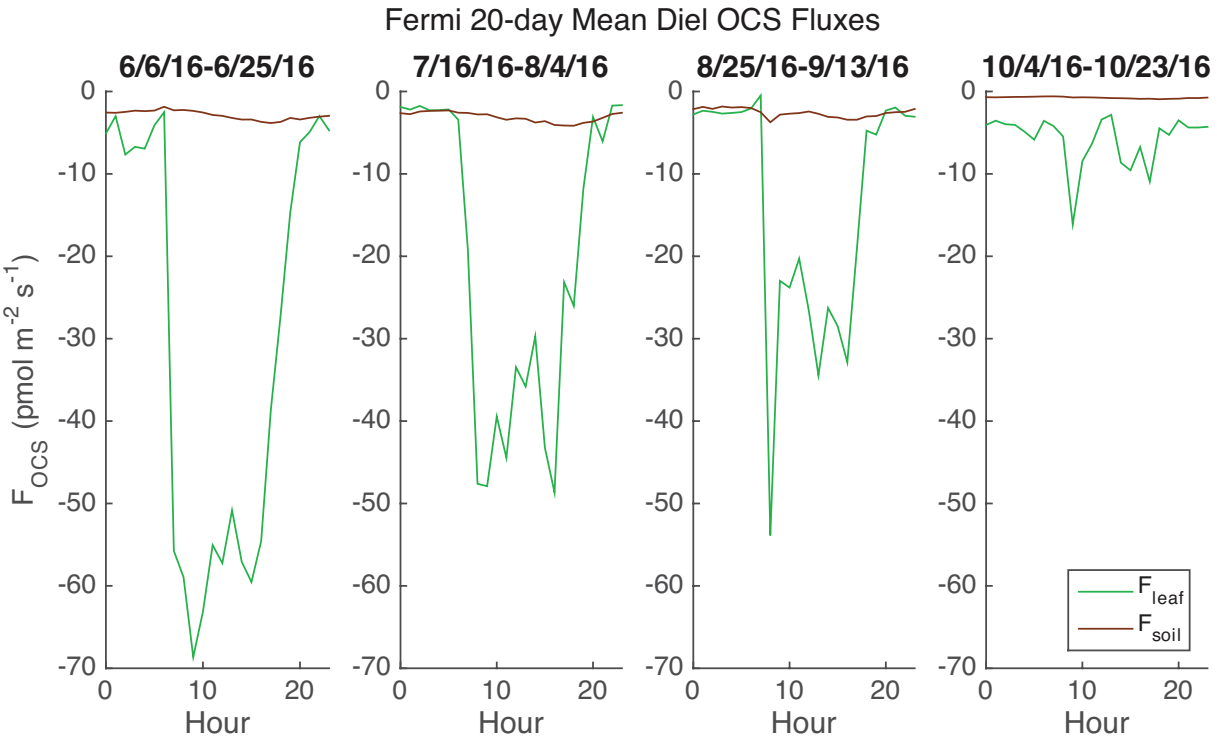

Figure 27. Select 20-day Fermi OCS flux diel cycles. The amplitude between F_{leaf} night and day is strongest in the middle of June, and diminished nearly to nighttime values by the middle of October. The amplitude of F_{soil} difference between day and night was much smaller than F_{leaf} throughout the season, and decreases to a nearly horizontal line just below 0 in mid-October.

3.7 Nighttime Carbonyl Sulfide Flux and Transpiration

Throughout the period of observation at Fermi, OCS flux continued in the absence of light, indicating incomplete stomatal closure. Boundary layer conditions at night (22:00–04:00) were often stratified due to low boundary layer turbulence, and filtering the data using a u* threshold as noted above, reduced the total number of nighttime values relative to the day. The tallgrass prairie ecosystem remained an OCS sink (F_{eco} mean = -6.05 ± 2.8 pmol m^{-2} s^{-1}), but F_{leaf} was occasionally a smaller sink than F_{soil} (mean = -3.60 ± 2.8 and -2.44 ± 2.8 pmol m^{-2} s^{-1} respectively), particularly during some period of the summer (Figure 28).

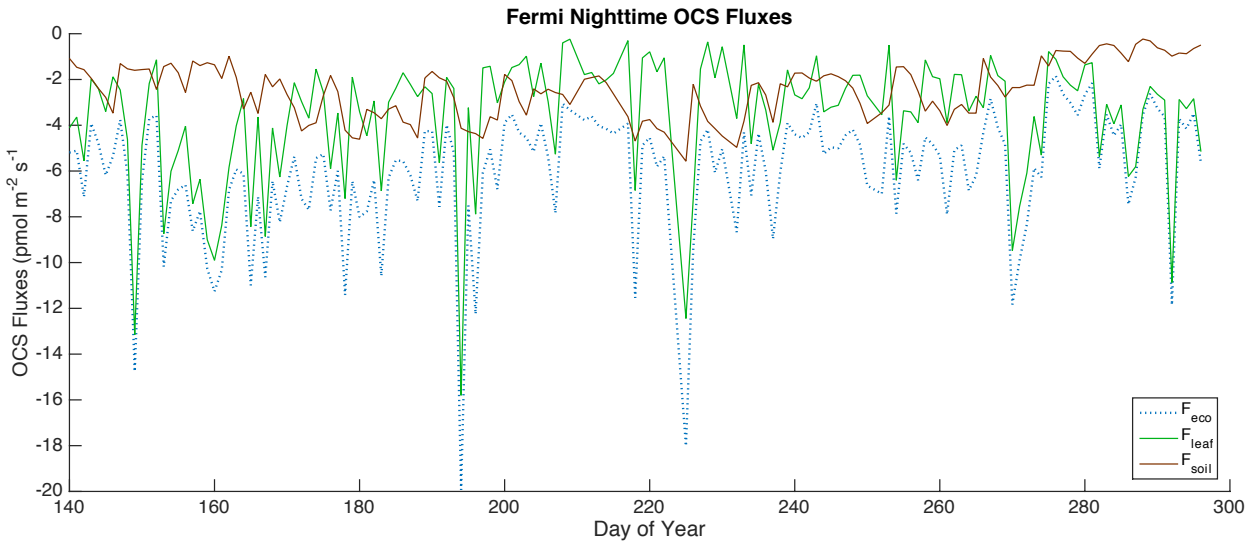

Figure 28. Fermi mean nighttime (22:00–04:00) OCS fluxes. In the absence of turbulence, nighttime F_{eco} fluxes are markedly smaller than the daytime, with soil fluxes (mean = -2.44 ± 2.8 pmol m^{-2} s^{-1}) often being larger than leaf uptake (mean = -3.60 ± 2.8 pmol m^{-2} s^{-1}).

Mean nighttime fluxes for all sites were smaller than daytime fluxes and occasionally were not statistically different from 0. Nighttime F_{leaf} at BND was nearly absent at the peak corn

site, but the measurement period was shorter relative to Fermi and it cannot be confirmed whether this short campaign was indicative of general behavior of the ecosystem. Only three nights of seven remained after filtering, one of which was a net OCS emission, for a mean nighttime F_{leaf} of -0.107 ± 1.4 pmol m^{-2} s^{-1}. Nighttime uptake of OCS in senescent corn at EF demonstrated one night of emission as well, but F_{leaf} was larger overall at -1.82 ± 2.5 pmol m^{-2} s^{-1}. The Fermi tallgrass prairie remained a sink during the same two periods at night (-2.06 ± 2.8 and -2.69 ± 2.8 pmol m^{-2} s^{-1}, respectively), but F_{soil} was often a stronger sink than leaf uptake.

Table 2. Mean nighttime OCS fluxes from tallgrass prairie (Fermi), peak-season corn (BND), and senescent corn (EF).

Site	*Vegetation*	*DOYs*	*F_{leaf} (pmol m^{-2} s^{-1})*	*F_{soil} (pmol m^{-2} s^{-1})*
Fermi	Tallgrass Prairie	138-297	-3.60 ± 2.8	-2.44 ± 2.8
BND	Corn	201-208	-0.107 ± 1.4	-0.0286 ± 1.4
Fermi	Tallgrass Prairie	201-208	-2.06 ± 2.8	-2.66 ± 2.8
EF	Corn	252-268	-1.82 ± 2.5	-0.382 ± 2.5
Fermi	Tallgrass Prairie	252-268	-2.69 ± 2.8	-2.71 ± 2.8

Leaf OCS flux was converted to nighttime transpiration in order to test the fourth hypothesis (*OCS flux can be used as a proxy for nighttime stomatal conductance and transpiration)*. As a function of leaf-level OCS fluxes, nighttime water loss (E_n) from the canopy is a unitless index (0–1) of observed nighttime transpiration. Photosynthesis is zero at night, but E_n will occur if stomata are partially open and humidity is less than 100%. With nighttime

transpiration measured here as a unitless index, qualitative assessments can now be made of the unknown nighttime variable, E_n can be made (see Figure 2). Elevated early season E_n values coincide with GPP maxima, but more sporadic E_n peaks (maximum = 0.323) were also observed at the end of the season when GPP was near its minimum during the day (Figure 29). Rates of E_n decreased to near 0 (E_n minimum = $7.09e^{-5}$) in the middle of the season (DOY 217 = August 4). The relationship between F_{leaf} and E_n proxy was significantly correlated (Figure 30A; R^2 = 0.537, $p < 0.001$) with higher rates of E_n during periods of higher F_{leaf}. However, E_n is better correlated with VPD (Figure 30B; R^2 = 0.749, $p < 0.001$), making it the more influential driver of E_n rather than g_s.

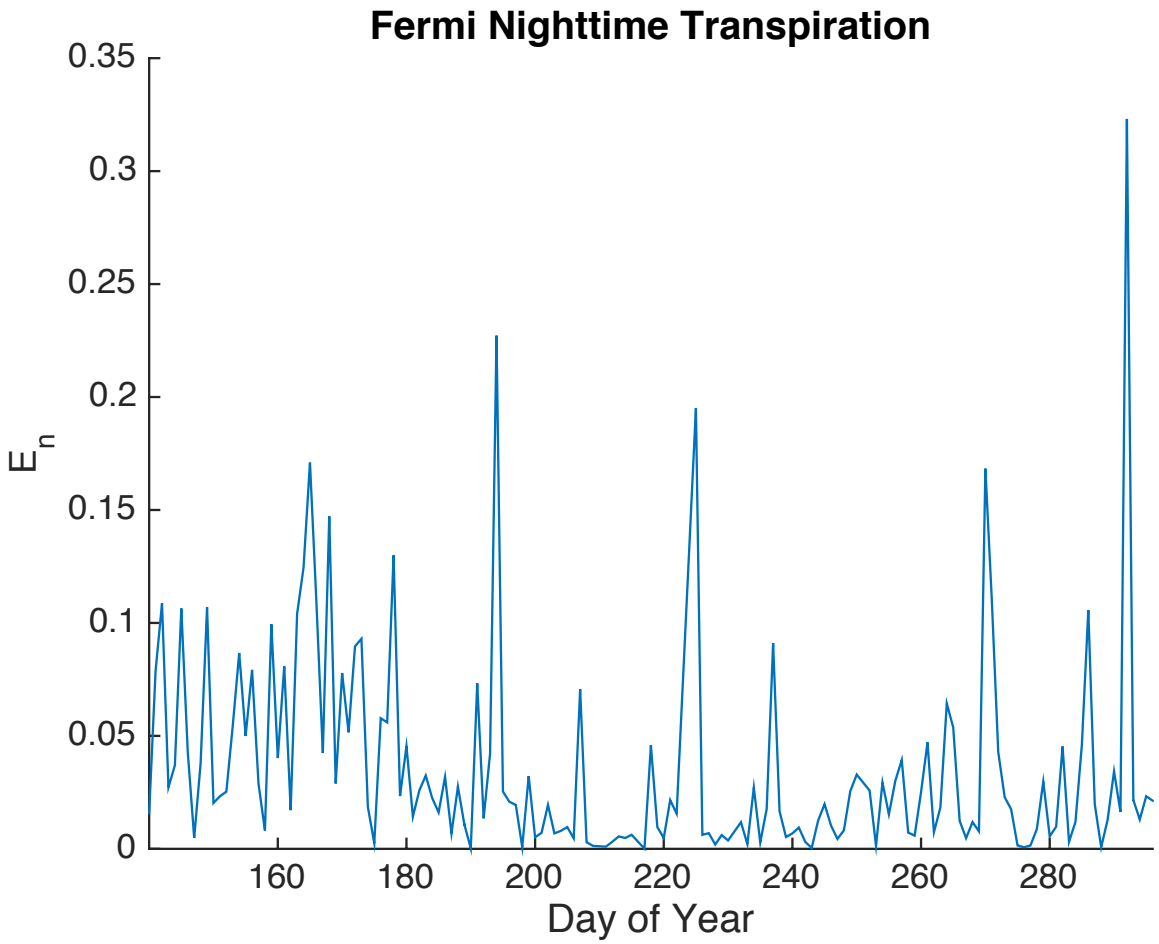

Figure 29. Fermi nighttime transpiration (mean = 0.0364). Sustained increased rates of nighttime transpiration were observed early in the season, followed by a mid-season decrease when E_n was reduced to minimum of $7.09e^{-5}$. The last portion of the season demonstrated an increase in transpiration, including the highest observation (0.323).

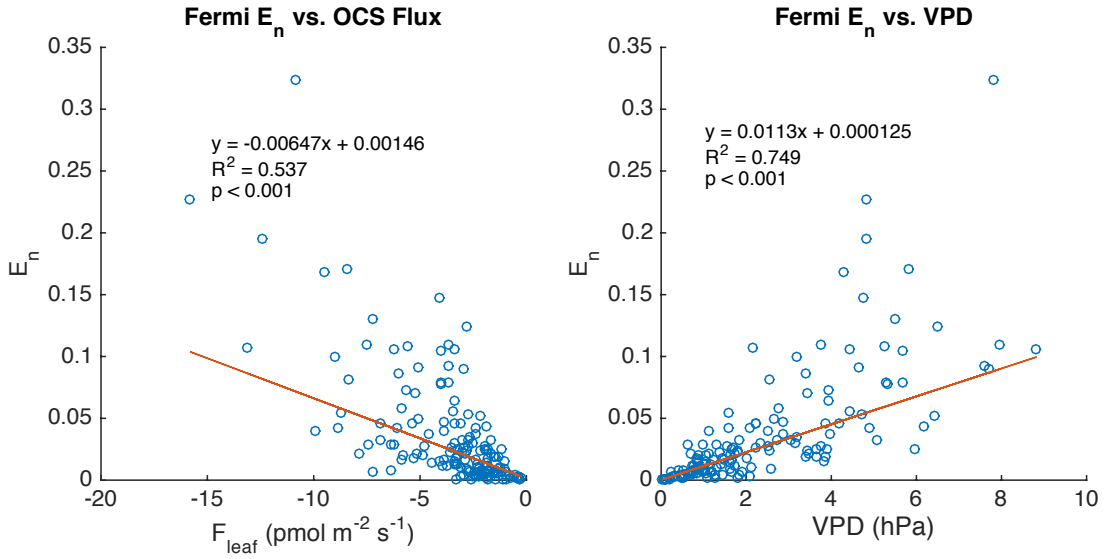

Figure 30. Fermi nighttime E_n vs. F_{leaf} (A) and E_n vs. VPD (B). Greater OCS uptake was observed as more water was transpired from leaves in the absence of photosynthesis (R^2 = 0.537, $p < 0.001$). However, VPD was much more correlated (R^2 = 0.749, $p < 0.001$), indicating that VPD drives E_n more than stomatal conductance.

Mean nighttime water loss at the two corn sites suggest that the agricultural ecosystems lost far less water at night than the prairie. Nighttime transpiration at BND approached zero (0.00300) and even the senescent corn at EF lost little water (0.0139). During these times at the Fermi prairie site, the medians were 0.0162 and 0.0235 during the BND and EF DOYs, respectively.

Table 3. Mean nighttime transpiration from the tallgrass prairie (Fermi), peak-season corn (BND), and senescent corn (EF). Values are normalized to the observed minimum and maximum E_n values from the three sites.

Site	*Vegetation*	*DOYs*	E_n
Fermi	Tallgrass Prairie	138-297	0.0364 ± 0.068
BND	Corn	201-208	0.00300 ± 0.0014
Fermi	Tallgrass Prairie	201-208	0.0162 ± 0.068
EF	Corn	252-268	0.0139 ± 0.023
Fermi	Tallgrass Prairie	252-268	0.0235 ± 0.068

3.8 Statistical Analysis of Nighttime Carbonyl Sulfide Flux

Numerous statistical approaches were used to determine the drivers of nighttime OCS flux as a proxy for stomatal conductance in order to test hypothesis five (*nighttime stomatal conductance and transpiration will vary with changes in atmospheric humidity and water stress*). Notable and statistically significant relationships will be presented here, with complete results from the statistical analyses being included in the appendix.

3.8.1 Linear Regressions

Eight ecosystem variables were selected as possible drivers of nighttime OCS flux based upon their reported effects on stomatal conductance. T_a and SWC have had demonstrated effects on F_{OCS} in multiple studies (*Commane et al.*, 2015), with high T_a and low SWC often resulting in emission from both soils and plants (*Commane et al.*, 2015). The enzyme controlling OCS hydrolysis, carbonic anhydrase, is also observed in soils. Carbonic anhydrase activity is driven by T_s and SWC (*Van Diest and Kesselmeier*, 2008; *Berry et al.*, 2013). Hot and dry soils

have been associated with soil OCS sources (*Berkelhammer et al.*, 2014; *Billesbach et al.*, 2014; *Maseyk et al.*, 2014; *Whelan et al.*, 2016). Whereas OCS does not require light to be taken up by plants, R_n from the previous day was selected because of the effects of light on stomatal conductance, with more light resulting in the stomata being more open (*Hetherington and Woodward*, 2003; *Commane et al.*, 2015), thus increasing the rate of OCS consumption. The ambient OCS and CO_2 concentrations were also selected as possible drivers. Concentrations of OCS vary with time in a diel cycle characterized by a morning increase with turbulence and a depletion at night in a still boundary layer as demonstrated earlier in this manuscript as well as in the literature (*Berkelhammer et al.*, 2014). Elevated ambient CO_2 concentrations have been linked with decreased g_s (*Hetherington and Woodward*, 2003; *Keenan et al.*, 2013). Fluctuations in WS would serve an indicator of turbulence, with higher WS resulting in more atmospheric OCS being mixed into the canopy from above. As VPD increases, evaporation rates increase but gs also responds negatively to higher VPD (*Herzog et al.*, 1998; *Benyon*, 1999; *Oren et al.*, 2001; *Daley and Phillips*, 2006; *Caird et al.*, 2007; *Fisher et al.*, 2007; *Kavanagh et al.*, 2007; *Coupel-Ledru et al.*, 2016) This indicates associations with g_s, and it is the basis for our E_n proxy (Equation 13).

These eight ecosystem variables were compared to both the whole-night mean leaf and ecosystem OCS fluxes using robust linear regression in Matlab. This fitting method is less affected by outliers in the data than the default ordinary least squares. Each data point is weighted by a process called “iteratively reweighted least squares” where subsequent iterations recompute the weights of predicted points that are farther than the prediction of the previous iteration. Linear model coefficients are then computed using the final weighted least

squares (https://www.mathworks.com/help/stats/robust-regression-reduce-outlier-effects.html). Among the whole-night comparisons, WS explained the largest variation of both F_{eco} and F_{leaf} at Fermi, but correlations were relatively low (Figure 31; R^2 = 0.299, $p < 0.001$; R^2 = 0.293, $p < 0.001$, respectively).

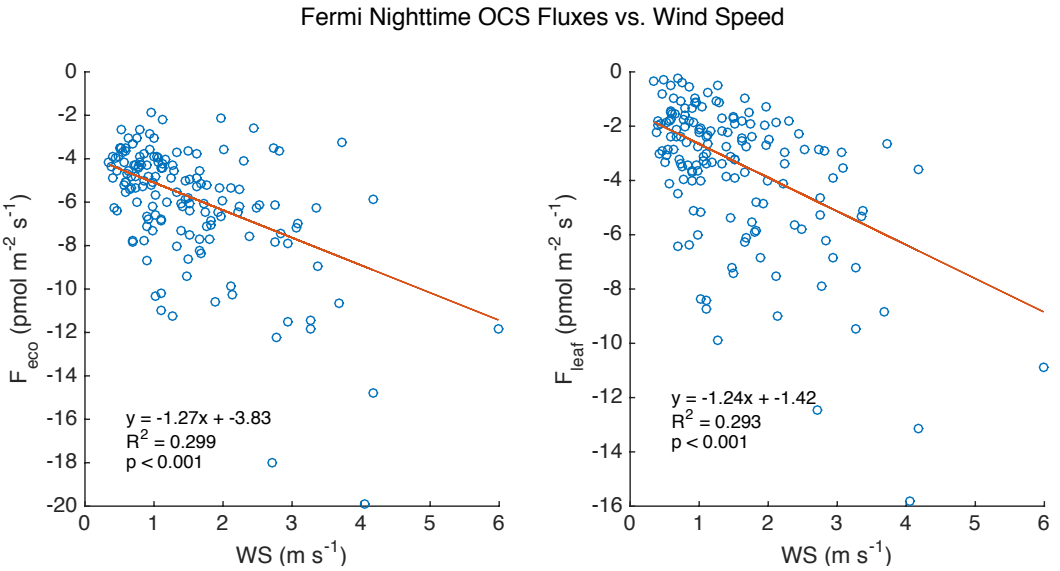

Figure 31. Fermi F_{eco} and F_{leaf} vs. WS. Among all variables compared with robust linear regression, WS explained the most observed variation of F_{eco} and F_{leaf}.

To test whether nighttime OCS fluxes were affected by different processes at different times of the night, the night was divided in half from 22:00–01:00 (n_1) and 01:00–04:00 (n_2). Robust linear regressions of these half-night fluxes were compared against the same eight ecosystem variables noted above. The variable most correlated to OCS fluxes among these 32 regressions was WS for n_1 F_{leaf} and n_1, F_{eco} (R^2 = 0.269, $p < 0.001$; R^2 = 0.304, $p < 0.001$, respectively) and n_2 F_{leaf} (R^2 = 0.309, $p < 0.001$). However, n_2 F_{eco} was best described by VPD (R^2

= 0.306, $p < 0.001$). The remaining results from these regressions were less correlated, but relationships with the amount of OCS and CO_2 were significant for F_{leaf} and F_{eco} in both n_1 and n_2 ($p < 0.001$).

3.8.2 High-Flux vs. Low-Flux Percentiles

The regression analyses were unable to reveal a clear univariate control on nighttime g_s. This may be due to the fact that mean nighttime fluxes were small (mean = -3.60 ± 2.8 pmol m^{-2} s^{-1}) and often close to the analytical uncertainty of the measurement. The next set of analyses was designed to probe the processes controlling nighttime g_s by separating nights with high fluxes (20^{th} percentile) and low fluxes (80^{th} percentile) over whole-nights (n) and the two half-nights (n_1 and n_2). The conditions associated with the high and low flux periods were assessed for each of the eight variables previously noted. If the conditions during high and low flux periods (represented by histograms) overlapped, it was assumed that the ecosystem variable was not significantly affecting nighttime OCS flux. Conversely, if there was separation between the histograms, it was not assumed that a given variable caused high or low nighttime flux, but rather that the high and low fluxes coincided with changes in these conditions (e.g., WS).

Confirming the results of the robust linear regressions, high WS resulted only in high fluxes (Figure 32). No low fluxes (F_{OCS} = 80^{th} percentile) were observed at WS greater than 3.84 m s^{-1}, but high fluxes (F_{OCS} = 20^{th} percentile) occurred throughout the range of observed mean WS (0.350–5.99 m s^{-1}).

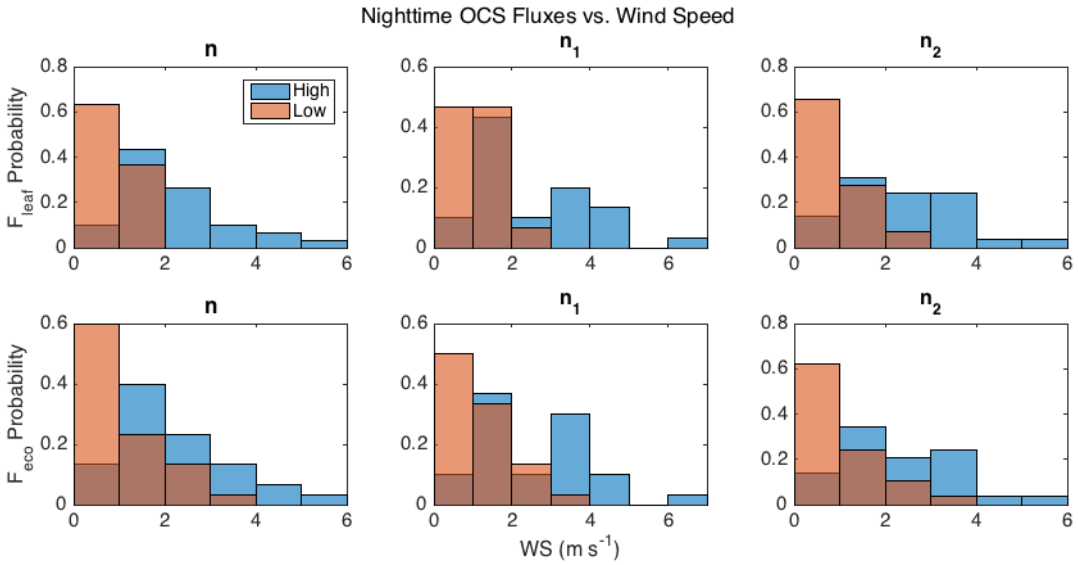

Figure 32. High (blue) and low (red) nighttime OCS fluxes vs. WS. High fluxes (20th percentile) occurred with higher WS. Low fluxes (80th percentile) only happened when WS was less than 3.84 m s^{-1}.

Vapor pressure deficits in n_2 were the second strongest correlation among the whole-night and half night regressions. In the percentile analysis, VPDs < 5.98 hPa were more likely to result in low OCS fluxes. High fluxes were also more likely at low VPD, but high fluxes were spread throughout the mean VPD range (0.00–8.79 hPa). In n_2, 86.2% of low fluxes occur at VPDs < 2.00 hPa (Figure 33).

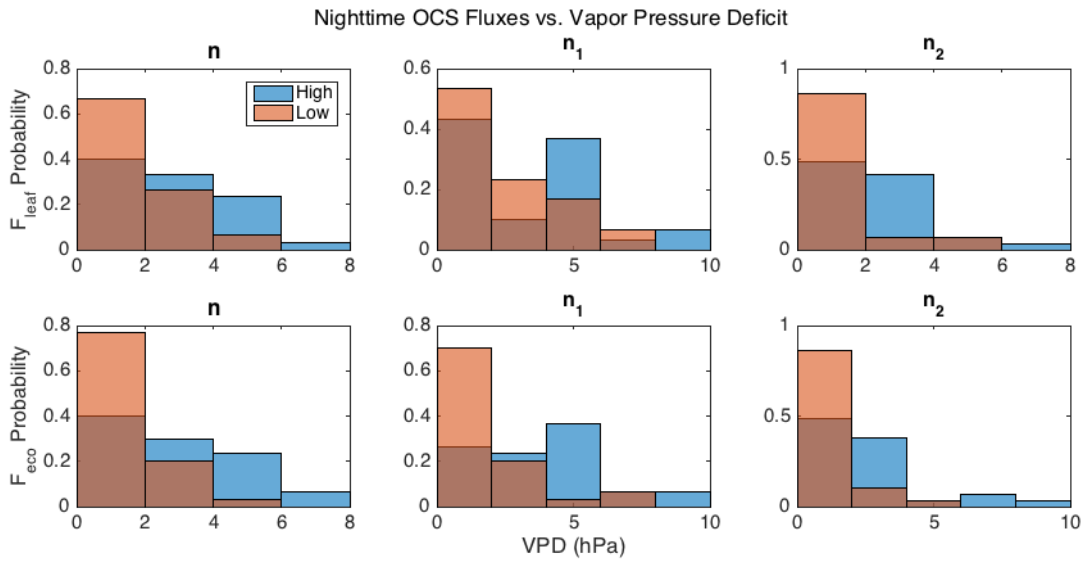

Figure 33. High (blue) and low (red) nighttime OCS fluxes vs. VPD. Low fluxes only occurred with VPD < 6.00 hPa, whereas high fluxes occurred throughout the range of observed VPD. Low fluxes in n_2 occurred almost exclusively (86.2%) with VPD < 2.00 hPa.

The most consistent histogram distributions across the six permutations of nighttime flux were provided by OCS and CO_2 (Figures 34 and 35, respectively). Concentrations of OCS at their lowest (210–280 ppt) resulted only in low fluxes. Conversely, the highest concentrations of OCS (490–560 ppt) usually resulted in only high fluxes, but low F_{eco} in n and n_1 also occurred in this range. As the night progressed (n_2), low F_{OCS} was more likely at the lower end of OCS concentrations as the stratified boundary layer becomes depleted in OCS. This result implies that the gradient of OCS, driven by atmospheric concentrations, was as important in determining the flux as the stomatal conductance.

The distributions of CO_2, on the other hand, were even more delineated and consistent. High F_{OCS} only happened when CO_2 was < 504 ppm. High and low F_{OCS} both occurred the majority of the time when CO_2 was 432–504 ppm. Above these concentrations, the probability

of low F_{OCS} diminished. From n_1 to n_2, low OCS fluxes occur at higher CO_2 as more CO_2 has been respired into the canopy throughout the night.

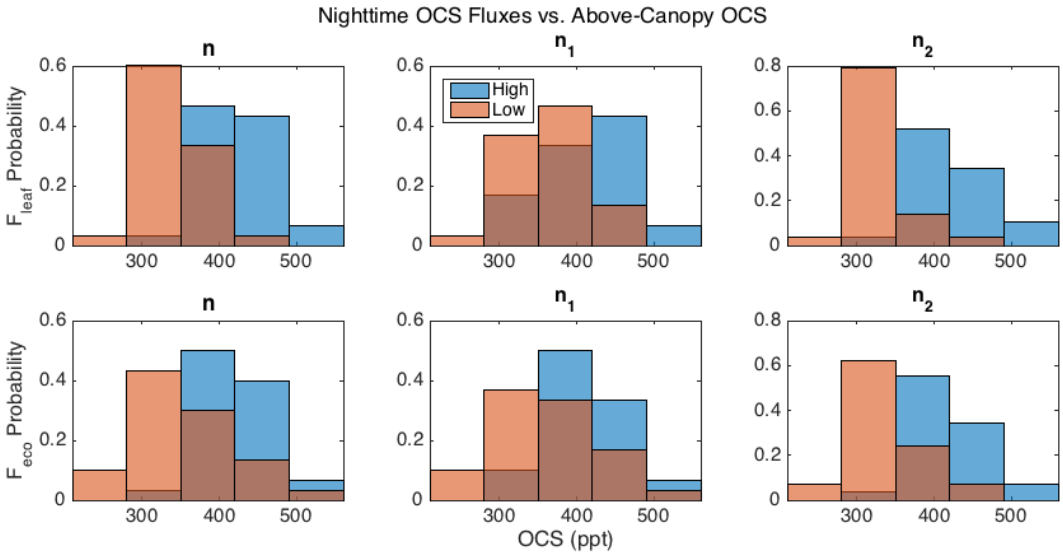

Figure 34. High (blue) and low (red) nighttime OCS fluxes vs. OCS. The lowest concentrations of OCS resulted in low F_{OCS}, and high OCS concentrations usually resulted in high F_{OCS}. As OCS in the stratified boundary layer gets depleted through the night, more low F_{OCS} was observed at low OCS.

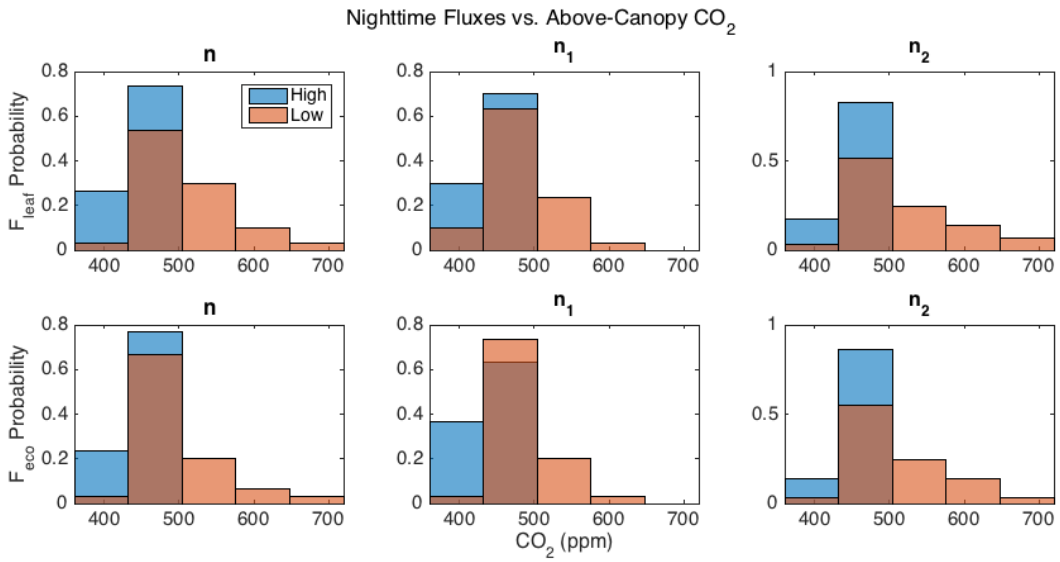

Figure 35. High (blue) and low (red) nighttime OCS fluxes vs. CO_2. High F_{OCS} only occurred when CO_2 was ≤ 500 ppm. Low F_{OCS} probability decreased with increasing CO_2 ≤ 500 ppm.

3.8.3 Nighttime Carbonyl Sulfide Flux Compared to the Previous Day

The final analysis tested if g_s during the day affected g_s during the night that followed. Whole-night F_{leaf} to previous whole-day F_{leaf} mean ratios were calculated, and in general, g_s stomatal conductance at night was ~8% of that from the previous day. The mean ratio of F_{leaf} night:day over the period of observation at Fermi was 9.94% (Figure 36A). Removing two outliers on DOY 242 and 243 (August 29–August 30, 2016) as well as the period of late-season senescence (DOY > 254) illustrates the consistency of the F_{leaf} night:day ratio (Figure 36B; mean = 8.15%, σ^2 = 7.75%). Removal of the 5th and 95th percentiles of the F_{leaf} night:day ratios reduced this to σ^2 = 4.69%.

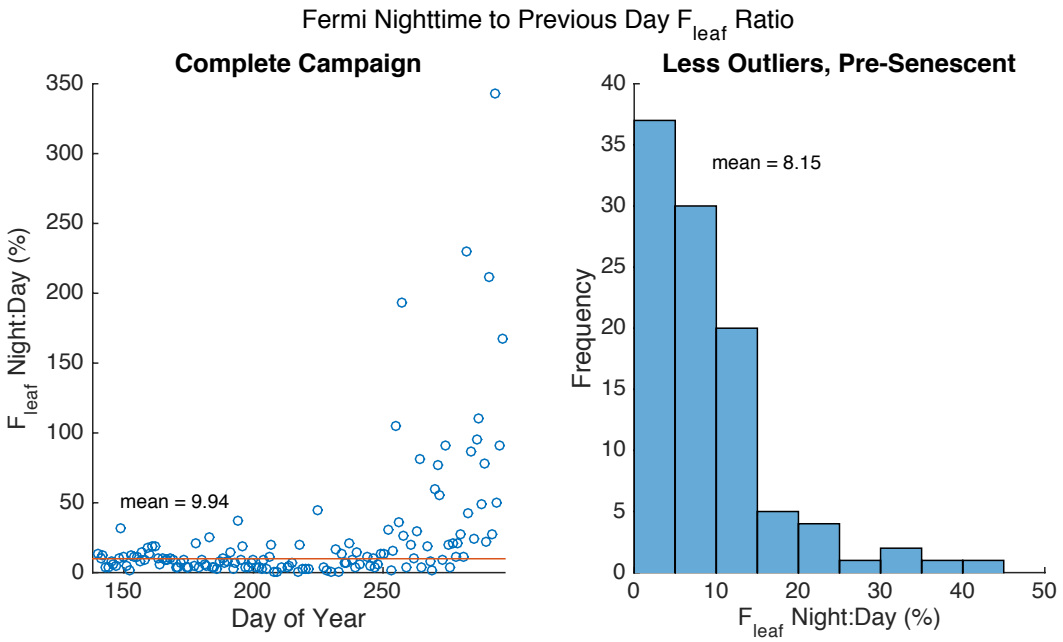

Figure 36. F_{leaf} night:day ratios at Fermi. The complete campaign ratio is shown (A; mean = 9.94%), with two outliers at DOY = 242 and 243 omitted from the scatter plot to highlight late-season instability of the ratio. With the two outliers and the senescent period removed (B; mean = 8.15%), the stability of nighttime flux relative to daytime flux becomes more apparent. With 5th and 95th percentiles removed, σ^2 = 4.69%.

The two corn sites presented significantly different night-to-day flux ratios. Nighttime fluxes at BND were two orders of magnitude smaller than daytime fluxes at Fermi, and the resulting F_{leaf} night:day ratio (mean = 0.134% ± 0.70) represents near complete stomatal closure. Senescent corn demonstrated another scenario, with a mixture of sources and sinks. Daytime and nighttime fluxes were both relatively small (-0.437 ± 15 and -1.82 ± 2.5 pmol m^{-2} s^{-1}, respectively), but F_{leaf} night was often larger by an order of magnitude, which resulted in a highly elevated F_{leaf} night:day (mean = 417% ± 430). Ratios of F_{leaf} night:day observed at the prairie site during BND DOYs were higher than BND values (mean = 5.93% ± 4.7), but EF DOYs at Fermi (mean = 12.6% ± 4.7) were far lower than at EF.

Table 4. F_{leaf} night:day ratios (%) at the tallgrass prairie (Fermi), peak-season corn (BND), and senescent corn (EF).

Site	*Vegetation*	*DOYs*	*F_{leaf} Night:Day (%)*
Fermi	Tallgrass Prairie	138-297	8.15 ± 4.7
BND	Corn	201-208	0.134 ± 0.70
Fermi	Tallgrass Prairie	201-208	5.93 ± 4.7
EF	Corn	252-268	417 ± 430
Fermi	Tallgrass Prairie	252-268	12.6 ± 4.7

Late in the season when vegetation began to die, the night:day ratio became very unstable. Fluxes in senescent corn hovered near 0. Late-season fluxes at Fermi swung from negligible daytime sinks with much larger nighttime fluxes one day, to highly elevated daytime sinks the next. Due to this instability, it may be appropriate to limit analysis of F_{leaf} night:day ratios to periods with pronounced daytime fluxes, thus allowing the sort of stable ratio observed for the majority of the season-scale Fermi campaign. It may be appropriate to limit this ratio analysis to the middle of the season when these ecosystems are actively photosynthesizing and carbon and water dynamics are most relevant.

4 DISCUSSION

4.1 Carbonyl Sulfide Flux in a Tallgrass Prairie

Hypothesis 1. Continuous measurements of OCS gradients can be used to derive OCS flux in a tallgrass prairie ecosystem.

The prairie demonstrated a strong daytime sink dominated by F_{leaf} (mean = -36.3 ± 9.5 pmol m^{-2} s^{-1}) throughout the study (Figure 21). The strength of the F_{leaf} OCS sink was highly correlated with FPAR (Figure 23; R^2 = 0.437, $p < 0.001$), with the strongest values of both (-103 ± 9.5 pmol m^{-2} s^{-1} and 94.6%, respectively) coinciding on DOY 170 (June 18; Figure 22). This result was hypothesized due to daytime OCS diffusion into leaves being regulated by g_s (*Protoschill-Krebs et al.*, 1996; *Sandoval-Soto et al.*, 2005; *Seibt et al.*, 2010; *Stimler et al.*, 2012; *Asaf et al.*, 2013; *Berkelhammer et al.*, 2014).

Nighttime fluxes in the prairie were consistently negative throughout the 159 days of observation Nighttime prairie fluxes were often one or two orders of magnitude smaller than daytime fluxes and frequently not distinguishable from zero (mean F_{eco} = -6.05 ± 2.8 pmol m^{-2} s^{-1}). Leaf and soil night fluxes had similar means with stronger night F_{leaf}, especially earlier in the season. The strongest nighttime F_{soil} occurred near the midpoint of the growing season, which is due to the effects of temperature and soil moisture on the magnitude of the soil flux.

The correlation between OCS and CO_2 concentrations (Figure 13; R^2 = 0.654, $p < 0.001$) is a function of the mirrored diel cycles of the two gases. Daytime turbulent conditions keep the OCS and CO_2 concentrations near atmospheric mixing ratios. Stratified nighttime conditions are dominated by canopy CO_2 respiration and OCS uptake. At dawn, turbulence mixes respired nighttime CO_2 into the atmosphere and canopy concentrations return to near atmospheric

concentrations. At the same time, turbulence mixes OCS into the canopy from the free troposphere. OCS concentrations at Fermi followed a distinct diel cycle (Figure 16) similar in structure to previous OCS field studies (*Berkelhammer et al.*, 2014; *Kooijmans et al.*, 2017, in discussion). Daytime maxima occurred around 15:00 h and tracked ambient OCS mixing ratios above the canopy. Within the canopy, daytime OCS concentrations were slightly lower (~30 ± 9.5 ppt) than atmospheric mixing ratios indicating the presence of a sink. At night, OCS concentrations within the canopy were routinely much lower (~100 ± 9.5 ppt) than above, which was a product of the nighttime stratification of the boundary layer.

The OCS diel cycle at BND (Figure 18A) showed midday concentrations in the canopy ~30 ± 13 ppt lower than above the canopy. At night, this difference increased to ~50 ± 13 ppt in the productive corn. Concentrations of OCS were nearly identical at EF regardless of sampling height or time of day (Figure 18B). The senescent corn and the nominal OCS flux confirmed that the seasonal OCS cycle is driven by plant uptake in this ecosystem. The corn at EF demonstrated a possible OCS emission when maximum in-canopy OCS concentrations rose to 780 ± 15 ppt (Figure 14), which was well above the concurrent atmospheric mixing ratios (419 ± 15 ppt). This possible emission happened despite SWC and T_s conditions (~50% and ~17°C, respectively) that would be unlikely to result in an OCS source (*Berkelhammer et al.*, 2014; *Billesbach et al.*, 2014; *Maseyk et al.*, 2014; *Whelan et al.*, 2016). It is possible that senesced plant material may have produced OCS through photo-degradation pathway.

OCS gradients were negative at the prairie throughout the season (Figure 20). These gradients followed a diel cycle similar to the concentrations, and increased in strength through the night as still air in the canopy was progressively depleted of OCS. Mid-season gradients

were most prominent at or around dawn (-35.6 ± 9.5 pmol m^{-1}), when turbulent convection resumed, and gradients weakened rapidly. Ambient OCS was mixed in from the free troposphere throughout the day, and this constant replenishment created a stable midday OCS gradient. Maximum daytime gradients (-11.8 ± 9.5 pmol m^{-1}) were observed early in the season, and coincided with maximum GPP (-38.7 µmol m^{-2} s^{-1}).

4.2 Carbonyl Sulfide Flux and Gross Primary Productivity

Hypothesis 2. OCS fluxes will follow a seasonal cycle associated with changes in local gross primary productivity.

Daytime F_{leaf} and GPP_{OCS} not only tracked GPP_{Re} throughout the growing season, but GPP_{OCS} may have demonstrated sensitivity to short-term variability that was absent from the GPP_{Re} estimate (Figure 37). Two late-season spikes in F_{leaf} on DOY 265 and 269 (-83.8 ± 9.5 and -99.1 ± 9.5 pmol m^{-2} s^{-1}, respectively) and the corresponding GPP_{OCS} may have indicated that opportunistic canopy undergrowth responded to increased PAR and abnormal seasonal warmth after taller species had senesced. A prolonged period hotter and more wet than the average for the time of year (Figure 38) made conditions favorable for a surge in productivity.

One reason that GPP_{Re} did not reproduce these spikes might be that seasonally uncharacteristic ecosystem conditions (e.g., T_a and SWC) contributed to a misrepresentation of daytime respiration by eddy covariance flux partitioning. Although, with short-term ecosystem variability, eddy covariance flux partitioning tends to overestimate respiration (*Reichstein et al.*, 2005), which would have resulted in a GPP_{Re} estimate larger than observed. This remains unresolved and highlights either a deficiency in one of the two methods to derive GPP.

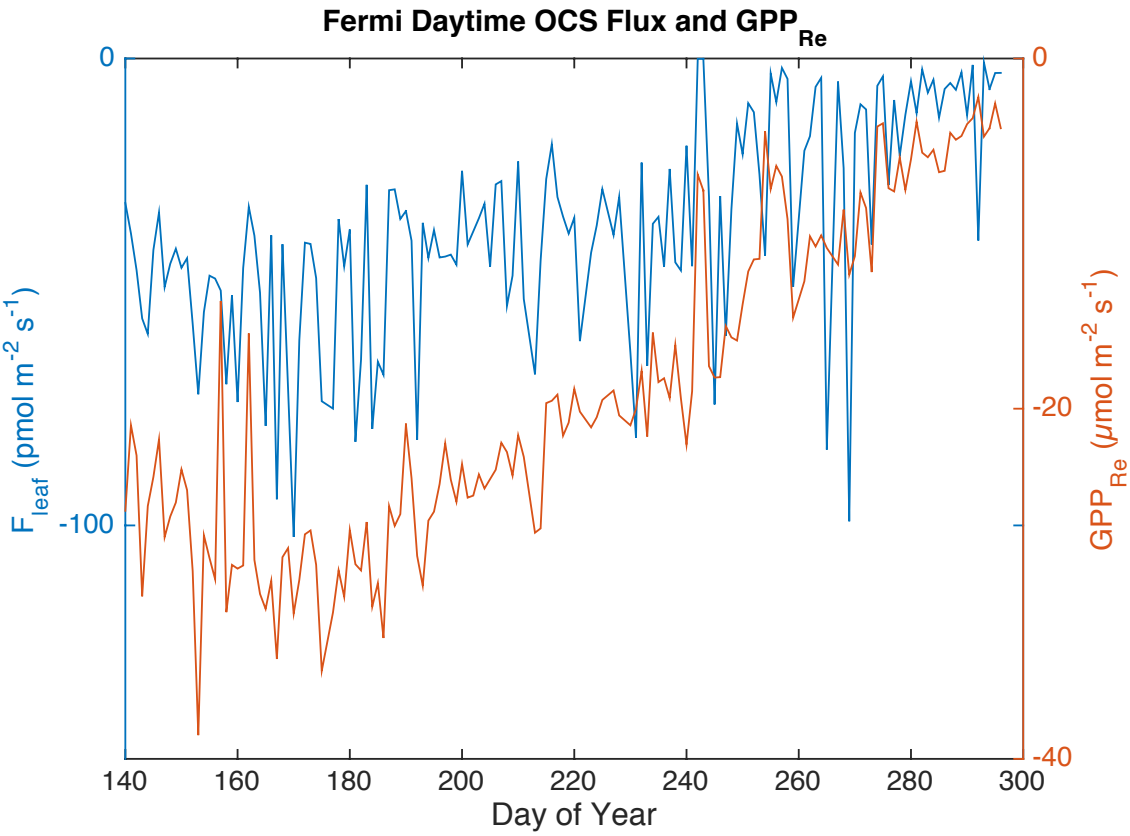

Figure 37. F_{leaf} and GPP_{Re} at Fermi. Maxima for F_{leaf} (-103 ± 9.5 pmol m^{-2} s^{-1}) and GPP_{Re} (-39 µmol m^{-2} s^{-1}) occur 23 days apart early in the growing season then diminish until fall senescence.

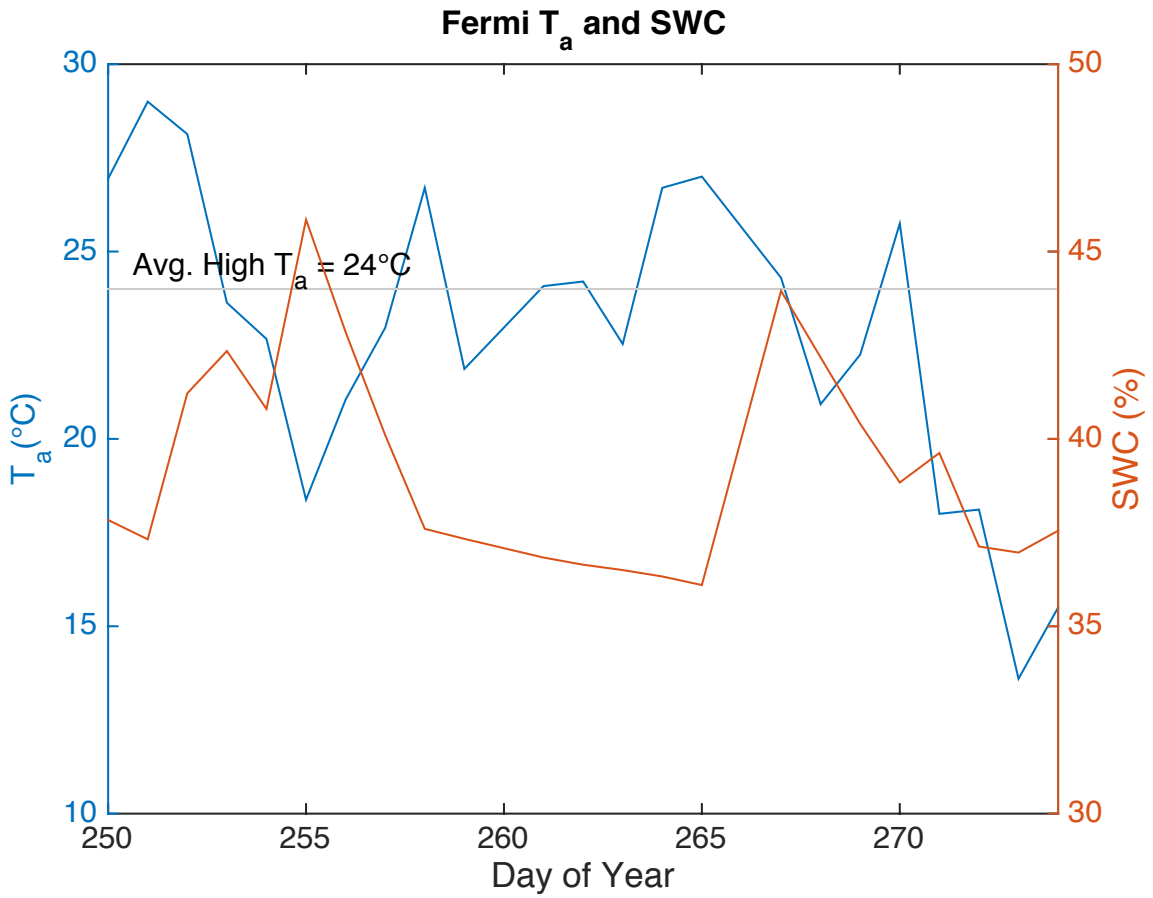

Figure 38. Air temperature and SWC at Fermi, DOY 250–275. Period brackets the late-season spikes in F_{leaf} observed on DOY 265 and 269. Observed air temperature had been elevated compared to historic averages for September, and SWC had increased prior to the observed OCS fluxes.

As an indicator of productivity, daytime fluxes of OCS at the prairie and two corn sites followed seasonal shifts. Prairie F_{leaf} was active for a longer portion of the growing season than corn. In the middle of the season, F_{leaf} at BND was more than double the prairie (-79.3 ± 13 and -36.3 ± 9.5 pmol m^{-2} s^{-1}, respectively). Senescent corn fluxes were essentially undetectable towards the end of the season (mean = -0.437 ± 15 pmol m^{-2} s^{-1}), whereas the prairie was still consuming OCS two orders of magnitude larger (-20.3 ± 9.5 pmol m^{-2} s^{-1}). This prolonged OCS uptake into the early fall indicated that the prairie likely store cumulatively more carbon than the corn site.

How and when photosynthesized carbon is released from an ecosystem should be considered when assessing the services provided by various ecosystems. For example, the prairie is productive for a longer portion of the growing season than corn, which is harvested before productivity stops in the prairie. Another factor affecting the carbon cycle of the prairie is managed burning. The Fermi tallgrass prairie was burned before the 2016 growing season. These carbon losses are not accounted for in R_{eco} estimates (*Petrie et al.*, 2016) and an overestimated NEE results in years when burning occurs. Other grasslands that undergo managed burning observe net neutral NEE (*Still et al.*, 2003) or net ecosystem carbon loss (*Zhang et al.*, 2011; *Vargas et al.*, 2012; *Logan and Brunsell*, 2015; *Petrie et al.*, 2016). Analysis of land use decisions should therefore track the carbon cycle beyond one growing season.

4.3 Comparison of Gross Primary Productivity Estimates

Hypothesis 3. Gross primary productivity derived from OCS flux (GPP_{OCS}) will be comparable to GPP derived from respiration (GPP_{Re}).

GPP_{OCS} overestimated GPP_{Re} by ~21% on average (-23.3 and -19.2 µmol m^{-2} s^{-1}, respectively) when using a constant LRU of 1.6. GPP_{OCS} estimates ranged from 55% to 121% of GPP_{Re} demonstrating the sensitivity of GPP_{OCS} to LRU estimates. Using the observed, site-specific LRU of 1.67, GPP_{OCS} overestimated GPP_{Re} by 12%.

GPP_{OCS} and GPP_{Re} were significantly correlated (Figure 25; R^2 = 0.566, p < 0.001, RMSE = 8.81, n = 150). Despite this correlation, GPP_{OCS} tended to overestimate $GPP_{Re.}$ This overestimate decreased to ~16% when comparing only the productive portion of the season before senescence. This difference is larger than the 4% reported by Blonquist et al. (2011), and the 6% average overestimation across five sites reported Asaf et al. (2013), though the previous studies

were based on short-term campaigns. Possible hypotheses for this disparity include (1), soil flux was underestimated, thus overestimating the leaf flux and resulting GPP_{OCS}; (2), LRU was underestimated, overestimating GPP_{OCS}; (3), daytime respiration was underestimated, underestimating GPP_{Re}; or (4), analytical bias in one or both methods, with an established GPP_{Re} bias of 20% (*Desai et al.*, 2008).

Adjusting the LRU within a range of published values (1.4–3.4; *Sandoval-Soto et al.*, 2005) demonstrated the sensitivity of GPP_{OCS} to LRU. Increasing the value beyond the calculated site-specific value of 1.67, an LRU of 2 resulted in GPP_{OCS} that underestimated GPP_{Re} by ~7%. Lastly, using the maximum observed LRU value of 3.4, GPP_{OCS} underestimated GPP_{Re} by ~45%.

A constant LRU of 1.6 is nearly the consensus in the literature (*Stimler et al.*, 2010, 2012; *Asaf et al.*, 2013; *Berkelhammer et al.*, 2014; *Billesbach et al.*, 2014; *Hilton et al.*, 2017). Even so, LRU can be highly variable, especially over the course of season-scale studies. One study using an LRU of 1.6 resulted in a 44% underestimation of GPP in direct sunlight, and a 19% overestimation in diffuse light, with calculated LRU ranging from 0.9 to 1.9 (*Maseyk et al.*, 2014). Regarding LRU values smaller than 1.6, a value of 1 is observed in C4 photosynthesizing plants (*Stimler et al.*, 2012), which would increase GPP_{OCS} relative to an LRU of 1.6. The Fermi prairie is a heterogeneous mix of C3 and C4 plants that shifts throughout the season, with C4 grasses dominating as the season progresses (*Still et al.*, 2003). Considering also that burning favors C4 plants (*Still et al.*, 2003), it should be noted that the Fermi site was burned prior to the 2016 growing season. A stronger C4 species distribution would have justified the use of an LRU lower than 1.6, which would have increased GPP_{OCS}. The observed LRU in the prairie

decreased as the season progressed, suggesting the increased influence of C4 plants. LRU instability occurred as plants senesced, which resulted in sporadic LRU spikes (Figure 39).

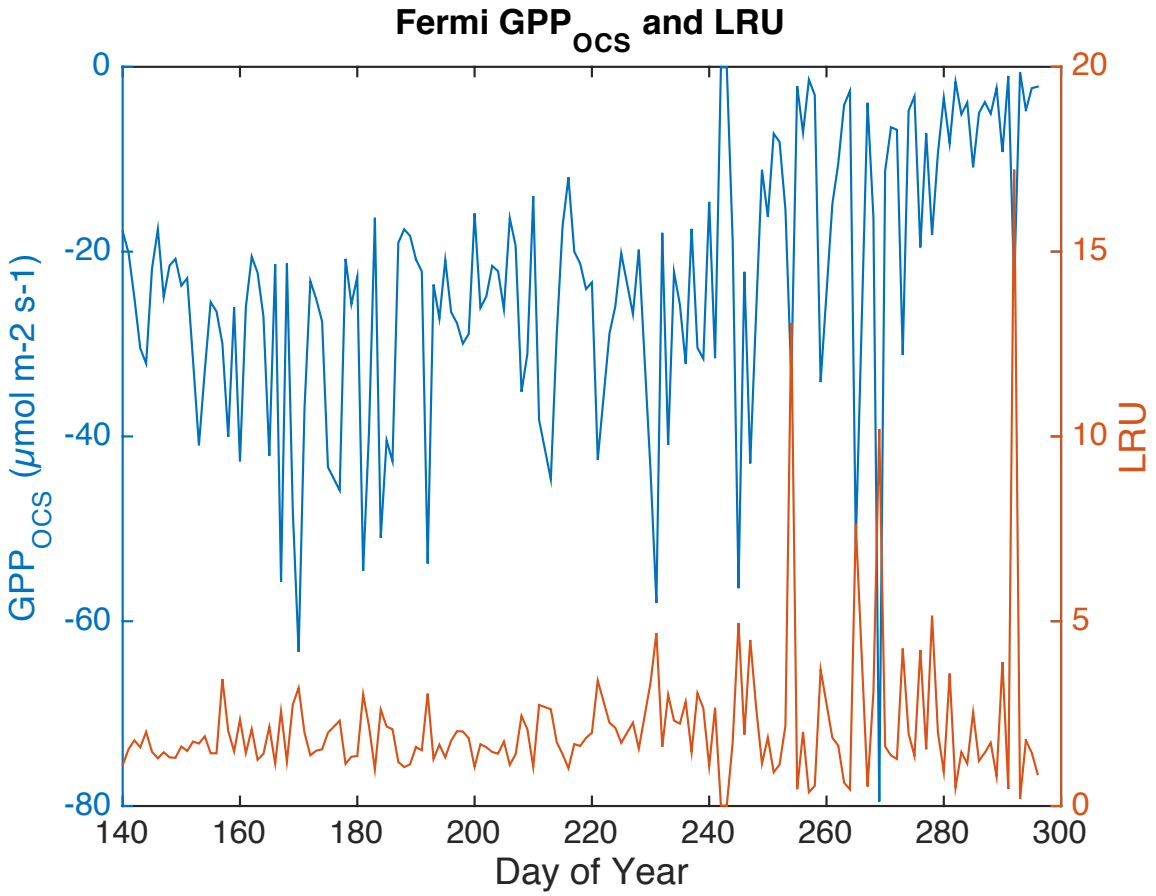

Figure 39. GPP_{OCS} and variable LRU through the period of observation. A constant LRU of 1.6 was used initially to calculate GPP_{OCS}. Resulting GPP_{OCS} during the main period of production (DOY < 254) was 16% higher than GPP_{Re}. Using the observed site-specific mean LRU of 1.67 resulted in GPP_{OCS} ~12% larger than GPP_{Re}.

4.4 Nighttime Stomatal Conductance and Transpiration

Hypothesis 4. OCS flux can be used as a proxy for nighttime stomatal conductance and transpiration.

Consistently negative nighttime F_{leaf} indicated that stomata were partially open and prairie stomata were more open at night than corn, on average (8.15% and 0.134%, respectively). The observed prairie E_n, however, was more correlated with VPD than nighttime F_{leaf} (Figure 30; $R^2 = 0.749$, $p < 0.001$ and $R^2 = 0.537$, $p < 0.001$, respectively). Therefore, VPD emerged as the main driver of E_n rather than g_s.

Linear regression models to determine the nighttime drivers of g_s were insufficient due to small nighttime flux signals and relatively high noise levels associated with nighttime fluxes. An alternative statistical approach isolated high fluxes and low fluxes by percentiles then compared them to eight ecosystem variables to determine drivers of g_s. As a first-order property, elevated WS resulted only in high fluxes. At low WS, low fluxes were more likely. This relationship suggests that WS acts as a mechanistic precondition for high nighttime OCS flux. Stratified and stable nighttime conditions in the boundary layer are the norm, and elevated nighttime OCS flux is thus an exception without turbulence increase OCS concentrations. High OCS concentrations are also a mechanistic precondition of high F_{leaf}, because they result from high WS.

Whereas WS and elevated OCS concentrations are associated with higher OCS fluxes, neither indicate a driver of g_s. Higher VPD was more associated with high OCS flux. If this indicates that higher VPD drives higher g_s, it would contradict studies showing an inverse relationship (*Muchow et al.*, 1980; *Oren et al.*, 2001; *Bucci et al.*, 2004; *Caird et al.*, 2007) or no relationship at all (*Barbour et al.*, 2005; *Caird et al.*, 2007).

Concentrations of CO_2 greater than ~500 ppm had a pronounced effect on OCS flux. No high OCS fluxes were observed at CO_2 concentrations > 500 ppm. Respired CO_2 accumulated to

elevated levels at low WS, but high fluxes occurred across the range of WS observed. This well-defined CO_2 threshold for F_{leaf} may indicate the effect of abscisic acid (ABA) in regulating stomatal conductance. ABA has been shown to reduce g_s (*Rawson and Clarke*, 1988; *Caird et al.*, 2007; *Howard and Donovan*, 2007), and this effect was more pronounced with increased CO_2 (*Leymarie et al.*, 1998, 1999; *Hetherington and Woodward*, 2003; *Caird et al.*, 2007; *Keenan et al.*, 2013). Above 500 ppm, it may be that CO_2 concentrations triggered the ABA effect, and reduced g_s and F_{leaf}. Although VPD drives E_n more than g_s, CO_2 concentrations still demonstrated an inverse correlation with E_n (Figure 40), with less water being transpired in the presence of elevated CO_2.

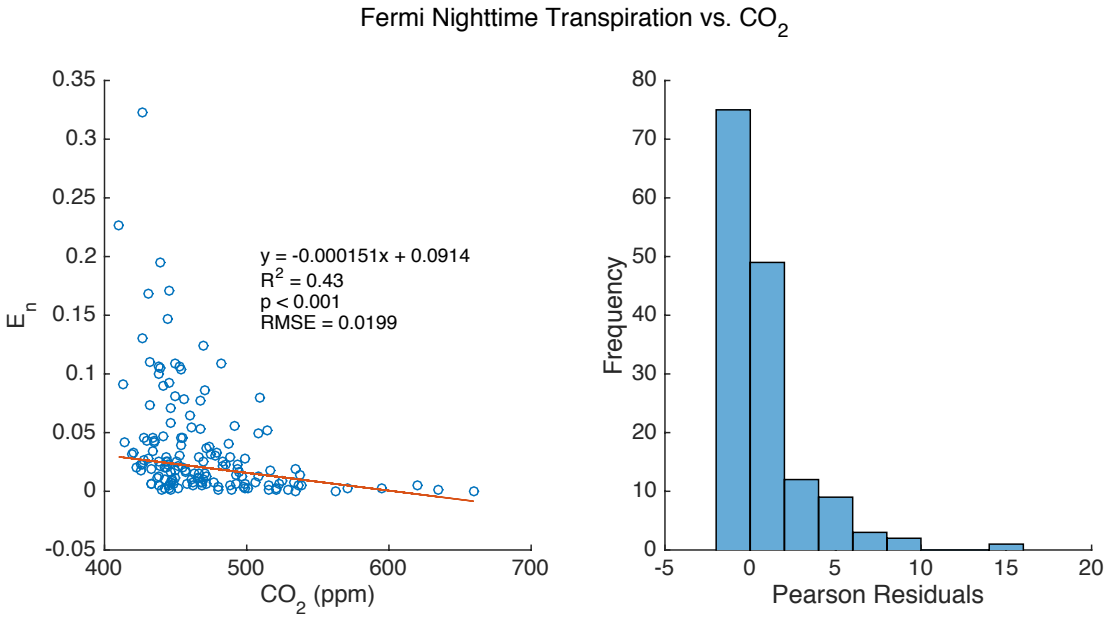

Figure 40. Fermi nighttime transpiration (E_n) vs. CO_2 concentration. Abscisic acid forces stomatal closure, especially when CO_2 is high (*Leymarie et al.*, 1998, 1999; *Hetherington and Woodward*, 2003; *Caird et al.*, 2007; *Keenan et al.*, 2013).

4.5 Humidity and Water Stress

Hypothesis 5. Nighttime stomatal conductance and transpiration will vary with changes in atmospheric humidity and water stress.

Minimal E_n occurred with relative humidity (R_h) > 90%. This relationship is predicted by the high correlation between E_n and VPD. Neither R_h nor SWC acted as primary drivers of nighttime g_s.

The relationship used to calculate the E_n proxy (Equation 13) is directly dependent on VPD. R_h is used to calculate VPD, so a high inverse correlation resulted between E_n and R_h (Figure 41A; $R^2 = 0.730$, $p < 0.001$). SWC correlated weakly with E_n with a nearly horizontal slope (Figure 41B; $R^2 = 0.334$, $p < 0.05$). This observation was in contrast to observations that g_s decreases with SWC (*Galmés et al.*, 2007) in order to minimize further water loss by E_n. The effect of R_h on E_n was much more direct, with R_h greater than ~80–90% being clearly associated with a decrease, if not total inhibition of nighttime water loss. At humidity < ~80% this relationship became more tenuous.

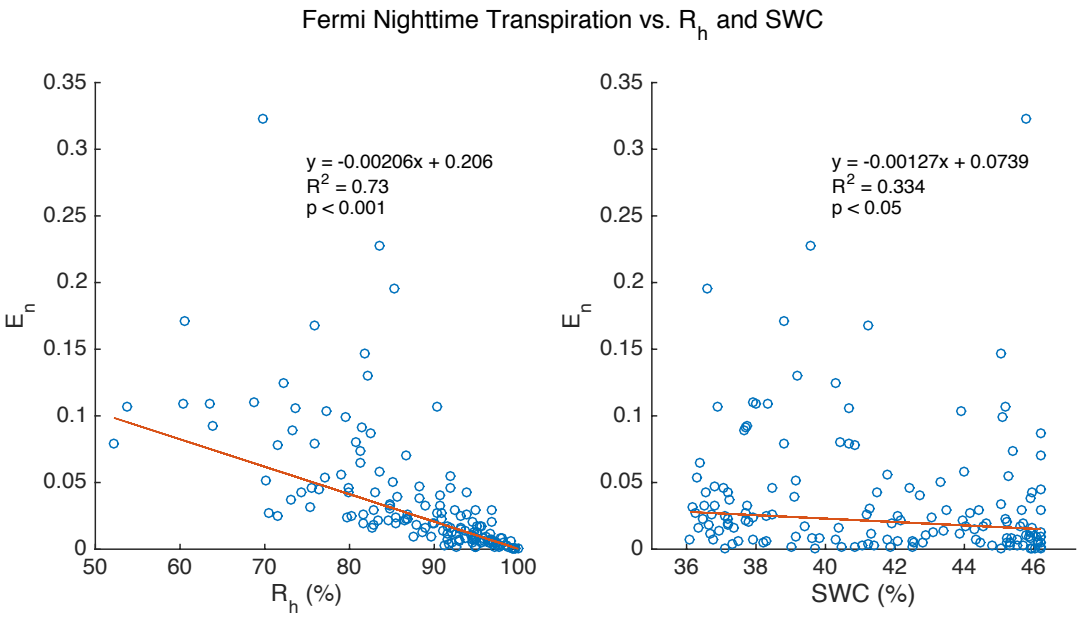

Figure 41. Fermi nighttime transpiration (E_n) vs. relative humidity (R_h) and soil water content (SWC). E_n is nearly completely shut off at R_h > ~90, indicating near complete stomatal closure. With a less defined relationship observed with E_n and SWC, all values of E_n occurred throughout the range of SWC, which is in contrast to literature indicating that E_n should decrease with SWC (*Galmés et al.*, 2007).

4.6 Inferring Ecosystem Responses to Climate Change

Driven by an increase in CO_2 emissions, climate change in Illinois will force higher temperatures with increased drought frequency over longer annual growing seasons (*Hayhoe et al.*, 2010). Our research suggests that these environmental changes will affect the carbon and water budgets of Illinois ecosystems in different ways.

Peak season corn E_n and F_{leaf} were both an order of magnitude lower than the prairie. Corn ecosystems therefore increase their WUE by minimizing E_n and photosynthesizing at rates higher than prairie ecosystems. Ratios of F_{leaf} night:day further illustrate this point with ~8% of prairie stomata remaining open at night compared to ~0.1% of corn stomata. But even though WUE estimates for corn can essentially ignore nighttime water loss, corn will still be subject to the increased daytime water budget demands expected with climate change.

The effects of increased atmospheric CO_2 reducing stomatal conductance are already triggering WUE increases in ecosystems (*Keenan et al.*, 2013, 2014). Therefore, it is anticipated that this "CO_2 fertilization effect" will decrease nighttime g_s in all ecosystems and force a concurrent WUE increase. Less water will be removed from the soil and transpired with less plant demand for water. Water runoff would also increase (*Wright and Wimberly*, 2013), especially in agricultural soils, which are more dense than undisturbed prairie soils (*Tisdall and Oades*, 1982; *Jastrow*, 1987). Ultimately, less plant transpiration would potentially make flood events more likely and increase soil moisture, which could increase respiration rates.

The tallgrass prairie was productive over a longer portion of the growing season than corn. Furthermore, the prairie demonstrated an opportunistic ability to turn production back on in the early fall when conditions were conducive to growth. The prairie has many other advantages in the context of climate change. Whereas prairies that undergo prescribed burning are often net carbon sources over the course of a year (*Zhang et al.*, 2011; *Vargas et al.*, 2012; *Logan and Brunsell*, 2015; *Petrie et al.*, 2016), photosynthesized carbon belowground in root and microbial biomass is retained. Belowground carbon assimilation is far more extensive in prairies than corn or soy. A 25-year-old prairie plot at Fermi restored from agriculture had more than twice the microbial biomass carbon than corn or soy plots in the same soil nearby (*Allison et al.*, 2005). These factors contribute to make soil carbon sequestration in prairies relatively quick and sustainable (*Matamala et al.*, 2008), as well as inexpensive (*Post et al.*, 2004).

Ecosystem services provided by prairies are not limited to carbon sequestration. The g_s of prairies allows them to draw down atmospheric pollutants at night when boundary layer stratification can make pollution especially harmful. Vegetation can act to reduce sulfur dioxide

(SO_2) and CO (*Nowak et al.*, 2006). Prairie grasses can also act as a sink for tropospheric ozone (*Mills et al.*, 2009). However, the ozone sink potential of grassland ecosystems may also hinder their productivity. Under elevated ozone concentrations, grasslands demonstrated a decreased response to ABA, and stomatal responses to drought conditions were impaired (*Mills et al.*, 2009).

Animal conservation and biodiversity also benefit from prairie ecosystems. A third of at-risk bird species are expected to lose 10% of their habitat between 2001 and 2051 (*Lawler et al.*, 2014). Prairie restorations increase the area endangered grassland birds have to nest and raise their young (*Heaton et al.*, 2008; *Pickett et al.*, 2008; *Wright and Wimberly*, 2013; *Lawler et al.*, 2014).

5 CONCLUSIONS

5.1 Overview

This first extended field application of the OCS flux-gradient method to constrain GPP and E_n demonstrated great potential in closing ecosystem carbon and water budgets. Therefore, this method could ultimately improve global estimates of how the biosphere will respond to climate change.

Vertical concentration gradients of OCS were continuously measured in a tallgrass prairie over 159 days of the 2016 growing season. These gradients were converted into OCS fluxes, which were dominated by plant uptake as demonstrated by the seasonal cycle of OCS flux coinciding with GPP from early season peak through senescence. On average, GPP_{OCS} compared well with absorbed PAR and the widely used GPP_{Re} method (-23.3 and -19.2 µmol m^{-2} s^{-1}, respectively), though the use of a constant LRU may have reduced the accuracy of GPP derived from the flux-gradient method. Nighttime g_s was observed using F_{leaf} as a proxy, revealing that prairie stomata remained more open at night and lost more water than corn. Prairie E_n was greatly inhibited when relative humidity was greater than 90%.

Corn demonstrated a near perfect absence of E_n, which may contribute to a higher WUE for corn. Both ecosystems—as well as others not studied here—are predicted to increase in WUE as atmospheric CO_2 concentrations rise, but the heterogeneous prairie provides a longer-term ecosystem service in sustainable soil carbon sequestration.

5.2 Further Study

Deploying season-scale OCS flux-gradient campaigns in other ecosystems will increase the accuracy of OCS-derived GPP and E_n as measurement techniques are inevitably refined. The influence of LRU values still needs more attention to determine whether a constant LRU is justified or if a variable LRU reduces bias. If a constant LRU is to be used, the 1.6 value requires further validation.

This study was conducted on terrain that is relatively flat with a short canopy. Campaigns conducted on terrain with more topographical relief or complex canopies will require more methodological considerations to account for differences in turbulent eddy diffusion and sub-canopy storage.

Field studies of OCS applying the flux-gradient method in as many ecosystems, on as many different terrains as possible would further our understanding of the potential of OCS to constrain GPP and E_n.

6 BIBLIOGRAPHY

Allison, V. J., R. M. Miller, J. D. Jastrow, R. Matamala, and D. R. Zak (2005), Changes in Soil Microbial Community Structure in a Tallgrass Prairie Chronosequence, *Soil Sci. Soc. Am. J.*, *69*(5), 1412, doi:10.2136/sssaj2004.0252.

Asaf, D., E. Rotenberg, F. Tatarinov, U. Dicken, S. A. Montzka, and D. Yakir (2013), Ecosystem photosynthesis inferred from measurements of carbonyl sulphide flux, *Nat. Geosci.*, *6*(3), 186–190, doi:10.1038/ngeo1730.

Barbour, M. M., L. A. Cernusak, D. Whitehead, K. L. Griffin, M. H. Turnbull, D. T. Tissue, and G. D. Farquhar (2005), Nocturnal stomatal conductance and implications for modelling $\delta^{18}O$ of leaf-respired CO_2 in temperate tree species, *Funct. Plant Biol.*, *32*(12), 1107, doi:10.1071/FP05118.

Barichivich, J., K. R. Briffa, R. B. Myneni, T. J. Osborn, T. M. Melvin, P. Ciais, S. Piao, and C. Tucker (2013), Large-scale variations in the vegetation growing season and annual cycle of atmospheric CO_2 at high northern latitudes from 1950 to 2011, *Glob. Chang. Biol.*, *19*(10), 3167–3183, doi:10.1111/gcb.12283.

Beniston, J. W., S. T. DuPont, J. D. Glover, R. Lal, and J. A. J. Dungait (2014), Soil organic carbon dynamics 75 years after land-use change in perennial grassland and annual wheat agricultural systems, *Biogeochemistry*, *120*(1–3), 37–49, doi:10.1007/s10533-014-9980-3.

Benyon, R. G. (1999), Nighttime water use in an irrigated Eucalyptus grandis plantation, *Tree Physiol.*, *19*(13), 853–859, doi:10.1093/treephys/19.13.853.

Berkelhammer, M., J. Hu, A. Bailey, D. C. Noone, C. J. Still, H. Barnard, D. Gochis, G. S. Hsiao, T. Rahn, and A. Turnipseed (2013), The nocturnal water cycle in an open-canopy forest, *J. Geophys. Res. Atmos.*, *118*(17), 10225–10242, doi:10.1002/jgrd.50701.

Berkelhammer, M., D. Asaf, C. Still, S. Montzka, D. Noone, M. Gupta, R. Provencal, H. Chen, and D. Yakir (2014), Constraining surface carbon fluxes using in situ measurements of carbonyl sulfide and carbon dioxide, *Global Biogeochem. Cycles*, *28*(2), 161–179, doi:10.1002/2013GB004644.

Berkelhammer, M., D. C. Noone, T. E. Wong, S. P. Burns, J. F. Knowles, A. Kaushik, P. D. Blanken, and M. W. Williams (2016a), Convergent approaches to determine an ecosystem's transpiration fraction, *Global Biogeochem. Cycles*, *30*(6), 933–951, doi:10.1002/2016GB005392.

Berkelhammer, M., H. C. Steen-Larsen, A. Cosgrove, A. J. Peters, R. Johnson, M. Hayden, and S. A. Montzka (2016b), Radiation and atmospheric circulation controls on carbonyl sulfide concentrations in the marine boundary layer, *J. Geophys. Res. Atmos.*, doi:10.1002/2016JD025437.

Berry, J. et al. (2013), A coupled model of the global cycles of carbonyl sulfide and CO 2: A possible new window on the carbon cycle, *J. Geophys. Res. Biogeosciences*, *118*(2), 842–852, doi:10.1002/jgrg.20068.

Billesbach, D. P., J. A. Berry, U. Seibt, K. Maseyk, M. S. Torn, M. L. Fischer, M. Abu-Naser, and J. E. Campbell (2014), Growing season eddy covariance measurements of carbonyl sulfide and CO_2 fluxes: COS and CO_2 relationships in Southern Great Plains winter wheat, *Agric. For. Meteorol.*, *184*, 48–55, doi:10.1016/j.agrformet.2013.06.007.

Bloem, E., S. Haneklaus, I. Salac, P. Wickenhäuser, and E. Schnug (2007), Facts and Fiction about Sulfur Metabolism in Relation to Plant-Pathogen Interactions, *Plant Biol.*, *9*(5), 596–607, doi:10.1055/s-2007-965420.

Blonquist, J. M., S. A. Montzka, J. W. Munger, D. Yakir, A. R. Desai, D. Dragoni, T. J. Griffis, R. K. Monson, R. L. Scott, and D. R. Bowling (2011), The potential of carbonyl sulfide as a proxy for gross primary production at flux tower sites, *J. Geophys. Res.*, *116*(G4), G04019, doi:10.1029/2011JG001723.

Bucci, S. J., F. G. Scholz, G. Goldstein, F. C. Meinzer, J. A. Hinojosa, W. A. Hoffmann, and A. C. Franco (2004), Processes preventing nocturnal equilibration between leaf and soil water potential in tropical savanna woody species, *Tree Physiol.*, *24*(10), 1119–1127, doi:10.1093/treephys/24.10.1119.

Caird, M. A., J. H. Richards, and L. A. Donovan (2007), Nighttime Stomatal Conductance and Transpiration in C3 and C4 Plants, *Plant Physiol.*, *143*(1).

Calderwood, A., and S. Kopriva (2014), Hydrogen sulfide in plants: From dissipation of excess sulfur to signaling molecule, *Nitric Oxide*, *41*, 72–78, doi:10.1016/j.niox.2014.02.005.

Campbell, J. E. et al. (2008), Photosynthetic Control of Atmospheric Carbonyl Sulfide During the Growing Season, *Science (80-.).*, *322*(5904).

Cheng, W., L. Zhang, C. Jiao, M. Su, T. Yang, L. Zhou, R. Peng, R. Wang, and C. Wang (2013), Hydrogen sulfide alleviates hypoxia-induced root tip death in Pisum sativum, *Plant Physiol. Biochem.*, *70*, 278–286, doi:10.1016/j.plaphy.2013.05.042.

Ciais, P. et al. (2005), Europe-wide reduction in primary productivity caused by the heat and drought in 2003, *Nature*, *437*(7058), 529–533, doi:10.1038/nature03972.

Commane, R., L. K. Meredith, I. T. Baker, J. A. Berry, J. W. Munger, S. A. Montzka, P. H. Templer, S. M. Juice, M. S. Zahniser, and S. C. Wofsy (2015), Seasonal fluxes of carbonyl sulfide in a midlatitude forest., *Proc. Natl. Acad. Sci. U. S. A.*, *112*(46), 14162–7, doi:10.1073/pnas.1504131112.

Cook, B. D., J. D. Jastrow, and R. M. Miller (1988), Root and mycorrhizal endophyte development in a chronosequence of restored tallgrass prairie, *New Phytol.*, *110*(3), 355–362, doi:10.1111/j.1469-8137.1988.tb00272.x.

Coupel-Ledru, A., E. Lebon, A. Christophe, A. Gallo, P. Gago, F. Pantin, A. Doligez, and T. Simonneau (2016), Reduced nighttime transpiration is a relevant breeding target for high water-use efficiency in grapevine., *Proc. Natl. Acad. Sci. U. S. A.*, *113*(32), 8963–8, doi:10.1073/pnas.1600826113.

Daley, M. J., and N. G. Phillips (2006), Interspecific variation in nighttime transpiration and stomatal conductance in a mixed New England deciduous forest, *Tree Physiol.*, *26*(4), 411–419, doi:10.1093/treephys/26.4.411.

Derner, J. D., T. W. Boutton, and D. D. Briske (2006), Grazing and Ecosystem Carbon Storage in the North American Great Plains, *Plant Soil*, *280*(1–2), 77–90, doi:10.1007/s11104-005-2554-3.

Desai, A. R. et al. (2008), Cross-site evaluation of eddy covariance GPP and RE decomposition techniques, *Agric. For. Meteorol.*, *148*(6–7), 821–838, doi:10.1016/j.agrformet.2007.11.012.

Van Diest, H., and J. Kesselmeier (2008), Soil atmosphere exchange of carbonyl sulfide (COS) regulated by diffusivity depending on water-filled pore space, *Biogeosciences*, *5*(2), 475–483.

Donovan, L. A., D. J. Grisé, J. B. West, R. A. Pappert, N. N. Alder, and J. H. Richards (1999), Predawn disequilibrium between plant and soil water potentials in two cold-desert shrubs, *Oecologia*, *120*(2), 209–217, doi:10.1007/s004420050850.

Elliott, E. T. (1986), Aggregate Structure and Carbon, Nitrogen, and Phosphorus in Native and Cultivated Soils1, *Soil Sci. Soc. Am. J.*, *50*(3), 627, doi:10.2136/sssaj1986.03615995005000030017x.

Field, C. B., R. B. Jackson, and H. A. Mooney (1995), Stomatal responses to increased CO_2: implications from the plant to the global scale, *Plant, Cell Environ.*, *18*(10), 1214–1225, doi:10.1111/j.1365-3040.1995.tb00630.x.

Fisher, J. B., D. D. Baldocchi, L. Misson, T. E. Dawson, and A. H. Goldstein (2007), What the towers don't see at night: nocturnal sap flow in trees and shrubs at two AmeriFlux sites in California, *Tree Physiol.*, *27*(4), 597–610, doi:10.1093/treephys/27.4.597.

Flanagan, L. B., L. A. Wever, and P. J. Carlson (2002), Seasonal and interannual variation in carbon dioxide exchange and carbon balance in a northern temperate grassland, *Glob. Chang. Biol.*, *8*(7), 599–615, doi:10.1046/j.1365-2486.2002.00491.x.

Flexas, J., and H. Medrano (2002), Drought-inhibition of Photosynthesis in C3 Plants: Stomatal and Non-stomatal Limitations Revisited, *Ann. Bot.*, *89*(2), 183–189, doi:10.1093/aob/mcf027.

Galmés, J., J. Flexas, R. Savé, and H. Medrano (2007), Water relations and stomatal characteristics of Mediterranean plants with different growth forms and leaf habits: responses to water stress and recovery, *Plant Soil*, *290*(1–2), 139–155, doi:10.1007/s11104-006-9148-6.

Green, S. ., K. . McNaughton, and B. . Clothier (1989), Observations of night-time water use in kiwifruit vines and apple trees, *Agric. For. Meteorol.*, *48*(3–4), 251–261, doi:10.1016/0168-1923(89)90072-5.

Guanter, L. et al. (2014), Global and time-resolved monitoring of crop photosynthesis with chlorophyll fluorescence., *Proc. Natl. Acad. Sci. U. S. A.*, *111*(14), E1327-33, doi:10.1073/pnas.1320008111.

Hayhoe, K., J. VanDorn, T. Croley, N. Schlegal, and D. Wuebbles (2010), Regional climate change projections for Chicago and the US Great Lakes, *J. Great Lakes Res.*, *36*, 7–21, doi:10.1016/j.jglr.2010.03.012.

Heaton, E. A., F. G. Dohleman, and S. P. Long (2008), Meeting US biofuel goals with less land: the potential of Miscanthus, *Glob. Chang. Biol.*, *14*(9), 2000–2014, doi:10.1111/j.1365-2486.2008.01662.x.

Herzog, K. M., R. Thum, G. Kronfus, H.-J. Heldstab, and R. Häsler (1998), Patterns and mechanisms of transpiration in a large subalpine Norway spruce (Picea abies (L.) Karst.), *Ecol. Res.*, *13*(2), 105–116, doi:10.1046/j.1440-1703.1998.00250.x.

Heskel, M. A., O. K. Atkin, M. H. Turnbull, and K. L. Griffin (2013), Bringing the Kok effect to light: A review on the integration of daytime respiration and net ecosystem exchange, *Ecosphere*, *4*(8), art98, doi:10.1890/ES13-00120.1.

Hetherington, A. M., and F. I. Woodward (2003), The role of stomata in sensing and driving environmental change, *Nature*, *424*(6951), 901–908, doi:10.1038/nature01843.

Hilton, T. W., M. E. Whelan, A. Zumkehr, S. Kulkarni, J. A. Berry, I. T. Baker, S. A. Montzka, C. Sweeney, B. R. Miller, and J. Elliott Campbell (2017), Peak growing season gross uptake of carbon in North America is largest in the Midwest USA, *Nat. Clim. Chang.*, *7*(6), 450–454, doi:10.1038/nclimate3272.

Howard, A. R., and L. A. Donovan (2007), Helianthus Nighttime Conductance and Transpiration Respond to Soil Water But Not Nutrient Availability, *Plant Physiol.*, *143*(1).

Huntzinger, D. N. et al. (2012), North American Carbon Program (NACP) regional interim synthesis: Terrestrial biospheric model intercomparison, *Ecol. Modell.*, *232*, 144–157, doi:10.1016/j.ecolmodel.2012.02.004.

Jasechko, S., Z. D. Sharp, J. J. Gibson, S. J. Birks, Y. Yi, and P. J. Fawcett (2013), Terrestrial water fluxes dominated by transpiration, *Nature*, *496*(7445), 347–350, doi:10.1038/nature11983.

Jastrow, J. D. (1987), Changes in Soil Aggregation Associated with Tallgrass Prairie Restoration, *Am. J. Bot.*, *74*(11), 1656, doi:10.2307/2444134.

Jastrow, J. D. (1996), Soil aggregate formation and the accrual of particulate and mineral-associated organic matter, *Soil Biol. Biochem.*, *28*(4–5), 665–676, doi:10.1016/0038-0717(95)00159-X.

Jastrow, J. D., R. M. Miller, and J. Lussenhop (1998), Contributions of interacting biological mechanisms to soil aggregate stabilization in restored prairie1The submitted manuscript has been created by the University of Chicago as operator of Argonne National Laboratory under Contract No. W-31-109-ENG-38 wit, *Soil Biol. Biochem.*, *30*(7), 905–916, doi:10.1016/S0038-0717(97)00207-1.

Jin, Z., J. Shen, Z. Qiao, G. Yang, R. Wang, and Y. Pei (2011), *Hydrogen sulfide improves drought resistance in Arabidopsis thaliana*.

Kavanagh, K. L., R. Pangle, and A. D. Schotzko (2007), Nocturnal transpiration causing disequilibrium between soil and stem predawn water potential in mixed conifer forests of Idaho, *Tree Physiol.*, *27*(4), 621–629, doi:10.1093/treephys/27.4.621.

Keenan, T. F., D. Y. Hollinger, G. Bohrer, D. Dragoni, J. W. Munger, H. P. Schmid, and A. D. Richardson (2013), Increase in forest water-use efficiency as atmospheric carbon dioxide concentrations rise., *Nature*, *499*(7458), 324–7, doi:10.1038/nature12291.

Keenan, T. F. et al. (2014), Net carbon uptake has increased through warming-induced changes in temperate forest phenology, *Nat. Clim. Chang.*, *4*(7), 598–604, doi:10.1038/nclimate2253.

Kesselmeier, J., N. Teusch, and U. Kuhn (1999), Controlling variables for the uptake of atmospheric carbonyl sulfide (COS) by soil, *J. Geophys. Res.*, *104*, 11577–11584.

Kimball, B. A., and S. B. Idso (1983), Increasing atmospheric CO_2: effects on crop yield, water use and climate, *Agric. Water Manag.*, *7*(1–3), 55–72, doi:10.1016/0378-3774(83)90075-6.

Kok, B. (1949), On the interrelation of respiration and photosynthesis in green plants, *Biochim. Biophys. Acta*, *3*, 625–631, doi:10.1016/0006-3002(49)90136-5.

Kooijmans, L. M. J. et al. (2017), Canopy uptake dominates nighttime carbonyl sulfide fluxes in a boreal forest, *Atmos. Chem. Phys. Discuss.*, 1–24, doi:10.5194/acp-2017-407.

Kuhn, U. (1999), Carbonyl sulfide exchange on an ecosystem scale: soil represents a dominant sink for atmospheric COS, *Atmos. Environ.*, *33*(6), 995–1008, doi:10.1016/S1352-2310(98)00211-8.

Lamers, L. P. M., L. L. Govers, I. C. J. M. Janssen, J. J. M. Geurts, M. E. W. Van der Welle, M. M. Van Katwijk, T. Van der Heide, J. G. M. Roelofs, and A. J. P. Smolders (2013), Sulfide as a soil phytotoxin-a review., *Front. Plant Sci.*, *4*, 268, doi:10.3389/fpls.2013.00268.

Lawler, J. J., D. J. Lewis, E. Nelson, A. J. Plantinga, S. Polasky, J. C. Withey, D. P. Helmers, S. Martinuzzi, D. Pennington, and V. C. Radeloff (2014), Projected land-use change impacts on ecosystem services in the United States., *Proc. Natl. Acad. Sci. U. S. A.*, *111*(20), 7492–7, doi:10.1073/pnas.1405557111.

Leymarie, J., G. Lascève, and A. Vavasseur (1998), Interaction of stomatal responses to ABA and CO_2 in Arabidopsis thaliana, *Aust. J. Plant Physiol.*, *25*(7), 785, doi:10.1071/PP98031.

Leymarie, J., G. Lasceve, and A. Vavasseur (1999), Elevated CO_2 enhances stomatal responses to osmotic stress and abscisic acid in Arabidopsis thaliana, *Plant, Cell Environ.*, *22*(3), 301–308, doi:10.1046/j.1365-3040.1999.00403.x.

Liu, J., C. Geng, Y. Mu, Y. Zhang, Z. Xu, and H. Wu (2010), Exchange of carbonyl sulfide (COS) between the atmosphere and various soils in China, *Biogeosciences*, *7*(2), 753–762, doi:10.5194/bg-7-753-2010.

Logan, K. E., and N. A. Brunsell (2015), Influence of drought on growing season carbon and water cycling with changing land cover, *Agric. For. Meteorol.*, *213*(213), 217–225, doi:10.1016/j.agrformet.2015.07.002.

Maseyk, K., J. A. Berry, D. Billesbach, J. E. Campbell, M. S. Torn, M. Zahniser, and U. Seibt (2014), Sources and sinks of carbonyl sulfide in an agricultural field in the Southern Great Plains., *Proc. Natl. Acad. Sci. U. S. A.*, *111*(25), 9064–9, doi:10.1073/pnas.1319132111.

Maseyk, K. S., U. Seibt, J. A. Berry, D. P. Billesbach, J. Campbell, and M. S. Torn (2012), Strong soil source of carbonyl sulfide in an agricultural field, in *American Geophysical Union, Fall Meeting 2012, abstract #B44A-04*.

Matamala, R., J. D. Jastrow, R. M. Miller, and C. T. Garten (2008), Temporal Changes In C And N Stocks Of Restored Prairie: Implications For C Sequestration Strategies, *Ecol. Appl.*, *18*(6), 1470–1488, doi:10.1890/07-1609.1.

Matyssek, R., M. S. Gunthardt-Goerg, S. Maurer, and T. Keller (1995), Nighttime exposure to ozone reduces whole-plant production in Betula pendula, *Tree Physiol.*, *15*(3), 159–165, doi:10.1093/treephys/15.3.159.

Meredith, L. K., R. Commane, J. W. Munger, A. Dunn, J. Tang, S. C. Wofsy, and R. G. Prinn (2014), Ecosystem fluxes of hydrogen: a comparison of flux-gradient methods, *Atmos. Meas. Tech.*, *7*(9), 2787–2805, doi:10.5194/amt-7-2787-2014.

Miller, R. M., and J. D. Jastrow (1990), Hierarchy of root and mycorrhizal fungal interactions with soil aggregation, *Soil Biol. Biochem.*, *22*(5), 579–584, doi:10.1016/0038-0717(90)90001-G.

Miller, R. M., S. P. Miller, J. D. Jastrow, and C. B. Rivetta (2002), Mycorrhizal mediated feedbacks influence net carbon gain and nutrient uptake in Andropogon gerardii, *New Phytol.*, *155*(1), 149–162, doi:10.1046/j.1469-8137.2002.00429.x.

Mills, G., F. Hayes, S. WIlkinson, and W. J. Davies (2009), Chronic exposure to increasing background ozone impairs stomatal functioning in grassland species, *Glob. Chang. Biol.*, *15*(6), 1522–1533, doi:10.1111/j.1365-2486.2008.01798.x.

Montzka, S. A., P. Calvert, B. D. Hall, J. W. Elkins, T. J. Conway, P. P. Tans, and C. Sweeney (2007), On the global distribution, seasonality, and budget of atmospheric carbonyl sulfide (COS) and some similarities to CO_2, *J. Geophys. Res.*, *112*(D9), D09302, doi:10.1029/2006JD007665.

Morgan, J. A. et al. (2004), Water relations in grassland and desert ecosystems exposed to elevated atmospheric CO_2, *Oecologia*, *140*(1), 11–25, doi:10.1007/s00442-004-1550-2.

Morgan, J. A., D. R. LeCain, E. Pendall, D. M. Blumenthal, B. A. Kimball, Y. Carrillo, D. G. Williams, J. Heisler-White, F. A. Dijkstra, and M. West (2011), C4 grasses prosper as carbon dioxide eliminates desiccation in warmed semi-arid grassland, *Nature*, *476*(7359), 202–205, doi:10.1038/nature10274.

Morison, J. I. L., and R. M. Gifford (1983), Stomatal Sensitivity to Carbon Dioxide and Humidity, *Plant Physiol.*, *71*(4).

Muchow, R., M. Ludlow, M. Fisher, and R. Myers (1980), Stomatal Behaviour of Kenaf and Sorghum in a Semiarid Tropical Environment. I. During the Night, *Aust. J. Plant Physiol.*, *7*(5), 609, doi:10.1071/PP9800609.

Nowak, D. J., D. E. Crane, and J. C. Stevens (2006), Air pollution removal by urban trees and shrubs in the United States, *Urban For. Urban Green. 4115-123*, *4*.

Oades, J. M. (1984), Soil organic matter and structural stability: mechanisms and implications for management, *Plant Soil*, *76*(1–3), 319–337, doi:10.1007/BF02205590.

Oren, R., J. S. Sperry, B. E. Ewers, D. E. Pataki, N. Phillips, and J. P. Megonigal (2001), Sensitivity of mean canopy stomatal conductance to vapor pressure deficit in a flooded Taxodium distichum L. forest: hydraulic and non-hydraulic effects, *Oecologia*, *126*(1), 21–29, doi:10.1007/s004420000497.

Papale, D. et al. (2006), Towards a standardized processing of Net Ecosystem Exchange measured with eddy covariance technique: algorithms and uncertainty estimation, *Biogeosciences*, *3*(4), 571–583.

Papenbrock, J., A. Riemenschneider, A. Kamp, H. N. Schulz-Vogt, and A. Schmidt (2007), Characterization of Cysteine-Degrading and H $_2$ S-Releasing Enzymes of Higher Plants - From the Field to the Test Tube and Back, *Plant Biol.*, *9*(5), 582–588, doi:10.1055/s-2007-965424.

Petrie, M. D., N. A. Brunsell, R. Vargas, S. L. Collins, L. B. Flanagan, N. P. Hanan, M. E. Litvak, and A. E. Suyker (2016), The sensitivity of carbon exchanges in Great Plains grasslands to precipitation variability, *J. Geophys. Res. Biogeosciences*, (121), 280–294, doi:10.1002/2015JG003205.

Piao, S. et al. (2008), Net carbon dioxide losses of northern ecosystems in response to autumn warming, *Nature*, *451*(7174), 49–52, doi:10.1038/nature06444.

Pickett, S. T. a. et al. (2008), Beyond Urban Legends: An Emerging Framework of Urban Ecology, as Illustrated by the Baltimore Ecosystem Study, *Bioscience*, *58*(2), 139.

Post, W. M., R. C. Izaurralde, J. D. Jastrow, B. A. McCarl, J. E. Amonette, V. L. Bailey, P. M. JARDINE, T. O. WEST, and J. ZHOU (2004), Enhancement of Carbon Sequestration in US Soils, *Bioscience*, *54*(10), 895, doi:10.1641/0006-3568(2004)054[0895:EOCSIU]2.0.CO;2.

Protoschill-Krebs, G., C. Wilhelm, and J. Kesselmeier (1996), Consumption of carbonyl sulphide (COS) by higher plant carbonic anhydrase (CA), *Atmos. Environ.*, *30*(18), 3151–3156, doi:10.1016/1352-2310(96)00026-X.

Rausch, T., and A. Wachter (2005), Sulfur metabolism: a versatile platform for launching defence operations, *Trends Plant Sci.*, *10*(10), 503–509, doi:10.1016/j.tplants.2005.08.006.

Rawson, H., and J. Clarke (1988), Nocturnal Transpiration in Wheat, *Aust. J. Plant Physiol.*, *15*(3), 397, doi:10.1071/PP9880397.

Reichstein, M., J. D. Tenhunen, O. Roupsard, J. Ourcival, S. Rambal, F. Miglietta, A. Peressotti, M. Pecchiari, G. Tirone, and R. Valentini (2002), Severe drought effects on ecosystem CO_2 and H_2O fluxes at three Mediterranean evergreen sites: revision of current hypotheses?, *Glob. Chang. Biol.*, *8*(10), 999–1017, doi:10.1046/j.1365-2486.2002.00530.x.

Reichstein, M. et al. (2005), On the separation of net ecosystem exchange into assimilation and ecosystem respiration: Review and improved algorithm, *Glob. Chang. Biol.*, *11*(9), 1424–1439, doi:10.1111/j.1365-2486.2005.001002.x.

Sandoval-Soto, L., M. Stanimirov, M. von Hobe, V. Schmitt, J. Valdes, A. Wild, and J. Kesselmeier (2005), Global uptake of carbonyl sulfide (COS) by terrestrial vegetation: Estimates corrected by deposition velocities normalized to the uptake of carbon dioxide (CO₂), *Biogeosciences*, *2*(2), 125–132, doi:10.5194/bg-2-125-2005.

Schaefer, K. et al. (2012), A model-data comparison of gross primary productivity: Results from the North American Carbon Program site synthesis, *J. Geophys. Res. Biogeosciences*, *117*(G3), n/a-n/a, doi:10.1029/2012JG001960.

Seibt, U., L. Wingate, J. Lloyd, and J. A. Berry (2006), Diurnally variable δ^{18}O signatures of soil CO_2 fluxes indicate carbonic anhydrase activity in a forest soil, *J. Geophys. Res. Biogeosciences*, *111*(G4), doi:10.1029/2006JG000177.

Seibt, U., J. Kesselmeier, L. Sandoval-Soto, U. Kuhn, and J. A. Berry (2010), A kinetic analysis of leaf uptake of COS and its relation to transpiration, photosynthesis and carbon isotope fractionation, *Biogeosciences*, *7*(1), 333–341, doi:10.5194/bg-7-333-2010.

Simmons, J. S., L. Klemedtsson, H. Hultberg, and M. E. Hines (1999), Consumption of atmospheric carbonyl sulfide by coniferous boreal forest soils, *J. Geophys. Res. Atmos.*, *104*(D9), 11569–11576, doi:10.1029/1999JD900149.

Snyder, K. A., J. H. Richards, and L. A. Donovan (2003), Night-time conductance in C3 and C4 species: do plants lose water at night?, *J. Exp. Bot.*, *54*(383), 861–865, doi:10.1093/jxb/erg082.

Still, C. J., J. A. Berry, M. Ribas-Carbo, and B. R. Helliker (2003), The contribution of C 3 and C 4 plants to the carbon cycle of a tallgrass prairie: an isotopic approach, *Oecologia*, *136*(3), 347–359, doi:10.1007/s00442-003-1274-8.

Stimler, K., D. Nelson, and D. Yakir (2009), High precision measurements of atmospheric concentrations and plant exchange rates of carbonyl sulfide using mid-IR quantum cascade laser, *Glob. Chang. Biol.*, *16*(9), 2496–2503, doi:10.1111/j.1365-2486.2009.02088.x.

Stimler, K., S. A. Montzka, J. A. Berry, Y. Rudich, and D. Yakir (2010), Relationships between carbonyl sulfide (COS) and CO_2 during leaf gas exchange, *New Phytol.*, *186*(4), 869–878, doi:10.1111/j.1469-8137.2010.03218.x.

Stimler, K., J. A. Berry, and D. Yakir (2012), Effects of carbonyl sulfide and carbonic anhydrase on stomatal conductance., *Plant Physiol.*, *158*(1), 524–30, doi:10.1104/pp.111.185926.

Stull, R. B. (2012), An introduction to boundary layer meteorology, *Springer Sci. Bus. Media*, *13*.

Sun, J., R. Wang, X. Zhang, Y. Yu, R. Zhao, Z. Li, and S. Chen (2013), Hydrogen sulfide alleviates cadmium toxicity through regulations of cadmium transport across the plasma and vacuolar membranes in Populus euphratica cells, *Plant Physiol. Biochem.*, *65*, 67–74, doi:10.1016/j.plaphy.2013.01.003.

Sun, J., J. Wu, D. Guan, F. Yao, F. Yuan, A. Wang, and C. Jin (2014), Estimating Daytime Ecosystem Respiration to Improve Estimates of Gross Primary Production of a Temperate Forest, edited by W. L. Araujo, *PLoS One*, *9*(11), e113512, doi:10.1371/journal.pone.0113512.

Taylor, K. E., R. J. Stouffer, G. A. Meehl, K. E. Taylor, R. J. Stouffer, and G. A. Meehl (2012), An Overview of CMIP5 and the Experiment Design, *Bull. Am. Meteorol. Soc.*, *93*(4), 485–498, doi:10.1175/BAMS-D-11-00094.1.

Tisdall, J. M., and J. M. Oades (1982), Organic matter and water-stable aggregates in soils, *J. Soil Sci.*, *33*(2), 141–163, doi:10.1111/j.1365-2389.1982.tb01755.x.

Vargas, R., S. L. Collins, M. L. Thomey, J. E. Johnson, R. F. Brown, D. O. Natvig, and M. T. Friggens (2012), Precipitation variability and fire influence the temporal dynamics of soil CO_2 efflux in an arid grassland, *Glob. Chang. Biol.*, *18*(4), 1401–1411, doi:10.1111/j.1365-2486.2011.02628.x.

Wand, S. J. E., G. F. Midgley, M. H. Jones, and P. S. Curtis (1999), Responses of wild C4 and C3 grass (Poaceae) species to elevated atmospheric CO_2 concentration: a meta-analytic test of current theories and perceptions, *Glob. Chang. Biol.*, *5*(6), 723–741, doi:10.1046/j.1365-2486.1999.00265.x.

Wang, B.-L., L. Shi, Y.-X. Li, and W.-H. Zhang (2010), Boron toxicity is alleviated by hydrogen sulfide in cucumber (Cucumis sativus L.) seedlings, *Planta*, *231*(6), 1301–1309, doi:10.1007/s00425-010-1134-9.

Wehr, R., J. W. Munger, J. B. McManus, D. D. Nelson, M. S. Zahniser, E. A. Davidson, S. C. Wofsy, and S. R. Saleska (2016), Seasonality of temperate forest photosynthesis and daytime respiration, *Nature*, *534*(7609), 680–683, doi:10.1038/nature17966.

Whelan, M. E., D.-H. Min, and R. C. Rhew (2013), Salt marsh vegetation as a carbonyl sulfide (COS) source to the atmosphere, *Atmos. Environ.*, *73*, 131–137, doi:10.1016/j.atmosenv.2013.02.048.

Whelan, M. E., T. W. Hilton, J. A. Berry, M. Berkelhammer, A. R. Desai, and J. E. Campbell (2016), Carbonyl sulfide exchange in soils for better estimates of ecosystem carbon uptake, *Atmos. Chem. Phys.*, *16*(6), 3711–3726, doi:10.5194/acp-16-3711-2016.

Wingate, L., U. Seibt, K. Maseyk, J. Ogée, P. Almeida, D. Yakir, J. S. PEREIRA, and M. MENCUCCINI (2008), Evaporation and carbonic anhydrase activity recorded in oxygen isotope signatures of net CO 2 fluxes from a Mediterranean soil, *Glob. Chang. Biol.*, *14*(9), 2178–2193, doi:10.1111/j.1365-2486.2008.01635.x.

Winner, W. E., A. S. Lefohn, I. S. Cotter, C. S. Greitner, J. Nellessen, L. R. McEvoy, R. L. Olson, C. J. Atkinson, L. D. Moore, and L. D. Moore (1989), Plant responses to elevational gradients of O(3) exposures in Virginia., *Proc. Natl. Acad. Sci. U. S. A.*, *86*(22), 8828–32.

Wright, C. K., and M. C. Wimberly (2013), Recent land use change in the Western Corn Belt threatens grasslands and wetlands., *Proc. Natl. Acad. Sci. U. S. A.*, *110*(10), 4134–9, doi:10.1073/pnas.1215404110.

Yakir, D., and X.-F. Wang (1996), Fluxes of CO_2 and water between terrestrial vegetation and the atmosphere estimated from isotope measurements, *Nature*, *380*(6574), 515–517, doi:10.1038/380515a0.

Zhang, H., Z.-Q. Tan, L.-Y. Hu, S.-H. Wang, J.-P. Luo, and R. L. Jones (2010a), Hydrogen Sulfide Alleviates Aluminum Toxicity in Germinating Wheat Seedlings, *J. Integr. Plant Biol.*, *52*(6), 556–567, doi:10.1111/j.1744-7909.2010.00946.x.

Zhang, L., B. K. Wylie, L. Ji, T. G. Gilmanov, and L. L. Tieszen (2010b), Climate-Driven Interannual Variability in Net Ecosystem Exchange in the Northern Great Plains Grasslands, *Rangel. Ecol. Manag.*, *63*(1), 40–50, doi:10.2111/08-232.1.

Zhang, L., B. K. Wylie, L. Ji, T. G. Gilmanov, L. L. Tieszen, and D. M. Howard (2011), Upscaling carbon fluxes over the Great Plains grasslands: Sinks and sources, *J. Geophys. Res.*, *116*(G3), G00J03, doi:10.1029/2010JG001504.

Zhang, Y., X. Xiao, S. Zhou, P. Ciais, H. McCarthy, and Y. Luo (2016), Canopy and physiological controls of GPP during drought and heat wave, *Geophys. Res. Lett.*, *43*(7), 3325–3333, doi:10.1002/2016GL068501.

Figure 42. BND soil map (https://websoilsurvey.nrcs.usda.gov).

Figure 43. EF soil map (https://websoilsurvey.nrcs.usda.gov).

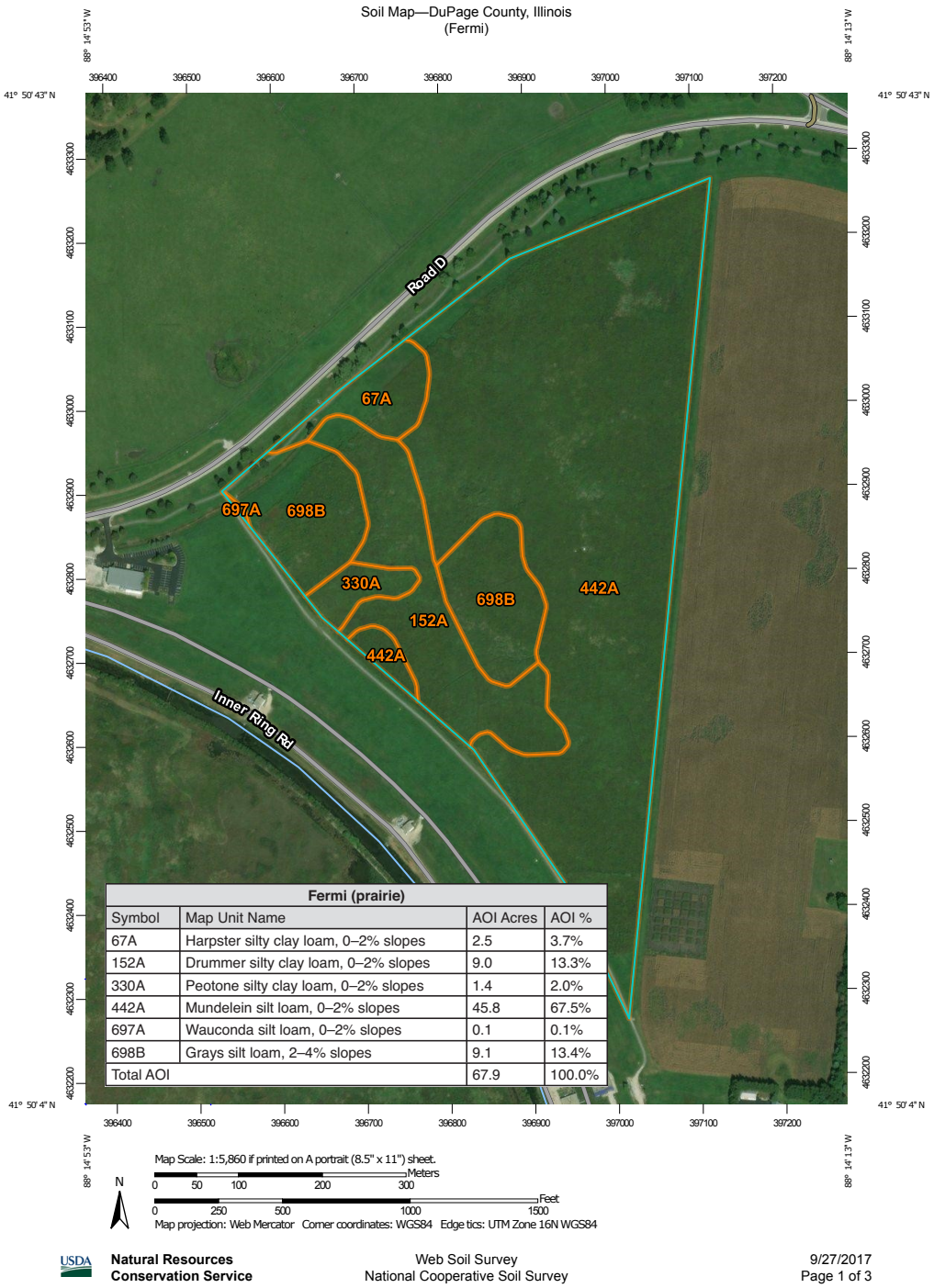

Fermi (prairie)

Symbol	Map Unit Name	AOI Acres	AOI %
67A	Harpster silty clay loam, 0–2% slopes	2.5	3.7%
152A	Drummer silty clay loam, 0–2% slopes	9.0	13.3%
330A	Peotone silty clay loam, 0–2% slopes	1.4	2.0%
442A	Mundelein silt loam, 0–2% slopes	45.8	67.5%
697A	Wauconda silt loam, 0–2% slopes	0.1	0.1%
698B	Grays silt loam, 2–4% slopes	9.1	13.4%
Total AOI		67.9	100.0%

Figure 44. Fermi soil map (https://websoilsurvey.nrcs.usda.gov).

Table 5. Whole-night (n) linear regressions, F_{leaf} vs. eight ecosystem variables, sorted by R^2.

F_{leaf} *vs.*	*Slope*	R^2	*p-Value*
WS	-1.24	0.293	2.79E-12
CO_2	0.0186	0.220	2.93E-07
OCS	-0.0154	0.204	3.88E-08
T_s	0.129	0.119	0.0191
T_a	0.0962	0.105	0.00965
R_n	0.0260	0.0905	0.0345
SWC	-0.0743	0.0894	0.115
VPD	-0.156	0.0874	0.0664

Table 6. First half-night (n_1) linear regressions, F_{leaf} vs. eight ecosystem variables, sorted by R^2.

F_{leaf} *vs.*	*Slope*	R^2	*p-Value*
WS	-1.09	0.269	1.52E-11
T_s	0.202	0.159	5.58E-05
T_a	0.136	0.148	5.93E-05
CO_2	0.0205	0.130	2.25E-05
OCS	-0.00956	0.0905	0.000446
SWC	-0.0740	0.0339	0.109
VPD	-0.0727	0.0290	0.282
R_n	0.0129	0.0268	0.254

Table 7. Second half-night (n_2) linear regressions, F_{leaf} vs. eight ecosystem variables, sorted by R^2.

F_{leaf} *vs.*	*Slope*	R^2	*p-Value*
WS	-1.35	0.309	1.40E-11
OCS	-0.0169	0.293	1.35E-08
CO_2	0.0154	0.275	7.96E-06
R_n	0.0505	0.257	8.22E-05
T_s	0.0801	0.190	0.197
T_a	0.0577	0.189	0.156
VPD	-0.343	0.188	0.00198
SWC	-0.0540	0.179	0.308

Table 8. Whole-night (n) linear regressions, F_{eco} vs. eight ecosystem variables, sorted by R^2.

F_{eco} *vs.*	*Slope*	R^2	*p-Value*
WS	-1.27	0.299	1.21E-12
OCS	-0.0170	0.225	2.94E-09
VPD	-0.380	0.176	8.23E-06
CO_2	0.0181	0.158	6.22E-06
SWC	0.176	0.149	0.000216
R_n	0.0387	0.110	0.00253
T_s	-0.111	0.0581	0.0668
T_a	-0.0537	0.0451	0.184

Table 9. First half-night (n_1) linear regressions, F_{eco} vs. eight ecosystem variables, sorted by R^2.

F_{eco} vs.	Slope	R^2	p-Value
WS	-1.15	0.304	2.65E-13
SWC	0.196	0.180	3.15E-06
CO_2	0.0228	0.139	3.54E-06
VPD	-0.275	0.118	4.07E-05
OCS	-0.0105	0.104	0.000114
R_n	0.0235	0.0427	0.0381
T_s	-0.0546	0.0154	0.334
T_a	-0.0192	0.0133	0.605

Table 10. Second half-night (n_2) linear regressions, F_{eco} vs. eight ecosystem variables, sorted by R^2.

F_{eco} vs.	Slope	R^2	p-Value
VPD	-0.544	0.306	3.92E-07
OCS	-0.0173	0.302	1.45E-08
WS	-1.177	0.300	9.92E-10
R_n	0.0600	0.229	2.90E-05
SWC	0.183	0.209	0.00119
CO_2	0.0154	0.186	0.000136
T_s	-0.139	0.186	0.0364
T_a	-0.0774	0.170	0.0790

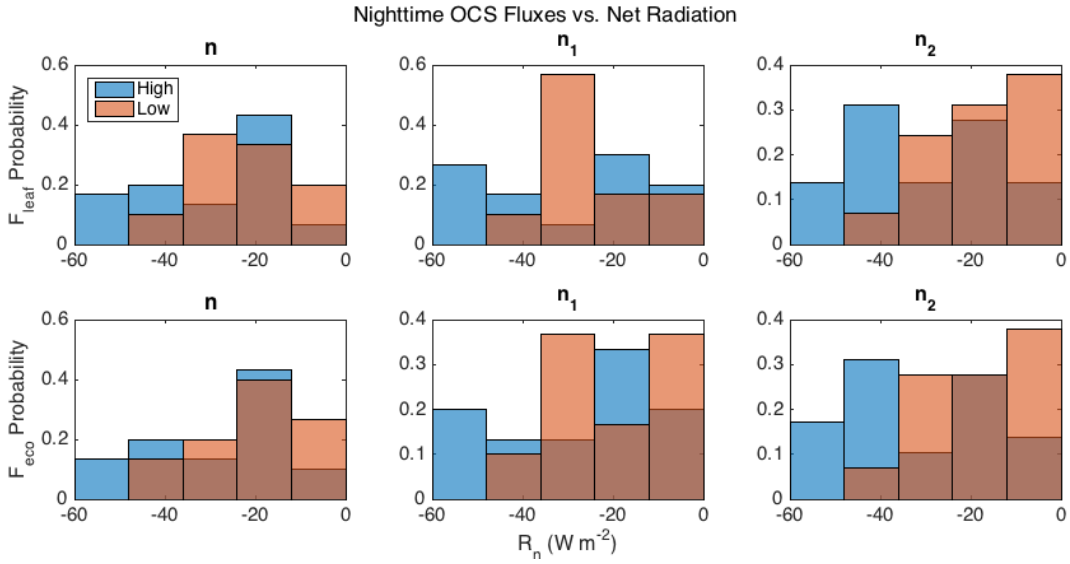

Figure 45. High (blue) and low (red) nighttime OCS fluxes vs. R_n.

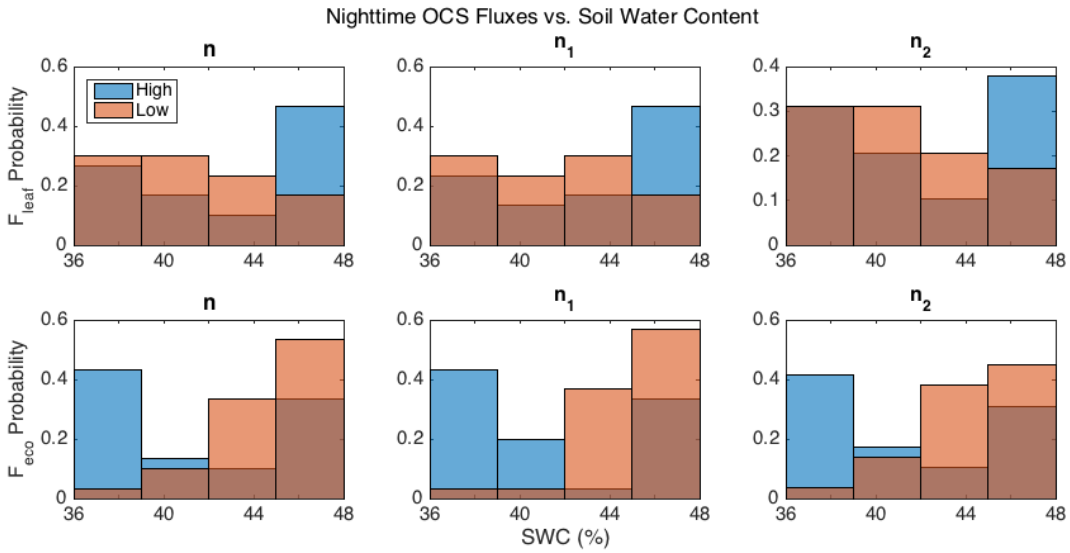

Figure 46. High (blue) and low (red) nighttime OCS fluxes vs. SWC.

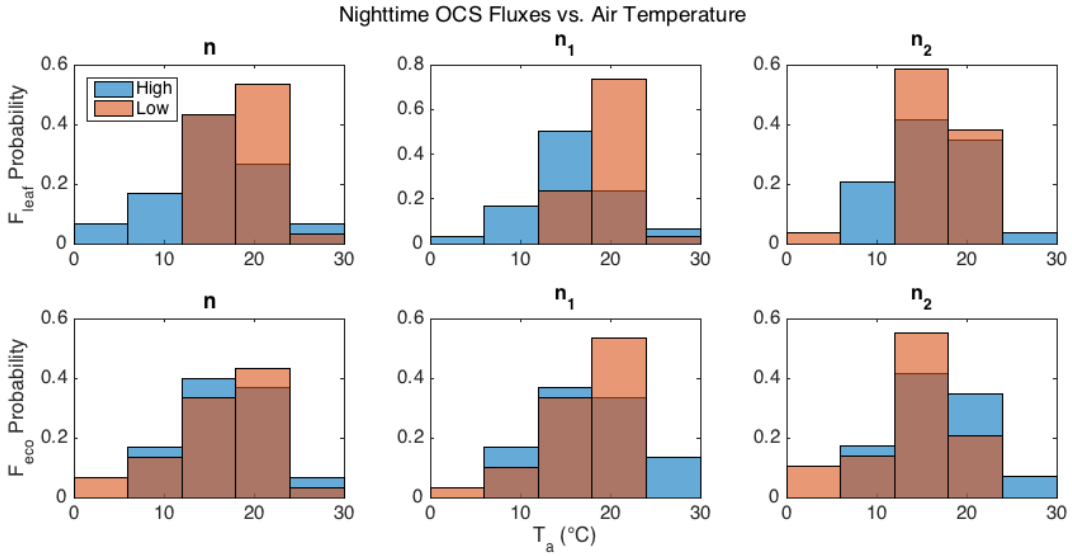

Figure 47. High (blue) and low (red) nighttime OCS fluxes vs. T_a.

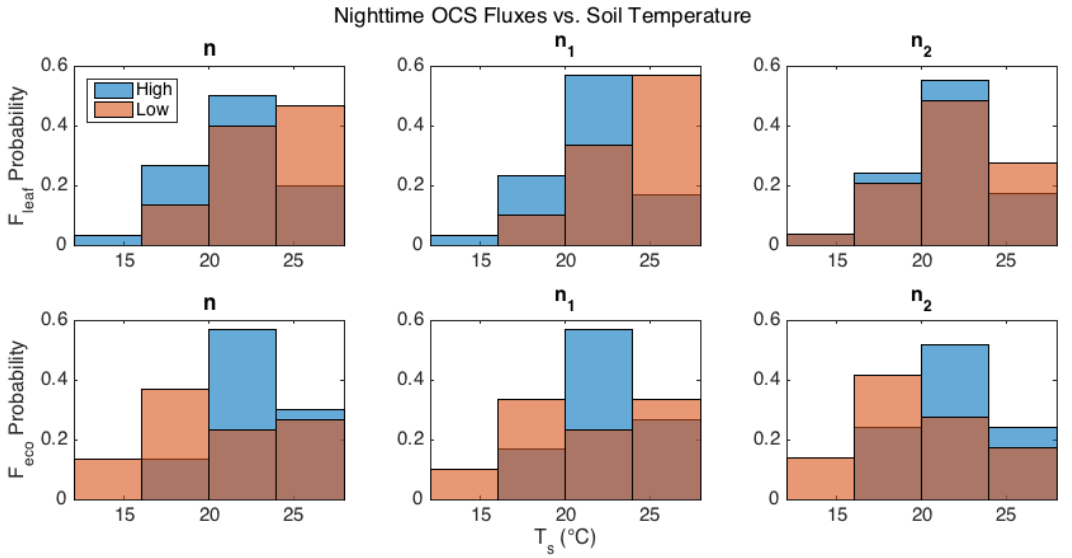

Figure 48. High (blue) and low (red) nighttime OCS fluxes vs. T_s.

8 VITA

Name	Benjamin M. Alsip
Education	B.A. English Literature, Knox College, Galesburg, IL, 2000
Teaching Experience	Department of Earth and Environmental Sciences, University of Illinois at Chicago, Chicago, IL: Global Environmental Change (EaES 101), 2016–2017
Honors	Illinois Water Resources Center Student Research Award, 2015
Abstracts	Alsip, B. M., M. Berkelhammer, R. Matamala, D. R. Cook, and C. Whelan (2016), Carbonyl Sulfide Fluxes from a Tall Grass Prairie Ecosystem Through a Growing Season, Abstract B53B-0527 presented at 2016 Fall Meeting, AGU, San Francisco, Calif., 12-16 Dec.